Neurovascular Coupling is Required for Amygdala Neuronal Activation and Associated Emotional Behaviors in Mice, Depending on NMDA Receptor Subunit 2D-expressing Cerebral Arteriolar Smooth Muscle Cells

Running title: Neurovascular Coupling Regulates Amygdala-dependent Emotion Homeostasis

Jiayu Ruan[1,2,3], Yiyi Zhang[2,3], Dongdong Zhang[2,3], Huiqi Xie[2,3], Xinghua Quan[2,3], Wentao Wang[2,3], Xu Hu[2,3], Yanmei Tao[5,6], Bingrui Zhao[2,3], Danping Lu[2,3], Jie-Min Jia[2,3,4*]

Affiliations

1. College of Life Sciences, Zhejiang University, Hangzhou, Zhejiang 310058, China.

2. Key Laboratory of Growth Regulation and Translational Research of Zhejiang Province, School of Life Sciences, Westlake University, Hangzhou 310024, China.

3. Westlake Laboratory of Life Sciences and Biomedicine, Hangzhou 310024, China.

4. Laboratory of Neurovascular Biology, Institute of Basic Medical Sciences, Westlake Institute for Advanced Study, Hangzhou 310024, China.

5. Key Lab of Organ Development and Regeneration of Zhejiang Province, Institute of Life Sciences, College of Life and Environmental Sciences, Hangzhou Normal University, Hangzhou 311121, China.

6. Department of Physiology, Medical College, Southeast University, Nanjing 210009, China.

*Correspondence: Jie-Min Jia (jiajiemin@westlake.edu.cn)

Abstract

Proper brain function depends on intact neurovascular coupling (NVC). Through NVC, local cerebral blood flow (CBF) is rapidly increased in activated cerebral regions to meet the corresponding demands of neural activities. NVC has been believed to support advanced cerebral functions such as complex emotional homeostasis. However, few studies provide causal link evidence with specific molecular and cellular identities. Here, using RNAscope, cell-type specific conditional knockout (cKO) perturbation in BL6/C57 mice, laser speckle contrast imaging, and mouse behavior assays, we demonstrated that the N-methyl-D-aspartic acid (NMDA) receptor noncore subunit NR2D is only expressed in cerebral arteriole smooth muscle cells (aSMCs) but not in peripheral aSMCs. Both aSMC-NR2D cKO and aSMC-NR2D+NMDA receptor subunit 1 (NR1) double cKO mice displayed a severe decline in functional hyperemia induced by whisker stimulation. In addition, the NR2D pathway was independent of previously demonstrated COX-2-PGE2-dependent mechanism and high-fat diet (HFD)-induced impairments in NVC. Caldesmon is a potential downstream protein in the NR2D pathway for NVC regulation. Notably, we demonstrated that NVC deficits caused abnormalities in complex emotional behaviors, such as anxiety-like behaviors (exhibiting increased defecation and urine), reduced curiosity and decreased fear instinct (displaying less fear of aggressive CD1 mice). Furthermore, fear-response gene c-FOS expression in the amygdala neurons was attenuated in aSMC-NR2D knockout mice after response to acute stresses. In contrast, its expression level remained unchanged in the non-fear-related cerebral regions such as the piriform cortex and hippocampus. These findings demonstrated that inadequate functional hyperemia impaired cerebral complex emotional functions and suggested a co-existence of anxiety and fearlessness in single individuals.

Introduction

Cerebral blood flow (CBF) provides logistic support for maintaining the homeostasis of the cerebral microenvironment by delivering oxygen and nutrients and clearing carbon dioxide and metabolic wastes as promptly and adequately as possible (1). CBF impacts the cerebral microenvironment by priming extracellular ion homeostasis, which could influence neuronal excitability (2). The emerging views are that moderate CBF dysregulation, not to such an extent as ischemia, leads to chronic cerebral dysfunction and disease (3). Cerebrovascular dysregulation becomes a feature not only of cerebrovascular pathologies but also of complex cognitive (4) and emotional disorders (5). Regionally rapid functional hyperemia induced by local neural activities, termed neurovascular coupling (NVC), is a functional interplay between the central nervous system

(CNS) and cerebrovascular systems by signaling neural messages, resulting in cerebral arterial smooth muscle cells (aSMCs) relaxation and hence vasodilation, leading the CBF increasing in regions of neural activating (6). NVC is a universally conserved biological process among mammalians that can effectively and spatiotemporally regulate cerebral blood supply distribution (7). The dynamics of CBF are widely assumed to represent neuronal activity in functional neuroimaging, which is the only non-invasive approach to measuring the cerebral cognitive and emotional status of humans. One of the known applications of NVC is functional magnetic resonance imaging (fMRI) (8).

With fMRI, high levels of the blood oxygenation level-dependent (BOLD) signal mirrored with an increased NVC are often repeatedly observed in some classic cerebral regions of patients with emotional disorders such as major depressive disorder (MDD), general anxiety disorder (GAD), and fear-related post-traumatic stress disorder (PTSD). For instance, MDD patients commonly manifest robust and persistent high BOLD signals in the lateral habenula (LHb), where excessive neural excitements were verified in many rodent animal models of depression (9). Besides, almost all PTSD patients and fear-stressed humans exhibit high BOLD signals in the amygdala (10, 11). Notably, induced by acute fear stress (e.g., instinct fear of a predator) or emotional disorders, the correlation between physiological or pathological neural excitement and an increased BOLD signal in the amygdala is an evolutionally conserved observation, crossing humans (12, 13), nonhuman primates (14), and rodents (15). However, the physiological roles of NVC in complex high-level cerebral functions (namely, how vital the increased amount of CBF beyond the resting CBF level is for advanced cerebral functions) remain largely unknown despite decades of extensive investigations on the underlying mechanisms of NVC.

Specifically, in emotional disorder studies, little insight has been drawn into how the increased magnitude of CBF over the resting level is involved in neuronal excitement in the amygdala and fear perception. On the other dimension, recent findings point out that in the *in vivo* experiments of rats, fluoxetine (a selective serotonin reuptake inhibitor) for rats has been proven to cause cerebral arterioles vasodilation (16) and reverse the deficit in escape latency in the learned helplessness model of the emotional disorder (17). It is well established that except neurons, aSMCs express a high level of serotonin transporter (18) and receptor subtypes (19, 20). These two facts together implicate that blood flow alteration caused by aSMCs may be involved in reversing emotional status. The consequence of ignoring the contributions of NVC to emotional disorders leads to stagnation in studies.

87

88 Compared with the study of the correlation between NVC and emotional disorders, the assessment of NVC is
89 more mature. The extent of NVC can be quantified by measuring CBF variation and vascular diameters during
90 the functional hyperemia in the barrel cortex of mice induced by the whisker stimulation, using laser doppler
91 imaging (21), laser speckle imaging (22), and two-photon Imaging (23). Previous studies have revealed
92 multiple signalling pathways mediating NVC: neurons or endothelial cells releasing nitric oxide (NO) to cerebral
93 arterioles SMCs (aSMCs) cause vasodilation (24-26); astrocyte-secreted small vasoactive molecules cause
94 the constriction of aSMCs (27-29). Although extensive manipulations have been established to enhance or
95 inhibit NVC, most depend on pharmacology or null mutations, which lack cellular specificity. Therefore, no
96 clear conclusion can be yielded by these means because both the neural circuit *per se* and the cerebrovascular
97 system are being affected, which confounds the contributions from vascular cell-dependent NVC inhibition.
98 Only the conditional knock-out genetic perturbation strategy developed during the recent decade can achieve
99 the goal of cell specificity (23, 30, 31). Most recent findings indicate that the N-methyl-D-aspartic acid (NMDA)
100 receptor expressed in aSMCs controls NVC robustly, revealed by cell-type specific genetic perturbation.
101 However, which noncore subunit of the NMDA receptor works with the obligatory NR1 core subunit in aSMCs
102 to mediate NVC remained unknown. The NMDA receptor has long been involved in emotional disorders. For
103 instance, the extinction of conditioned fear is mediated by NMDA receptors in the amygdala (32, 33); in
104 emotional disorders patients, it can be found that NMDA receptors decreased in the prefrontal cortex (34);
105 NR2D (one of a noncore subunit of NMDA receptor) total knock-out mice exhibited anxiety-like and depression
106 behavior phenotypes (35). Since the total knock-out strategy and widespread nature of drug interruption lose
107 the cellular specificity manipulation, the contribution and cellular identity of NMDA receptors in fear-like and
108 anxiety-like behavior presentation are unclear.

109

110 Here, we first reported that NR2D is a unique noncore subunit of the NMDA receptor expressed in cerebral
111 aSMCs. In whisker stimulation-mediated functional hyperemia, conditional knockout (cKO) of NR2D in aSMCs
112 of mice resulted in reduced functional hyperemia. The NVC regulatory pathway involving NR2D was similar to
113 that mediated by NR1 but independent of the COX-2 and high-fat diet (HFD) pathways. Caldesmon is a
114 potential downstream protein in the NR2D pathway for NVC regulation. Notably, behaviors that represent fear
115 status were significantly diminished in aSMC-specific NR2D cKO mice. Furthermore, neuronal c-Fos
116 expressions in the amygdala, which usually represents neurons activated in response to fear stimuli, were
117 robustly attenuated in aSMC-specific NR2D cKO mice. More interestingly, aSMC-specific NR2D cKO mice

118 exhibited a higher level of anxiety-like behavior by producing more defecation, similar to that in anxiety patients
119 (36). Based on the above evidence, being less fearful and having a higher anxiety level can coexist in the
120 same individuals. Our findings may shed light onto a new angle of emotional disorder treatment development.
121

122 # Materials and methods

123 **Animal and animal care**

124 All mice procedures complied with the Institutional Animal Care and Use Committee (IACUC) guidelines of the
125 School of Life Sciences, Westlake University. All mice housed in Westlake University Laboratory Animal
126 Resource Center with standard animal rooms provided a 12-h light/dark cycle at 25°C. No more than six mice
127 were fed in each cage, and standard chow and water were provided to the mice *ad libitum*. All the genetic
128 information of mice is in Table 1. All mice were B6 background. Unless otherwise specified, the age of all male
129 adult mice was from 2-month-old to 3-month-old.
130

131 **Cell culture**

132 P0 mice anesthetized with ice. Surgical tweezers were used to quickly extract pial membrane or cortex from
133 the brains of mice in DMEM (Gibico, Cat# 11965092, USA). Then, 0.25% Trypsin (Thermo Scientific, Cat#
134 25200072, USA) was used to digest pia or cortex for 15min at 37℃ in the incubator. After that, cells were
135 added with FBS (Gibico, Cat# 10099, USA) and filtered by a 40μm filter (Falcon, Cat# 352340, CHN). Finally,
136 cells were centrifuged 1,600*g at 4℃ for 5min and resuspended by SMCM (ScienCell, Cat# 1101, USA) in T25
137 flasks (Corning, Cat# 430639, USA).
138

139 **TMX administration**

140 **1. Tamoxifen for mice**

141 Tamoxifen (MCE, Cat# HY-13757A, USA) was orally administrated to mice. Tamoxifen was dissolved in corn
142 oil (Aladdin, Cat# C116023-500ml, CHN), and the dose for each mouse per day was 0.2ml (10mg/ml). In almost
143 all cases, for adult mice, tamoxifen was orally administered to mice from postnatal day 60 to postnatal day 63
144 (P60 to P63). Otherwise, for the P5 conditional knock-out group and its littermate control group, infant mice
145 got tamoxifen through breast milk. On the fifth day after the birth of mice (P5), the mother of infant mice was
146 orally administrated with tamoxifen for four days (from P5 to P8). In particular cases, tamoxifen administration
147 time refers to the results and figures of the corresponding experiments.

148

149 **2. Tamoxifen for cell culture (include cell sorting)**

150 When cells reached approximately 80% full of the bottom surface of T25 flasks, tamoxifen was administrated
151 to cells. tamoxifen was dissolved in DMSO (Solarbio, Cat# D8371, CHN), and the final concentration of
152 tamoxifen for SMCM was 5μM. After four-day culture, EGFP or Tdtomato in cells were expressed. Cells were
153 sorted by MA-900 (Sony, FCCF-MBR, JPN) to obtain EGFP-positive or Tdtomato-positive cells, and these cells
154 were pure sorted cerebral arterioles smooth muscle cells (aSMCs). Sorted cells were cultured in SMCM for
155 further assay. The purity of cells sorted by the same method had been verified in the paper published by our
156 laboratory (37).

157

158 **RNA scope *in situ* hybridization**

159 Horizontal sections (15μm) of tamoxifen administrated SMAcre^{ER+}:Ai14 mice brains were obtained by CM1950
160 (Lecia, Histo-CM1950, DEU). All RNA scope *in situ* hybridisation productions were obtained from ACDbio,
161 including RNAcope Multiplex Fluorescent Reagent Kit v2 (ACDbio, Cat# 323100, USA), *Grin2d* probe (ACDbio,
162 Cat# 425951-C3, USA) and *Grin1* probe (ACDbio, Cat# 431611, USA). All operations were carried out following
163 the reagent instructions of ACDbio company and a published study that used RNA scope *in situ* hybridization
164 (38).

165

166 **RT-PCR**

167 aSMCs from triple transgenic mouse lines, SMAcre^{ER+}:*grin2d*$^{f/f}$:Ai47 (conditional knock-out group) and
168 SMAcre^{ER+}:*grin2d*$^{+/+}$:Ai47 (littermate control group), were used as a source for RNA extraction. Briefly, after
169 obtaining pure sorted EGFP/Tdtomato-positive aSMCs from pia (pial aSMCs) and cortex (parenchymal
170 aSMCs) of the conditional knock-out group and its littermate control group, cells were cultured in 6cm dishes
171 (Corning, Cat# 430166, USA) with SMCM. After cells reached around 90% density, Trizol (Sangon Biotec, Cat#
172 B511311-0100, CHN) was used for the RNA extraction. RNA from P0 SMAcre^{ER+}:*grin2d*$^{+/+}$:Ai47
173 cortex/cerebellum was used as a positive control. After the P0 mice were anesthetized with ice, the cerebellum
174 of the mice was directly taken out, and TRIzol was used for RNA extraction.

175

176 After RNA extraction, all RNA samples were reverse transcription to cDNA (50ng/μl) using HiScript III 1st Strand
177 cDNA Synthesis Kit (Vazyme, Cat# R312-02, CHN). For the PCR amplification system, each reaction
178 contained 10μl of Green Taq Mix (Vazyme, Cat# P131-AA, CHN), 2μl of cDNA, 2μl of primer pairs (10μM), and

179 6μl of RNAase-free water. Except the amplification cycle of *18s* was 20, the amplification cycle of other primers
180 was 35. Agarose gel electrophoresis used 2% agarose gel (BIOWESTE, Cat# 111860, ESP) and ran at 220V
181 for 30min. RT-PCR gel images were obtained by Tanon imager (Tanon, 1600 Geil imager, CHN). All operations
182 were carried out in strict accordance with the reagent instructions. A list of primer pairs is in Table 2.
183
184 **Western-bolt**
185 For tissue sample collection, tissue samples were ground together with RIPA (Thermo Scientific, Cat# 89901,
186 USA) on ice for 30min. For cell samples, after cells reached around 90% density, the RIPA was used for protein
187 extraction on ice for 30min. Protease Inhibitor Cocktail (CWBIO, Cat# CW22008, CHN) was used to prevent
188 protein enzymolysis during the protein extraction. After that, samples were centrifuged 12,000*g at 4℃ for
189 5min, and supernatant were collected. Concentrations of proteins were measured by Micro BCA Protein Assay
190 Kit (CWBIO, Cat# CW2011S, CHN), and after the concentration measurement, all samples were boiled with
191 SDS-PAGE loading buffer (CWBIO, Cat# CW0027S, CHN) for 10min at 100℃. 8% SDS-polyacrylamide
192 electrophoresis gels were used for gel running, and a protein marker (GenStar, Cat# M221-05, CHN) was used
193 to identify the protein size. After 90min gels running at 120V (80V for the first 30min), gels were transferred to
194 0.45μm PVDF membranes (Millipore, Cat# IPVH00010, USA) at 400mA for 120min. After transfer, PVDF
195 membranes were blocked by 5% non-fat milk in 1X TBST buffer for 60min at room temperature with a mild
196 horizontal shake.
197
198 After the block, for each particular assay, the first antibody diluted with 5% non-fat milk in 1X TBST buffer was
199 used to incubate the membrane overnight at 4℃ with a mild horizontal shake. After the first antibody incubation,
200 the membrane was washed by 1X TBST 10min (3 replicates). The corresponding second HRP-conjugated
201 antibody diluted with 5% non-fat milk in 1X TBST buffer was used to incubate the membrane 45min at room
202 temperature with a mild horizontal shake. After the second antibody incubation, the membrane was washed
203 by 1X TBST 10min (3 replicates). ECL kits (Abbkine, Cat# BMU102-CN, CHN) and gel image system (GE,
204 GEL Imaging System AI680RGB v.2.0, USA) were used for exposure photography. All operations were carried
205 out in strict accordance with the reagent instructions. A list of antibodies is in Table 3.
206
207 **Immunofluorescence staining**
208 For tissue Immunofluorescence (IF) staining, briefly, after anesthesia with 1% pentobarbital sodium, the mice
209 were perfused with 1X PBS (5min) and 4%PFA in 1X PBS (5min) through the left ventricle to empty blood and

fix tissue. Afterwards, tissue was extracted and fixed by 4%PFA in 1X PBS overnight at 4℃ with a mild horizontal shake. The next day, for MCA branches IF staining, MCA branches were carefully extracted from the brain using surgical tweezers. Then, treated isolated MCA branches by 0.5% Triton X-100 (Diamond, Cat# A110694-0500, CHN) in 1X PBS for 30min at room temperature, and then isolated MCA branches were washed with 1X PBS for 10min (3 replicates). Next, 5% BSA (BBI, Cat# A600332-0100, CHN) in 1X PBS was used to block isolated MCA branches for 30min at room temperature. After the block, isolated MCA branches were rewashed as described before. For other tissue like brain and peripheral organs, all organs were sliced into 50μm (Leica, Histo-VT1200S, DEU) after fixed by 4%PFA in 1X PBS overnight at 4℃ with a mild horizontal shake. The subsequent process was similar to that of isolated MCA branches.

For cultured cell immunofluorescence staining. After cells reached around 90% density, cells were passed by into 12-well plates (Corning, Cat# 3515, USA) with glass slices (30k cells per well). After cells in 12-well plates reached around 70% density, cells in glass slices were fixed by 4%PFA in 1X PBS for 10min at room temperature. Washed cell slices with 1X PBS 10min (3 replicates), treated cells with 0.3% Triton X-100 in 1X PBS for 10min at room temperature, and then washed again with 1X PBS 10min (3 replicates). Next, 5% BSA in 1X PBS was used to block cell slices for 30min at room temperature. After the block, cell slices were rewashed as described above.

In the staining process, the first antibody diluted with 1% BSA+0.1% Triton X-100 in 1X PBS was used to incubate samples overnight at 4℃. After the first antibody incubation, samples were washed with 1X PBS 10min (3 replicates). The corresponding second fluorescence-conjugated antibody diluted with 1% BSA+0.1% Triton X-100 in 1X PBS was used to incubate samples 120min at room temperature. After the second antibody incubation, samples were washed with 1X PBS 10min (3 replicates). After that, 1000X diluted Hoechst (AbMole, Cat# M5112, CHN) was used for nucleus staining. The operation was slightly different for the co-staining of NR2D and NR1 in MCA. After incubating with the first antibody of NR2D, Goat Anti-Mouse IgG (H+L) was used as the second antibody for 120min incubating at room temperature. Then, Donkey anti-Goat IgG (H+L) Cross-Adsorbed Secondary Antibody, Alexa Fluor™ 647, was used as the third antibody to incubate at room temperature for 120min. After incubating the third antibody, 5% BSA in 1X PBS was used to block isolated MCA branches for 30min at room temperature. Then, the first antibody of NR1 was incubated overnight at 4℃. After the first antibody of NR1 incubation, samples were incubated with Goat anti-Mouse IgG (H+L)

240 Cross-Adsorbed Secondary Antibody, Alexa Fluor™ 488 at room temperature for 120min. 1X PBS was used
241 for washing after each step (10min, 3 replicates). Tissue slices and cell culture slices were covered by a glass
242 slice with the mounting medium (SouthernBiotech, 0100-01, USA). Zeiss LSM800 (Zeiss, LSM800, DEU)
243 microscopy was used for photography. All operations were carried out in strict accordance with the reagent
244 instructions. A list of antibodies is in Table 3.
245
246 **Whisker stimulation**
247 The whisker was trimmed to only remain lane three and lane four on one side of the face, and the scalp was
248 exposed on the same day. The mice did not perform any operation the day before the assay to reduce potential
249 interference (Particular set-up diagrams refers to the results and figures of the corresponding experiments).
250 On the day of the assay, mice were anesthesia with 1% pentobarbital sodium, and stable fixated on the
251 platform. The electro-motor-driven brush stimulated the whisker longitudinally for 1 minute at a frequency of
252 4Hz. The principle of laser speckle contrast imaging has been described in the previous study (39), and the
253 operation referred to the published study (40). Laser Speckle Image System (LSIS, RWD, RFSLI ZW/RFSLI
254 III, CHN) was used to monitor the CBF variation in the region of interest (ROI) of the opposite barrel cortex of
255 mice. The recording parameters were: 512*512 resolution, 10FPS, and 2min recording (the 30s before
256 stimulation, 1min during stimulation, and 30s after stimulation).
257
258 **Cisternal injection and whisker stimulation**
259 All operations were followed by study ***Cannula Implantation into the Cisterna Magna of Rodents***
260 *(https://doi.org/10.3791/57378)*. NS-398 (MCE, Cat# HY-13913, USA) was mixed with FITC (10mg/ml, Sigma,
261 FD40S-1G, USA) for injection, and the final concentration of NS-398 in the CSF was 100μM. 10min after the
262 injection, remove the scalp, and the FITC signal was detected by microscope (Zeiss, Axio Zoom v16, DEU).
263 20min after the injection, whisker stimulation (parameters were similar to that described above in “Whisker
264 stimulation” part) was performed for successfully injected mice.
265
266 **Physical examination of mice and the HFD challenge experiment**
267 Electronic scales were used for weighing mice and high-fat food (SYSEbBio, Cat# D12492, CHN). The body
268 fat/lean/total water content of mice was measured with EchoMRI™-100H (Echo MRI, Cat# 100H, USA). The
269 blood pressure of mice was measured by Kent Noninvasive blood pressure measurement system for
270 animals/Biopac physiological signal analytical system (Kent/Biopac, Cat#, USA). HFD challenge kept for 8-

weeks. The food consumption and the body fat/lean/total water content of mice were monitored during the HFD challenge. Whisker stimulation was performed after the HFD challenge (parameters were similar to that described above in “Whisker stimulation” part).

Immunoprecipitation assay (include lentivirus infection)

Tdtomato-positive pure aSMCs from P0 pial culture of SMAcre^{ER+}:Ai14 mice were collected for lentivirus infection and further immunoprecipitation (IP) assay. Cells were cultured in 6cm dishes with SMCM. After cells reached around 90% density, add lentivirus (Lenti-EF1-EGFP-CMV-*grin2d*-3XFlag-WPRE) into the culture and keep for one week (virus titer: $2.6*10^9$). Infected cells were green. MA-900 sorted out EGFP and Tdtomato double-positive cells, and these cells were lentivirus-infected aSMCs. These cells were then cultured in 10cm dishes. After cells reached around 90% density, cells were collected by RIPA reagent. A Protein G Magnetic beads kit (Epizyme, Cat# YJ002, CHN) was used for the immunoprecipitation assay. NR2D antibody and IgG control antibody were mixed with Protein G Magnetic beads respectively to pull down NR2D and its related protein. Pull-down products were verified by western-bolt and analyzed through mass spectrometry. All operations were carried out in strict accordance with the reagent instructions. Data analysis and inclusion criteria methods are described in “Statistical analysis software and code” part. A list of antibodies is in Table3.

Open field test and open field-like test

The setup of open field test (OFT) referred to published studies (41-44). Each mouse was placed in the central area of a 40*40 cm box for the OFT. The camera recorded their path, fecal/urine production and movement parameters within 15 minutes. The setup of open field-like test (OFLT) referred to published studies (45). Each mouse was placed in the central area of a 23*23 cm box for the OFLT. An iron mesh wall replaced one wall of the box. Sketch paper was put on the bottom of the box to collect urine. A transparent acrylic plate covered the top of the box. Symmetric space is on the opposite side of the iron mesh wall. The camera recorded their path, fecal/urine production and movement parameters within 20 minutes. During the analysis, the box was divided into three parts (left area, central area, and right area) to analyze the preference of mice for iron mesh wall.

CD-1 fear assay

The setup of CD-1 fear assay referred to published papers (45-48). CD-1 mice that were never exposed to wild-type (WT, SMAcre^{ER-}:*Grin2d*$^{f/f}$) and cKO (SMAcre^{ER+}:*Grin2d*$^{f/f}$) mice were used for the assay. Before the assay, simultaneously put a single WT or cKO mouse and a CD-1 mouse into a cage. The cage contains new

302 padding and a metal lid on the top. One side of the metal lid is used for placing food and water bottles, so the
303 height is lower than another side. After that, the camera was used to record all behaviors of C57 mice (WT or
304 cKO mouse) and CD-1 mice, including but not limited to fighting behaviors within 10 minutes. After the assay,
305 CD-1 and C57 mice were separated again. C57 mice were fed alone in a clean new cage for 90 minutes and
306 then used for brain extraction to detect neural c-Fos expression in the amygdala, S1BF, Pir cortex, and
307 hippocampus.
308
309 **Elevated plus-maze test**
310 The setup of elevated plus-maze (EPM) referred to published studies (38, 49). The EPM comprises two open
311 arms (65×5 cm) and two close arms (65×5 cm). Each mouse was placed in the center, facing one of the two
312 open arms, and allowed to explore for 5 minutes. Time spent in open arms, center of arms, and close arms
313 were recorded.
314
315 **Statistical analysis software and code**
316 All the analysis of fluorescence intensity and grey value used Zeiss Zen Lite (v2.3) and ImageJ (v1.53u). All
317 whisker stimulation original data were measured by LSIS-self software (v5.0). Visualization of CBF variation,
318 CBF plateau mean value, CBF plateau maximum value, CBF "Time to plateau", CBF increase value (K-slope),
319 data inclusion criteria before bioinformatics analysis of mass spectrometry data, and OFLT heat map were
320 calculated using self-compiled MATLAB codes. Besides, The Veen map was made by Hello jvenn!
321 (http://jvenn.toulouse.inra.fr/app/example.html). KEGG and GO analysis referred to DAVID Bioinformatics
322 Resources (https://david.ncifcrf.gov/home.jsp) and Kyoto Encyclopedia of Genes and Genomes
323 (https://www.genome.jp/kegg/). The figure of KEGG pathway map made by self-compiled R code. All codes
324 were available at https://github.com/JialabEleven/Neurovascular_coupling. All the original behavioral data of
325 OFLT were recorded using any-maze (v4.73). OFT and EPM original behavioral data were recorded using
326 Noldus. All statistical data were processed by Numbers (v12.2), and all figures were made by Prism (v9.4.1).
327
328 **Brief description of codes**

329 1. **Data and code availability.** All image processing, analysis, and visualization, as detailed below, were
330 performed in ImageJ (v1.53u), R studio and MATLAB (MathWorks). All quantitative analyses were done
331 in a blinded manner. The codes were divided into four parts, visualization of cerebral blood flow variation,
332 analysis of cerebral blood variation periods, data pre-analysis of mass spectrum, and the heat map of mice

tracking of OFLT. All codes can be found at https://github.com/JialabEleven/Neurovascular_coupling.

2. **Visualization of the CBF change collected by LSIS.** Using custom-written scripts, the LSIS data were analyzed in MATLAB (version R2021a; MathWorks). It generates relative perfusion values (arbitrary units), and the CBF was expressed as a percentage change over baseline values in whisker stimulation experiments. For the whisker stimulation experiments, the imaging sampling frequency is 10Hz for a total of 120 seconds, and the first frame per second of the image (512 pixels × 512 pixels) was taken as the analysis object. A 30-second-long period (typically 30 images) was averaged and considered as the baseline image, and which grey value of every pixel was recorded at the beginning of the imaging session. Then every whisker stimulation image (60 seconds) and after-stimulation image (30 seconds) were normalized to the baseline image. To demonstrate the differences in CBF variation between SMAcre^{ER-}:*Grin2d*$^{f/f}$ mice and SMAcre^{ER+}:*Grin2d*$^{f/f}$ mice, the ROI of barrel cortex opposite to the whisker stimulation side was chosen, and the diagram of CBF change over baseline of the ROI was presented in Figure 2B.

3. **Analysis of CBF periods.** Acquired laser speckle data of relative perfusion values were processed in MATLAB using custom-written scripts for the automated detection and analysis of perfusion change parameters. To find the endpoint of the rising period of CBF value under whisker stimulation, the local maximum intensity threshold was determined visually for each image and the cubic interpolation calculated the time to 20% and 80% of the local maximum. Within the threshold range, the inflection point where the value rises rapidly to a stable level was selected as the end point to reach the blood flow plateau. The beginning of the whisker stimulation (30 seconds) to the time of the selected local maximum was the rising period, and the local maximum to the end of the whisker stimulation (90 seconds) was the plateau period. Their kinetics of them were characterized as rise20-80 time in the rising period (from 20% to 80% of local maximum amplitude), K-slope (slope of rising speed) in the rising period, and maximum and mean value in the plateau period, as shown in Figure 2C-F, Figure 3B/E-G, Figure 4F/H-J, Figure S3, and Figure S4.

4. **Mass spectrum analysis for IP products of NR2D.** Acquired mass spectrum data was analyzed in MATLAB and R studio using a custom algorithm. Firstly, the data is filtered through the rules set by

362 MATLAB as below, the proteins needed to appear at least once in the three IP experiments and the
363 peptide-spectrum match (PSM) value was higher than ten. Furthermore, the proteins would be preserved
364 for subsequent analysis if the PSM value of this protein existed in the NR2D-IP group and not in the IgG
365 control group. If the PSM value of proteins exists in both groups, the proteins would be preserved if the
366 PSM value of NR2D-IP groups was greater than twice that of the corresponding IgG control group. The
367 selected mass spectrum data was further analyzed by R studio to achieve KEGG pathway enrichment, as
368 shown in Figure 5.

369

370 **5. Heat map of mice tracking.** Acquired Open Field-Like Test data of mice activity was analyzed using a
371 custom algorithm in MATLAB. To compare the location preference in an OFT between SMAcre^{ER-}:*Grin2d*$^{f/f}$
372 mice and SMAcre^{ER+}:*Grin2d*$^{f/f}$ mice, the track map of mice was transformed into heat map which employed
373 the Gaussian blur operation, as shown in Figure 6B.

374

375 # Results

376 **Expression of NR2D in cerebral aSMCs**

377 We first confirmed the expression of NR2D/*Grin2d* (the gene name of NR2D) in cerebral aSMCs through a
378 series of measurement approaches. First, we used RT–PCR to detect the gene expression of all NMDA
379 receptors in aSMCs collected from the brain parenchyma (Figure 1A/B). The functional NMDA receptor
380 comprises two core subunits of NR1 and two noncore subunits, NR2/3 (50). The PCR results showed that
381 among the seven known NMDA receptors, only the gene of the core subunit, *Grin1*, and the gene of the
382 noncore subunit, *Grin2d*, were expressed in cerebral aSMCs. This result suggests that the NMDA receptor in
383 cerebral aSMCs may comprise NR1 (encoded by *Grin1*) and NR2D (encoded by *Grin2d*) only. In addition, we
384 also measured the expression of *Grin2d* in cerebral aSMCs *in situ* by RNAscope. We first tested the specificity
385 of the RNAscope probe (Figure S1A). According to previous reports, with increasing age, the expression of
386 *Grin2d* and its encoded protein NR2D in the cerebellum is significantly reduced, while that of *Grin1* and its
387 encoded protein NR1 increased (51, 52). We used RNAscope probes of *Grin1* and *Grin2d* to measure the
388 gene expression of *Grin1* and *Grin2d* in the cerebellum of young (postnatal day 14, P14) and adult (3-month-
389 old) mice. In the cerebellum of young mice, *Grin2d* was expressed at high levels, but *Grin1* was expressed at
390 low levels. In contrast, in adult mice, *Grin2d* was expressed at low levels, but *Grin1* was expressed at high

391 levels. This trend is consistent with previous reports. Next, we measured the gene expression of *Grin2d* in the
392 cerebral arterioles *in situ* in brain slices from adult SMACre^{ER+}:Ai14 mice (Figure 1C). One week after oral
393 administration of tamoxifen, the aSMCs of mice specifically expressed tdTomato fluorescent protein. We used
394 the expression of this red fluorescent protein to confirm the location of cerebral aSMCs. The results of
395 RNAscope showed that although the density of the *Grin2d* probe signal was less than that of neurons, gene
396 expression of *Grin2d* occurred in cerebral aSMCs. This result supported the PT-PCR data and further
397 confirmed the expression of *Grin2d* in cerebral aSMCs.
398
399 Next, we introduced the Cre-loxp system to knockout NR2D in aSMCs. We tested whether Cre protein was
400 expressed in neurons and endothelial cells, leading to the leakage of Cre protein to non-aSMCs in the CNS.
401 The IF results demonstrated negligible tdTomato signal in NeuN-positive cells and CD-31 positive cells in brain
402 slices of SMACre^{ER+}:Ai14 mice (Figure S1B). Then, due to the extensive-expression of Cre protein in all
403 aSMCs of SMACre^{ER+} mice, we used SMACre^{ER+}:Ai14 mice to detect the colocalization of NR2D protein and
404 tdTomato protein in the peripheral organs of mice after the administration of tamoxifen. The
405 immunofluorescence (IF) staining showed no colocalization of NR2D protein and tdTomato protein in the heart,
406 liver, spleen, lung, kidney or small intestine (Figure S1C). The above evidence showed that even though
407 SMACre^{ER+} mice could express Cre protein in SMCs of other peripheral organs outside the CNS, the
408 expression of NR2D in cerebral aSMCs was specific.
409
410 After validating the reliability of SMACre^{ER+} mice, we also validated the reliability of *Grin2d*-flox mice. Nestin-
411 Cre^{+}:*Grin2d*$^{f/f}$ mice were obtained by mating Nestin-Cre^{+} mice with *Grin2d*$^{f/f}$ mice. By verifying the expression
412 of NR2D protein in the cerebellum of P0 Nestin-Cre^{+}:*Grin2d*$^{f/f}$ mice through western-blot (WB), we determined
413 that, compared with Nestin-Cre^{-}:*Grin2d*$^{f/f}$ mice, the expression of NR2D in the cerebellum was significantly
414 reduced in Nestin-Cre^{+}:*Grin2d*$^{f/f}$ mice, to levels even lower than those in the cerebellum of adult Nestin-
415 Cre^{-}:*Grin2d*$^{f/f}$ mice (Figure 1D/H). Moreover, we used SMACre^{ER+}:*Grin2d*$^{f/f}$ mice to verify the expression of
416 NR2D in the whole cerebellum at P10. On the fifth day after the birth of mice, the infant mothers received oral
417 administration of tamoxifen for four days (from P5 to P8 of infant mice). Since this strain of mice had NR2D
418 knocked out only in aSMCs, the expression of NR2D in other non-aSMCs was not affected. In addition,
419 because cerebral aSMCs accounted for only approximately 3‰ of the total number of cells in the brain, the
420 loss of NR2D expression in cerebral aSMCs did not significantly impact the expression of NR2D in the whole

421 cerebellum. The WB results showed that there was no significant difference in the expression of NR2D in the
422 cerebellum between the WT(SMACre^{ER-}:*Grin2d*$^{f/f}$) mice and cKO (SMACre^{ER+}:*Grin2d*$^{f/f}$) mice (Figure 1E/I).
423
424 Based on the above results, we mated SMACre^{ER+}:*Grin2d*$^{f/f}$ mice with SMACre^{ER+}:Ai47 mice to generate triple-
425 positive SMACre^{ER+}:*Grin2d*$^{f/f}$:Ai47 mice to obtain pure pial aSMCs. Then, we used RT–PCR, WB, and IF to
426 measure *Grin2d*/NR2D expression (Figure 1F/J, Figure 1G/K, and Figure 1L/M/O). The results confirmed the
427 expression of *Grin2d* in cerebral aSMCs and showed the expression level of *Grin2d*/NR2D in cKO
428 (SMACre^{ER+}:*Grin2d*$^{f/f}$) mice was significantly lower than that in WT (SMACre^{ER-}:*Grin2d*$^{f/f}$) mice. In the *ex vivo*
429 experiment, we extracted the middle cerebral artery (MCA) from the cortex surface of adult mice to determine
430 whether there was NR2D protein expression. The expression of NR2D protein was detected in the aSMCs of
431 the MCA in WT mice, and the expression of NR2D in the MCA of SMACre^{ER+}:*Grin2d*$^{f/f}$ mice decreased
432 significantly. The above results again confirm that the expression of the *Grin2d* gene and the NR2D protein in
433 mouse cerebral aSMCs and the Cre-loxp system was a suitable genetic tool to significantly reduce the
434 expression of *Grin2d* and the encoded NR2D protein in mouse cerebral aSMCs. Finally, we verified the effect
435 of aSMCs-NR2D cKO on the expression of biomarkers in aSMCs by WB and IF. The results showed that the
436 expression of both smoothelin (Figure 1N) and SMA (Figure 1P) did not significantly change with the cKO of
437 NR2D in aSMCs.
438
439 **Conditional knock-out of NR2D in aSMCs leads to a decrease in functional hyperemia**
440 We tested the functional hyperemia capacity with the conventional whisker stimulation assay. We set two time
441 points (P5 and P60) for tamoxifen administration to knockout *Grin2d* in aSMCs in SMACre^{ER+}:*Grin2d*$^{f/f}$ mice to
442 determine the contribution of NR2D to functional hyperemia. Moreover, we also used platelet-derived growth
443 factor receptor beta (Pdgfrβ)$^{ER+}$:*Grin2d*$^{f/f}$ mice to knockout *Grin2d* at P60 to validate the contribution of NR2D
444 in all mural cells. All mice underwent whisker stimulation at the same age (P65) (Figure 2A). The laser speckle
445 image system (LSIS) was used to monitor blood volume variation during the whisker stimulation assay (Figure
446 2B). The results showed that compared with WT mice, all cKO mice exhibited dysfunctional hyperemia during
447 the whisker stimulation period, regardless of whether cKO NR2D mice were SMACre^{ER+} at P5/P60 or Pdgfrβ^{ER+}
448 at P60 (Figure 2C). Specifically, during the period in which whisker stimulation-induced changes in CBF had
449 reached a plateau, the mean CBF changes of P5 SMACre^{ER+}:*Grin2d*$^{f/f}$ mice, P60 SMACre^{ER+}:*Grin2d*$^{f/f}$ mice,
450 and P60 Pdgfrβ^{ER+}:*Grin2d*$^{f/f}$ mice were 4.88%, 4.75%, and 3.14%, respectively. Compared with WT mice
451 (14.13%), the CBF changes in cKO mice were attenuated by at least 65%, a significant difference. In addition,

452 there were no significant differences in the mean CBF changes among all cKO groups. The maximum CBF
453 changes during the whisker stimulation exhibited a similar trend as the mean CBF changes in the four groups.
454 The maximum CBF changes of WT mice, P5 SMACre^{ER+}:*Grin2d*$^{f/f}$ mice, P60 SMACre^{ER+}:*Grin2d*$^{f/f}$ mice, and
455 P60 Pdgfrβ^{ER+}:*Grin2d*$^{f/f}$ mice were 18.38%, 8.23%, 7.34% and 5.31%, respectively. The WT group significantly
456 differed from all three cKO groups. Moreover, the maximum CBF increase rate of P60 Pdgfrβ^{ER+}:*Grin2d*$^{f/f}$ mice
457 was significantly lower than that of P5 and P60 SMACre^{ER+}:*Grin2d*$^{f/f}$ mice (Figure 2D). Next, we quantified the
458 CBF change from the beginning of whisker stimulation to the time the CBF variations began to stabilize
459 (plateau). We defined the latency between whisker stimulation and the start of the plateau period as the "time
460 to plateau". This period reflected how long the whisker stimulation-induced CBF change took to reach a
461 plateau. Next, we used the "K-slope" to describe the rate of slope increase of CBF during the "time to plateau",
462 reflecting the initial rate of CBF change. Time to plateau did not significantly differ among all four groups (Figure
463 2E); however, due to different mean and maximum CBF changes during the plateau period, the K-slope of the
464 WT group was significantly higher than that of all cKO groups. In addition, the K-slopes of the three cKO groups
465 did not significantly differ (Figure 2F). In summary, cKO of NR2D in mural cells led to dysfunctional hyperemia
466 during the whisker stimulation assay. No differences in parameters were observed between the P5
467 SMACre^{ER+}:*Grin2d*$^{f/f}$ mice and the P60 SMACre^{ER+}:*Grin2d*$^{f/f}$ mice. Only the maximum CBF change in P60
468 Pdgfrβ^{ER+}:*Grin2d*$^{f/f}$ mice was lower than that in the two SMACre^{ER+}:*Grin2d*$^{f/f}$ groups. There is no significant
469 difference between aSMCs-NR2D cKO during development and adulthood, suggesting that the original effect
470 of functional hyperemia is aSMCs.
471
472 As each mouse underwent at least two rounds of whisker stimulation during the whisker stimulation assay, we
473 wondered whether high-frequency whisker stimulation led to desensitization or hypersensitization of CBF
474 change. We used SMACre^{ER-}:*Grin2d*$^{f/f}$ mice to validate whether long-term continuous whisker stimulation led
475 to desensitization or hypersensitization of functional hyperemia (Figure S3). We collected data on twenty-one
476 consecutive days of whisker stimulation (ten times per day, each time lasting 1 minute). Comparison of the
477 data obtained before and after the long-term stimulation revealed no significant difference in any parameter
478 (mean CBF change, maximum CBF change, time to plateau, or K-slope). Therefore, the results suggest that
479 long-term continuous whisker stimulation did not induce desensitization or hypersensitization of the CBF
480 change.
481
482 **aSMC-expressed NR2D and NR1 may work together to regulate functional hyperemia**

483 Previous reports have suggested that the NR1 core subunits of NMDA receptors are always present in
484 functional NMDA receptors in neurons. To verify whether NMDA receptors containing NR2D and NR1 subunits
485 are present in cerebral aSMCs and whether these subunits work together, we measured the CBF change
486 induced by whisker stimulation in NR1 plus NR2D double-knockout mice (SMACre^{ER+}:*Grin1*$^{f/f}$:*Grin2d*$^{f/f}$ mice)
487 before and after tamoxifen administration (Figure 3A). If the NR1 and NR2D subunits in aSMCs are similar to
488 those in neurons and form complexes to work together, the CBF decrease caused by a double knockout of
489 these two genes should be similar to that caused by a single knockout of NR2D or NR1 alone. In contrast, if
490 the CBF decrease differs, these two proteins work independently. First, we performed the whisker stimulation
491 assay before and after tamoxifen administration in WT (SMACre^{ER-}:*Grin1*$^{f/f}$:*Grin2d*$^{f/f}$) mice to confirm whether
492 this experimental procedure plus the administration of tamoxifen affected functional hyperemia. All parameters
493 measured (the mean CBF change, maximum CBF change, time to plateau, and K-slope) showed no significant
494 differences in WT (SMACre^{ER-}:*Grin1*$^{f/f}$:*Grin2d*$^{f/f}$) mice before and after tamoxifen administration (Figure S4).
495 This means that the experimental operation itself could not affect functional hyperemia. Then, we administered
496 the whisker stimulation assay to SMACre^{ER+}:*Grin2d*$^{f/f}$ mice and SMACre^{ER+}:*Grin1*$^{f/f}$:*Grin2d*$^{f/f}$ mice before and
497 after tamoxifen administration. Before tamoxifen administration, SMACre^{ER+}:*Grin2d*$^{f/f}$ mice and
498 SMACre^{ER+}:*Grin1*$^{f/f}$:*Grin2d*$^{f/f}$ mice showed normal functional hyperemia. However, after tamoxifen
499 administration, both groups of mice exhibited a decreased CBF change during the whisker stimulation plateau
500 period (Figure 3B). Specifically, during the plateau period, the mean CBF change (9.98% and 11.55%) and
501 maximum CBF change (14.07% and 16.07%) before tamoxifen administration in SMACre^{ER+}:*Grin2d*$^{f/f}$ mice
502 and SMACre^{ER+}:*Grin1*$^{f/f}$:*Grin2d*$^{f/f}$ mice, respectively, showed no significant differences. However, after
503 tamoxifen administration, these two groups of mice showed significantly decreased mean values (3.42% and
504 3.85%, respectively) and maximum CBF change (6.01% and 7.05%, respectively) during the plateau period.
505 There was no significant difference between SMACre^{ER+}:*Grin2d*$^{f/f}$ mice and SMACre^{ER+}:*Grin1*$^{f/f}$:*Grin2d*$^{f/f}$ mice
506 after tamoxifen administration (Figure 3E). Regarding time to plateau, SMACre^{ER+}:*Grin1*$^{f/f}$:*Grin2d*$^{f/f}$ mice had a
507 longer time to plateau after tamoxifen administration than SMACre^{ER+}:*Grin1*$^{f/f}$:*Grin2d*$^{f/f}$ mice before tamoxifen
508 administration and SMACre^{ER+}:*Grin2d*$^{f/f}$ mice after tamoxifen administration (Figure 3F). Before the tamoxifen
509 administration, the K-slopes of the SMACre^{ER+}:*Grin2d*$^{f/f}$ mice and SMACre^{ER+}:*Grin1*$^{f/f}$:*Grin2d*$^{f/f}$ mice showed no
510 significant difference; similar results were observed after tamoxifen administration. Nevertheless, the K-slope
511 showed significant differences from before to after tamoxifen administration in each group (Figure 3G). Except
512 for the functional assay, IF staining demonstrated the colocalization of the NR1 and NR2D subunits in aSMCs
513 of the MCA (Figure 3C/D). In summary, based on the structural and functional evidence shown above, cKO of

514 NR2D and NR2D plus NR1 in aSMCs of mice led to similar patterns of functional hyperemia, which highly
515 suggests that the NR2D and NR1 subunits work together as a complex to form functional NMDA receptors in
516 cerebral aSMCs to regulate functional hyperemia. Hence, in later experiments, we used *Grin2d* knockouts to
517 yield similar results (knockout of NMDA receptors) in aSMCs.
518
519 **aSMC-expressed NR2D works independently of COX-2 and HFD pathways to regulate functional**
520 **hyperemia**
521 Previous studies demonstrated that COX-2 is a molecule involved in NVC regulation. When COX-2 is knocked
522 out or inhibited, functional hyperemia is attenuated by approximately 50%. However, total knockout of COX-2
523 in mice can lead to severe peripheral defects, such as kidney dysfunction (53). Thus, NVC impairment may be
524 partially due to other global side effects. We wanted to study the similarities and differences between the
525 aSMCs-NR2D-related pathway and the reported COX-2-related pathway through more local and precise
526 intervention in the NVC regulation. We administered NS-398, a specific inhibitor of COX-2, locally through the
527 cistern magnum to inhibit the activity of COX-2 (Figure 4A). By injecting fluorescein isothiocyanate (FITC) at
528 the same time, we could track the diffusion of NS-398. We selected only mice with successful cistern magnum
529 administration for the further whisker stimulation assay. The successful injection of NS-398 and FITC clearly
530 labelled the Virchow-Robin spaces of arterioles (Figure 4B). Through analysis of the whisker stimulation data,
531 we found that administration of NS-398 to WT (SMACre^{ER-}:*Grin2d*$^{f/f}$) mice significantly decreased the mean
532 CBF change during the plateau period by approximately 42% (from 13.70% to 7.91%), which is consistent with
533 the currently known reports. Moreover, in cKO mice administered NS-398, the mean CBF change was further
534 attenuated to 2.99%, significantly lower than that of the cKO (SMACre^{ER+}:*Grin2d*$^{f/f}$) group without NS-398
535 (5.96%). A similar trend was observed in the maximum CBF change during the plateau period: the maximum
536 CBF change of the WT group without NS-398 administration was 20.09%, significantly decreasing to 11.58%%
537 after NS-398 administration. In the cKO group, the maximum CBF changes without and with NS-398 were
538 9.48% and 6.88%, respectively, which significantly differed (Figure 4F/H). However, regarding time to plateau,
539 no significant differences were found among the four groups of mice (Figure 4I). Regarding K-slopes, the WT
540 group without NS-398 had significantly higher values than the other groups (Figure 4J). Interestingly, through
541 IF and RT–PCR, we found that *Ptgs2* (gene name of COX-2) and COX-2 were expressed not only in neurons
542 but also in cerebral aSMCs (Figure 4C/D). Moreover, the RT–PCR results of *Ptgs2* expression in adult cortex
543 lysates were even lower than those in cultured cerebral aSMCs (Figure 4G). This evidence suggests that COX-
544 2 expressed in cerebral aSMCs may also contribute to the COX-2 pathway to regulate CBF. The conclusions

545 drawn from previous studies are not comprehensive. In addition, WB did not detect COX-2 expression in the
546 immunoprecipitated (IP) products of NR2D (Figure 4E). The above evidence suggests that COX-2 and the
547 NR2D subunit in cerebral aSMCs may independently regulate functional hyperemia.
548
549 Moreover, we also administered a high-fat diet (HFD) to WT (SMACre^{ER-}:*Grin2d*$^{f/f}$) and cKO
550 (SMACre^{ER+}:*Grin2d*$^{f/f}$) mice because a previous study reported a relationship between HFD challenge and
551 functional hyperemia (54). We monitored the food consumption of mice during the HFD challenge (Figure S2G)
552 and the fat/lean/total water content of mice (Figure S2H). These parameters confirmed the successful
553 establishment of the HFD model. After HFD administration, mice underwent whisker stimulation (Figure 4F).
554 During the plateau period, the mean CBF change of HFD_SMACre^{ER-}:*Grin2d*$^{f/f}$ mice was 5.00%, and the mean
555 CBF change of HFD_SMACre^{ER+}:*Grin2d*$^{f/f}$ mice was 1.33%, which significantly differed. A similar trend was
556 observed in maximum CBF change; in HFD_WT mice, it was 7.62%, and in HFD_cKO mice, it was 3.03%
557 (Figure 4H). The time to the plateau of HFD_WT and HFD_cKO mice after the HFD challenge was not
558 significantly different (Figure 4I). The K-slope of HFD_cKO mice was significantly lower than that of HFD_WT
559 mice, which indicated that HFD and aSMC-NR2D cKO have a superimposed effect on functional hyperemia.
560 Compared with WT and cKO mice in the control groups, after the HFD challenge, all parameters significantly
561 decreased in both WT and cKO mice (Figure 4J). The above evidence suggests that HFD and the NR2D
562 subunit in cerebral aSMCs may independently regulate functional hyperemia.
563
564 **Impact of NR2D cKO in aSMCs on physical parameters**
565 In addition to functional experiments, we also physical monitored SMACre^{ER-}:*Grin2d*$^{f/f}$ and SMACre^{ER+}:*Grin2d*$^{f/f}$
566 mice. We tracked the weight of P5 tamoxifen-administered SMACre^{ER+}:*Grin2d*$^{f/f}$ (P5) mice and p60
567 SMACre^{ER+}:*Grin2d*$^{f/f}$ tamoxifen-administered (P60) mice. There was a significant difference in body weight
568 between the P5 group during part of the period from P38 to P60. Specifically, the weight of cKO
569 (SMACre^{ER+}:*Grin2d*$^{f/f}$) mice was lower than that of their WT (SMACre^{ER-}:*Grin2d*$^{f/f}$) littermates (controls) (Figure
570 S2A/B). However, in the P60 group, even at P92, WT and cKO mice exhibited no significant difference in body
571 weight (Figure S2C/D). Moreover, at P65, we also monitored the blood pressure of mice. The results showed
572 no significant differences among WT mice, SMACre^{ER+}:*Grin2d*$^{f/f}$ mice, and SMACre^{ER+}:*Grin1*$^{f/f}$:*Grin2d*$^{f/f}$ mice
573 before/after tamoxifen administration in terms of diastolic blood pressure, systolic blood pressure, and mean
574 arterial pressure (Figure S2E). In addition, we monitored the weight of mice before the whisker stimulation

575 assay at P65 by sampling survey and found no significant difference between the SMACre^{ER-}:*Grin2d*$^{f/f}$ group
576 and the SMACre^{ER+}:*Grin2d*$^{f/f}$ group (Figure S2F).
577
578 **Caldesmon may be the key downstream molecule of NR2D-regulated functional hyperemia in cerebral**
579 **aSMCs**
580 We wanted to discover the critical downstream molecule of the NR2D subunit that regulates functional
581 hyperemia. We first used the lentivirus to overexpress NR2D in cultured SMCs. After NR2D was fully
582 overexpressed, NR2D and the proteins interacting with NR2D were pulled down by immunoprecipitation (IP).
583 Next, we drew a Venn diagram after mass spectrometry analysis of the products from three independent IPs;
584 we found that 75 proteins were detected in all three independent IP experiments (Figure 5A). We selected the
585 proteins that met the following criteria: appeared at least once in the three IP experiments, had a PSM value
586 higher than ten, and were observed in only the NR2D-IP groups or existed in both NR2D-IP groups and
587 immunoglobulin (IgG) control groups, but the PSM values in NR2D-IP groups were more than twice that in the
588 IgG control groups. A total of 916 proteins were selected for Kyoto Encylopedia of Genes and Genomes
589 (KEGG) and Gene Ontology (GO) analyses. According to the KEGG pathway analysis, the signalling pathway
590 related to vascular SMC contraction was enriched in the IP products of NR2D (Figure 5B). In this pathway, we
591 found that caldesmon was detected in all three independent IP experiments. Caldesmon is critical for cell
592 contraction and dilation. We further verified the reliability of bioinformatics analysis data through WB. In WB,
593 we first assessed the expression of NR2D in IP products. Then, we assessed caldesmon expression in IP
594 products by WB. Caldesmon was detected in the "Input" and the "NR2D-IP" lanes (Figure 5C). Three types of
595 GO analysis of the 916 selected proteins were shown in Figure 5D-F. In short, by analyzing bioinformatics
596 data and performing WB, we found that caldesmon may be the critical downstream molecule that regulates
597 functional hyperemia by altering the contractional and relaxational homeostasis of aSMCs.
598
599 **Conditional knock-out of NR2D in aSMCs leads mice to express a unique anxiety-like behavior and**
600 **reduced curiosity**
601 We designed a new open field test (OFT), the open field-like test (OFLT), to explore whether the defect in
602 functional hyperemia induced by NR2D cKO in aSMCs affected a series of emotional functions in mice. In the
603 initial experimental proposal, we aimed to use the OFLT to simultaneously detect anxiety, curiosity, and
604 instinctive fear. In the experiment, we placed WT (SMACre^{ER-}:*Grin2d*$^{f/f}$) mice and cKO (SMACre^{ER+}:*Grin2d*$^{f/f}$)
605 mice in the left part of the box, with the middle of the box blocked with an iron mesh wall (Figure 6A). This area

606 was similar to the classic OFT, which is used to observe the anxiety-like behavior of mice. A mirrored,
607 symmetrical area was on the opposite side of the iron mesh wall. A CD-1 mouse was placed behind the iron
608 mesh wall. Because CD-1 mice are aggressive, they usually fight with C57 mice when placed them together.
609 Thus, CD-1 mice could generate fear memories in C57 mice. C57 mice were predicted to exhibit spontaneous
610 curiosity and exploration of the iron mesh wall and areas behind it. However, the fear of the CD-1 mouse was
611 predicted to motivate the C57 mouse to avoid the iron mesh wall as much as possible, creating a behavioral
612 conflict between curiosity and fear. However, the pilot experiment did not detect fear behavior from cKO mice
613 in the OFLT. This finding raised doubts about whether the fear intensity generated by the OFLT was sufficient
614 for C57 mice, which would make the OFLT unable to detect fear. Therefore, in the formal experiment, we
615 changed the experimental procedure to assess fear behavior separately.
616
617 During the formal behavioral test, SMACre^{ER-}:*Grin2d*$^{f/f}$ and SMACre^{ER+}:*Grin2d*$^{f/f}$ mice were placed in the left
618 area of the box, which was lined with sketch paper to absorb urine produced by mice to enable urine weighing.
619 The top of the box was covered with a transparent acrylic plate (Figure 6A). After a 20-minute behavioral test,
620 we analyzed some parameters. First, we analyzed the distance travelled by mice. WT (SMACre^{ER-}:*Grin2d*$^{f/f}$)
621 mice were more curious about the iron mesh wall and were more willing to stay near the iron mesh wall for
622 exploration. However, cKO (SMACre^{ER+}:*Grin2d*$^{f/f}$) mice seemed less interested in the iron mesh wall. The
623 heatmap showed that the distance travelled by cKO mice was increased compared with that by WT mice, but
624 that exploration near the iron mesh wall was reduced in cKO mice (Figure 6B). Specifically, during the 20-
625 minute behavioral test, the average distance travelled by cKO mice was 30.24 m, significantly higher than that
626 of WT mice (22.98 m) (Figure 6C). In addition, the mean urine weight of cKO mice was 247.81 mg, significantly
627 higher than that of WT mice (78.06 mg) (Figure 6D). The fecal results were similar to those of urine volume,
628 as the number of feces produced was significantly higher in the cKO group (4.9) than in the WT group (2.8)
629 (Figure 6E). In addition, we assessed the preference of the mice for the iron mesh wall and found that the
630 proportion of the time that cKO mice stayed near the iron mesh wall (on the right side of the left half of the
631 whole box) was significantly lower than that of WT mice (60.75% vs. 70.60%). Instead, cKO mice spent more
632 time in the central area of the box than WT mice (19.96% vs. 14.53%) (Figure 6F). Finally, we analyzed the
633 ratio of time spent in the right and left areas (Figure 6G) and the ratio of time spent in the right and all the
634 remaining areas (Figure 6H) in WT and cKO mice. Both of these parameters significantly decreased. Based
635 on the above results, cKO mice exhibited unconventional urine-specific and fecal-specific anxiety-like
636 behaviors and showed reduced curiosity toward the iron mesh wall and the area behind it.

637

638 Then, we used a 40-cm square box to conduct the traditional OFT (Figure S5A) to verify our conclusion
639 obtained by the OFLT. In the 15-minute OFT, we found no significant differences between WT
640 (SMACre^{ER-}:*Grin2d*$^{f/f}$) mice and cKO (SMACre^{ER+}:*Grin2d*$^{f/f}$) mice in terms of time spent in the center area
641 (Figure S5B), time spent in the periphery (Figure S5C) and the total distance travelled (Figure S5D).
642 Surprisingly, the probabilities of defecation (Figure S5E) and urination (Figure S5F) were higher in cKO mice
643 than in WT mice. In addition, the number of feces produced by the cKO group was much greater than that
644 produced by the WT group (Figure 6E, 3.38 vs. 0.79). Moreover, regarding the latency to fecal production, the
645 WT group produced the first feces at 517.40s on average, while the cKO group produced the first feces at
646 285.67s on average, nearly half the latency of the WT group (Figure S5G). In summary, the fecal production
647 latency of cKO mice was shorter than that of WT mice, and the number of feces produced was greater than
648 that of WT mice. The increase in urine and fecal volume in the OFT was consistent with that in the OFLT.
649 Urination and defecation-specific anxiety were conservative in two independent experiments.

650

651 **Conditional knock-out of NR2D in aSMCs leads mice to exhibit less fear in the CD-1 fear assay**

652 Due to the lack of fear responses in the OFLT, we conducted an acute fear-induction experiment to test
653 whether NVC regulates the fear response. Glutamatergic neurons are present in the amygdala (49), but
654 whether NR2D expressed in cerebral aSMCs in the amygdala are regulated by local glutamatergic neurons
655 and thus influence the fear response is unknown. First, we demonstrated the presence of arterioles and
656 capillaries in the amygdala (Figure S6A), which is the structural fundamental of the behavioral test. Then, we
657 placed CD-1 mice and WT (SMACre^{ER-}:*Grin2d*$^{f/f}$) or cKO (SMACre^{ER+}:*Grin2d*$^{f/f}$) mice together in a cage to
658 directly induce acute fear in WT or cKO mice (Figure 7A). The amygdala is involved in regulating fear memory.
659 Therefore, in addition to recording behavioral parameters, we also performed IF staining of c-Fos in the
660 amygdala of WT and cKO mice to detect the activation of neurons in this area. In this assay, we first exposed
661 WT or cKO mice to CD-1 mice for 10 minutes and recorded their fighting and social behaviors with video
662 cameras. Then, brain extraction of C57 mice was performed 90 minutes later to detect the activation of neurons
663 in the amygdala through c-Fos IF staining.

664

665 Behavioral data showed no difference between the WT and cKO groups in the amount (number of bouts) of
666 active sniffing (Figure 7B). Nevertheless, the latency to the first fight in the WT group was significantly shorter
667 than that in the cKO group (58.13 s vs. 201.3 s, Figure 7C). The number of fights in the WT group (4.63 on

668 average) was also significantly higher than that in the cKO group (1.9 on average) (Figure 7D). In addition,
669 regarding the space use of mice (i.e., close proximity), cKO mice were more willing to share a small space
670 with CD-1 mice than WT mice (161.3 s of cKO mice vs. 88.63 s of WT mice, Figure 7E). The total duration of
671 fighting of the WT group (25.25 s) was greater than that of the cKO group (10.40 s) (Figure 7F). In addition,
672 we conducted a deeper analysis of the fight data of WT and cKO mice. In the WT group, 7/37 (18.92%) fights
673 were initiated by WT C57 mice, and CD-1 mice initiated 30/37 (81.08%) fights. In the cKO group, 5/19 (26.32%)
674 fights were initiated by cKO C57 mice, and 14/19 (73.68%) fights were initiated by CD-1 mice (Figure 7G). In
675 terms of flighted after fights, in 36/37 fights (97.3%), WT mice lost and fled; only one CD-1 mouse lost.
676 However, in the cKO group, cKO C57 mice lost and fled in 7/19 (36.94%) fights, and CD-1 mice lost and fled
677 in 12/19 (63.16%) fights (Figure 7H).
678
679 The IF results showed that significantly more amygdala neurons were activated in WT mice than in cKO mice
680 (88.19/mm^2 vs. 25.99/mm^2, Figure 7I). Additionally, the activation of neurons in the barrel cortex (S1BF area)
681 in the WT group (219.18/mm^2) was significantly higher than in the cKO group (109.59/mm^2) (Figure 7J). S1BF
682 is also the location of the ROI used for CBF detection by whisker stimulation. This result indicates that CBF
683 and neuronal activity decrease in this region is conservative across experiments. However, in cerebral regions
684 unrelated to fear or social interaction, such as the piriform (Pir) cortex and hippocampus, there was no
685 significant difference in the level of neuronal activation between WT and cKO mice (Figure 7K/L). We
686 additionally established control groups without CD-1 mouse exposure (Figure S6 B-E). All statistical data are
687 presented in Figure 7M. Based on the above data, cKO mice exhibited less fear than WT mice in the CD1-1
688 fear assay, as seen most obviously in the reduced activation of amygdala neurons and the reduced probability
689 of fleeing a fight.
690
691 **No significant behavioral differences in the elevated plus-maze (EPM) test between SMACre^{ER-}:*Grin2d*$^{f/f}$**
692 **and SMACre^{ER+}:*Grin2d*$^{f/f}$ mice**
693 Based on the OFT, OFLT and CD-1 fear assay results, we concluded that SMACre^{ER+}:*Grin2d*$^{f/f}$ mice exhibit
694 anxiety-like and fear-attenuated behaviors. Therefore, we additionally performed an elevated plus-maze (EPM)
695 test. The EPM test evaluates mouse anxiety as a trade-off between curiosity (exploring open arms) and fear
696 (staying in closed arms). In a 5-minute EPM test, we found that the behavior of WT (SMACre^{ER-}:*Grin2d*$^{f/f}$) and
697 cKO (SMACre^{ER+}:*Grin2d*$^{f/f}$) mice were similar. There were no significant differences between WT mice and
698 cKO mice in terms of distance travelled, time spent in the central area, time spent in the closed arms, time

699 spent in the open arms, the proportion of time in the open/closed arms, and proportion of time in the
700 center/periphery (Figure S7). This may be due to the behavior of cKO mice, which both exhibited anxiety-like
701 and fear-attenuated behaviors, which may have led to no net difference in preference for open or closed arms,
702 leading the behavior of cKO mice to be similar to that of WT mice.
703

704 # Discussion

705 Unlike previous studies, we abandoned the use of drugs and null mice to study the molecular function of NR2D
706 but adopt Cre-dependent transgenic mice, which makes our conclusion more cell-specific. According to the
707 current data, the maximum CBF change during the plateau stage in Pdgfrβ^{ER+}:*Grin2d*$^{f/f}$ mice was lower than
708 that in SMACre^{ER+}:*Grin2d*$^{f/f}$ mice (Figure 2D), which suggests that there may be low levels of NR2D expression
709 in pericytes and/or venous SMCs. Subsequent studies should investigate the expression and role of NR2D in
710 these cells.
711

712 Conditional knock-out of NR2D in aSMCs caused an approximately two-thirds decrease in the CBF variation
713 during the whisker stimulation (Figure 2C). Compared with an approximately 50% decrease in the CBF
714 variation in the COX-2 total knock-out model (55), it can be inferred that NR2D on aSMCs contributes more to
715 NVC regulation than COX-2 in all organs. The drawback of COX-2 total knock is the loss of cell specificity and
716 systemic side effects. Our study found that COX-2 was expressed in not only neurons but also cerebral aSMCs.
717 Therefore, COX-2 total knock-out also impacts the function of COX-2 in aSMCs. Previous studies found that
718 COX-2 is expressed only in neurons in the brain (55-58). Thus, these conclusions may not be entirely correct.
719 Besides, previous studies found that after whisker stimulation, c-Fos-positive cells were enriched in layer IV of
720 the cortex, but the distribution of COX-2-positive cells was enriched in layers II/III of the cortex (59, 60). Hence,
721 it would be inaccurate to attribute COX-2-induced regulation of functional hyperemia to neurons alone. Hence,
722 in subsequent experiments, we plan to explore the contribution of COX-2 expressed in aSMCs to cerebral
723 functional hyperemia in SMACre^{ER+}:*Ptgs2*$^{f/f}$ mice.
724

725 The “time to plateau” and “K-slope” parameters innovative reflect the impact of a particular pathway in two
726 periods of functional hyperemia. The first period encompasses increases in hyperemia (how quickly CBF
727 reaches a plateau), and the next reflects hyperemia maintenance (how much CBF increased). If a particular
728 pathway impacts only the first period, interfering with this pathway will increase the time to plateau and
729 decrease the K-slope. If a particular pathway impacts only the second period, interfering with this pathway will

730 decrease the time to the plateau without impacting the K-slope (61). This study is the first to distinguish these
731 two periods by using parameters “time to plateau” and “K-slope”. For example, we can consider data shown
732 in Figure 2, compared with SMACre^{ER-}:*Grin2d*$^{f/f}$ mice, SMACre^{ER+}:*Grin2d*$^{f/f}$ mice did not differ in the time to
733 plateau but had a lower K-slope, which means that NR2D was involved in both the increasing and maintenance
734 periods of hyperemia. Therefore, NR2D could influence two potential pathways in cerebral aSMCs to regulate
735 functional hyperemia. If NR2D contributed only to glutamate signalling, SMACre^{ER+}:*Grin2d*$^{f/f}$ mice would exhibit
736 decreased K-slope and increased time to plateau, with the CBF change equal to that of WT mice. If NR2D
737 contributed only to the maintenance of cellular dilation, SMACre^{ER+}:*Grin2d*$^{f/f}$ mice would exhibit no changes in
738 K-slope and decreased time to plateau, with the CBF change lower than that in WT mice. However,
739 SMACre^{ER+}:*Grin2d*$^{f/f}$ mice did not differ in time to plateau, although the K-slope decreased. Hence, based on
740 these parameters, we speculate that NR2D in cerebral aSMCs participates in glutamate signalling and the
741 maintenance of cellular dilation. These two parameters make it possible to accurately analyze the increase of
742 CBF in the future.
743
744 We identified caldesmon, a critical downstream protein of NR2D, as regulating CBF in aSMCs through IP data.
745 Previous reports have revealed that nonphosphorylated caldesmon binds with actin and myosin to prevent
746 their interaction, thereby inhibiting the contraction of the cell skeleton (62-65). Through phosphorylation of
747 MAPK (66) and PAK (67) or binding with calcium-activated CaM (68), caldesmon is removed from the binding
748 site of actin and myosin, leading to the contraction of the cytoskeleton. Therefore, if the knockout of NR2D in
749 aSMCs affects the phosphorylation of caldesmon or calcium activation of CaM, it is likely to lead to abnormal
750 cell contraction and relaxation. In addition, caldesmon and arp2/3 are antagonistic, and increased caldesmon
751 expression will affect the expression of arp2/3 (69, 70). Arp2/3 is responsible for the assembly and extension
752 of the actin skeleton to maintain an angle of 70° between two actin filaments. If the loss of NR2D in aSMCs
753 leads to the abnormal expression of caldesmon, it is likely to further lead to the abnormal expression of arp2/3,
754 which affects the assembly of actin and the angle of actin skeletons, thus affecting the normal contraction and
755 relaxation of cells. Therefore, future experiments should focus on manipulate caldesmon in aSMCs-NR2D cKO
756 mice to further study the role of the NR2D-caldesmon pathway in regulating cerebral aSMC contraction and
757 relaxation.
758
759 The change in emotional behavior is the most important discovery of this study. We first link the correlation of
760 NVC and emotional disorders in one study by the transgenic strategy. Compared with the extensive behavioral

761 changes produced by the traditional anxiety-like model, SMACre^{ER+}:*Grin2d*$^{f/f}$ mice showed an increase in the
762 production of urine and defecation, which may indicate that the cKO of NR2D in aSMCs specifically affected
763 the cerebral regions of anxiety related to urination and defecation in mice. Clinical studies have confirmed that
764 patients with anxiety show a significant increase in defecation (36), which is consistent with our report. The
765 correlation between anxiety and increased defecation is conservative across species. This precise effect may
766 find a more specific target for treating this type of anxiety and avoiding the side effects caused by the
767 widespread use of drugs.
768
769 In addition, the fecal production of both SMACre^{ER-}:*Grin2d*$^{f/f}$ and SMACre^{ER+}:*Grin2d*$^{f/f}$ mice was higher in the
770 OFLT than in the OFT. On the one hand, the OFLT lasted for 20 minutes, while the OFT lasted for 15 minutes.
771 On the other hand, the OFLT box (26 × 26 cm) was smaller than the OFT box (40 × 40 cm). The overall anxiety
772 level of mice may be higher in a narrower space. Based on physical monitoring during the HFD challenge,
773 food consumption and changes in fat content of SMACre^{ER-}:*Grin2d*$^{f/f}$ mice and SMACre^{ER+}:*Grin2d*$^{f/f}$ mice were
774 similar (Figure S2 G/H). These findings indicated that the increase in defecation of SMACre^{ER+}:*Grin2d*$^{f/f}$ mice
775 in the OFT and OFLT may not be due to differences in food consumption.
776
777 The increase of CBF in the amygdala during fear is conservative across species. A previous study on
778 depressed adolescents showed a decreased CBF baseline in the amygdala (71). Hence, a stable CBF supply
779 in the amygdala is critical for emotional homeostasis. We hypothesize that the "CBF-Neuron-Behavior" axis is
780 how NVC regulates the cerebral complex emotional behaviors. Our manipulation only influenced the
781 expression of NR2D in aSMCs (CBF level), and this manipulation decreased c-Fos expression in neurons of
782 the amygdala (neuronal level). Finally, it caused the fear attenuation of mice (behavioral level). Therefore, this
783 study is the first to show the high correlation between NVC regulation and advanced cerebral functions.
784 Besides, what makes us curious is the cellular identity of neurons not activated in SMACre^{ER+}:*Grin2d*$^{f/f}$ mice
785 after the acute fear stimulation. So, we expected to explore the identity of these groups of neurons, and these
786 neurons may both blood supply-sensitive and participate in the regulation of fear.
787
788 In the EPM test, mice can explore open arms. However, their preference for dark areas and fear of heights
789 leads them to fear open arms. The conflict between exploration (curiosity) and avoidance (fear) can thus be
790 assessed. In our study, SMACre^{ER+}:*Grin2d*$^{f/f}$ mice showed anxiety-like and fear-attenuated behaviors, leading
791 to contradictory behavior. Because of their increased anxiety, SMACre^{ER+}:*Grin2d*$^{f/f}$ mice did not want to explore

open arms. However, because these mice felt less fear of heights (fear-attenuated behavior), they did not fear open arms. Thus, there was no difference between WT and SMACre^{ER+}:*Grin2d*$^{f/f}$ mice regarding exploring open arms and closed arms in the EPM test (Figure S7). Because SMACre^{ER+}:*Grin2d*$^{f/f}$ mice exhibited both anxiety-like and fear-attenuated behaviors, there was no net change in behavior. The results of the EPM test further confirm that SMACre^{ER+}:*Grin2d*$^{f/f}$ mice exhibited increased anxiety-like behaviors and attenuated fear simultaneously.

Encouragingly, we only intervened in the expression of NR2D in cerebral aSMCs, which only occupied 0.3% of total cells in the mouse brain, enough to change the CBF variation and advanced emotional behaviors of mice. This phenomenon suggested that continually decreased CBF supply during neuron activation is a vital trigger factor for advanced behavioral dysfunction. As the absence of NR2D in cerebral aSMCs leads to abnormalities in higher-order cognitive functions, NR2D is a promising target for treating anxiety-related and amygdala-related mental disorders or diseases. This study provides new strategies and ideas for treating psychiatric diseases and can inform drug development by interfering with molecules expressed in cerebral aSMCs to treat mental disorders.

Acknowledgments

We thank Yanmei Tao for sharing Nestin-Cre mice. We thank Bo Zhou for sharing SMAcre^{ER} mice. We thank Zilong Qiu for sharing Ai47 mice. We thank Xiang Yu for sharing PdgfrβCre^{ER} mice. We thank Yangang Sun for sharing *Grin1* mice. We thank Yajie Liu from Westlake University Laboratory Animal Resource Center for guiding behaviors assays. We thank Yuxiao Niu from Yanxiao Zhang lab of Westlake University for drawing KEGG pathway map.

Fundings

J.‐M.J. acknowledges supports from Westlake University startup funding, the Westlake Education Foundation, the Zhejiang Province Natural Science Foundation (Project # 2022XHSJJ004), the Westlake Laboratory of Life Sciences and Biomedicine (Project# 202109013).

Conflict of Interest

We declare that we do not have any financial or personal relationships with other people or organizations, which may affect our work inappropriately, and there are no professional or other personal interests of any nature or kind in any products, services and/or companies. These interests may be interpreted as affecting or reviewing the positions in the following manuscripts.

References

1. Attwell D, Buchan AM, Charpak S, Lauritzen M, Macvicar BA, Newman EA. Glial and neuronal control of brain blood flow. Nature. 2010;468(7321):232-43.
2. Lauritzen M, Dreier JP, Fabricius M, Hartings JA, Graf R, Strong AJ. Clinical relevance of cortical spreading depression in neurological disorders: migraine, malignant stroke, subarachnoid and intracranial hemorrhage, and traumatic brain injury. J Cereb Blood Flow Metab. 2011;31(1):17-35.
3. Girouard H, Iadecola C. Neurovascular coupling in the normal brain and in hypertension, stroke, and Alzheimer disease. J Appl Physiol (1985). 2006;100(1):328-35.
4. Ruitenberg A, den Heijer T, Bakker SL, van Swieten JC, Koudstaal PJ, Hofman A, et al. Cerebral hypoperfusion and clinical onset of dementia: the Rotterdam Study. Ann Neurol. 2005;57(6):789-94.
5. Pico-Perez M, Radua J, Steward T, Menchon JM, Soriano-Mas C. Emotion regulation in mood and anxiety disorders: A meta-analysis of fMRI cognitive reappraisal studies. Prog Neuropsychopharmacol Biol Psychiatry. 2017;79(Pt B):96-104.
6. Iadecola C. Neurovascular regulation in the normal brain and in Alzheimer's disease. Nat Rev Neurosci. 2004;5(5):347-60.
7. Drew PJ. Neurovascular coupling: motive unknown. Trends Neurosci. 2022;45(11):809-19.
8. Hillman EM. Coupling mechanism and significance of the BOLD signal: a status report. Annu Rev Neurosci. 2014;37:161-81.
9. Clemm von Hohenberg C, Weber-Fahr W, Lebhardt P, Ravi N, Braun U, Gass N, et al. Lateral habenula perturbation reduces default-mode network connectivity in a rat model of depression. Transl Psychiatry. 2018;8(1):68.
10. Kamiya K, Abe O. Imaging of Posttraumatic Stress Disorder. Neuroimaging Clin N Am. 2020;30(1):115-23.

849 11. Ahmed-Leitao F, Spies G, van den Heuvel L, Seedat S. Hippocampal and amygdala volumes in adults
850 with posttraumatic stress disorder secondary to childhood abuse or maltreatment: A systematic review.
851 Psychiatry Res Neuroimaging. 2016;256:33-43.
852 12. Pitman RK, Rasmusson AM, Koenen KC, Shin LM, Orr SP, Gilbertson MW, et al. Biological studies of
853 post-traumatic stress disorder. Nat Rev Neurosci. 2012;13(11):769-87.
854 13. Whalen PJ, Kagan J, Cook RG, Davis FC, Kim H, Polis S, et al. Human amygdala responsivity to
855 masked fearful eye whites. Science. 2004;306(5704):2061.
856 14. Hadj-Bouziane F, Bell AH, Knusten TA, Ungerleider LG, Tootell RB. Perception of emotional
857 expressions is independent of face selectivity in monkey inferior temporal cortex. Proc Natl Acad Sci U S A.
858 2008;105(14):5591-6.
859 15. Harris AP, Lennen RJ, Marshall I, Jansen MA, Pernet CR, Brydges NM, et al. Imaging learned fear
860 circuitry in awake mice using fMRI. Eur J Neurosci. 2015;42(5):2125-34.
861 16. Ofek K, Schoknecht K, Melamed-Book N, Heinemann U, Friedman A, Soreq H. Fluoxetine induces
862 vasodilatation of cerebral arterioles by co-modulating NO/muscarinic signalling. J Cell Mol Med.
863 2012;16(11):2736-44.
864 17. Malberg JE, Duman RS. Cell proliferation in adult hippocampus is decreased by inescapable stress:
865 reversal by fluoxetine treatment. Neuropsychopharmacology. 2003;28(9):1562-71.
866 18. Li RW, Yang C, Kwan YW, Chan SW, Lee SM, Leung GP. Involvement of organic cation transporter-
867 3 and plasma membrane monoamine transporter in serotonin uptake in human brain vascular smooth muscle
868 cells. Front Pharmacol. 2013;4:14.
869 19. Maddahi A, Edvinsson L. Enhanced expressions of microvascular smooth muscle receptors after focal
870 cerebral ischemia occur via the MAPK MEK/ERK pathway. BMC Neurosci. 2008;9:85.
871 20. Cao L, Xu CB, Zhang Y, Cao YX, Edvinsson L. Secondhand cigarette smoke exposure causes
872 upregulation of cerebrovascular 5-HT(1) (B) receptors via the Raf/ERK/MAPK pathway in rats. Acta Physiol
873 (Oxf). 2013;207(1):183-93.
874 21. Li W, Prakash R, Chawla D, Du W, Didion SP, Filosa JA, et al. Early effects of high-fat diet on
875 neurovascular function and focal ischemic brain injury. Am J Physiol Regul Integr Comp Physiol.
876 2013;304(11):R1001-8.
877 22. Remzso G, Nemeth J, Toth-Szuki V, Varga V, Kovacs V, Domoki F. NMDA attenuates the
878 neurovascular response to hypercapnia in the neonatal cerebral cortex. Sci Rep. 2019;9(1):18900.

879 23. Chow BW, Nunez V, Kaplan L, Granger AJ, Bistrong K, Zucker HL, et al. Caveolae in CNS arterioles
880 mediate neurovascular coupling. Nature. 2020;579(7797):106-10.
881 24. Offenhauser N, Thomsen K, Caesar K, Lauritzen M. Activity-induced tissue oxygenation changes in
882 rat cerebellar cortex: interplay of postsynaptic activation and blood flow. J Physiol. 2005;565(Pt 1):279-94.
883 25. St Lawrence KS, Ye FQ, Lewis BK, Frank JA, McLaughlin AC. Measuring the effects of indomethacin
884 on changes in cerebral oxidative metabolism and cerebral blood flow during sensorimotor activation. Magn
885 Reson Med. 2003;50(1):99-106.
886 26. Busija DW, Bari F, Domoki F, Louis T. Mechanisms involved in the cerebrovascular dilator effects of
887 N-methyl-d-aspartate in cerebral cortex. Brain Res Rev. 2007;56(1):89-100.
888 27. Roman RJ. P-450 metabolites of arachidonic acid in the control of cardiovascular function. Physiol
889 Rev. 2002;82(1):131-85.
890 28. Alkayed NJ, Narayanan J, Gebremedhin D, Medhora M, Roman RJ, Harder DR. Molecular
891 characterization of an arachidonic acid epoxygenase in rat brain astrocytes. Stroke. 1996;27(5):971-9.
892 29. Amruthesh SC, Boerschel MF, McKinney JS, Willoughby KA, Ellis EF. Metabolism of arachidonic acid
893 to epoxyeicosatrienoic acids, hydroxyeicosatetraenoic acids, and prostaglandins in cultured rat hippocampal
894 astrocytes. J Neurochem. 1993;61(1):150-9.
895 30. Hogan-Cann AD, Lu P, Anderson CM. Endothelial NMDA receptors mediate activity-dependent brain
896 hemodynamic responses in mice. Proc Natl Acad Sci U S A. 2019;116(21):10229-31.
897 31. Lu L, Hogan-Cann AD, Globa AK, Lu P, Nagy JI, Bamji SX, et al. Astrocytes drive cortical vasodilatory
898 signaling by activating endothelial NMDA receptors. J Cereb Blood Flow Metab. 2019;39(3):481-96.
899 32. Davis M. NMDA receptors and fear extinction: implications for cognitive behavioral therapy. Dialogues
900 Clin Neurosci. 2011;13(4):463-74.
901 33. Shultz B, Farkash A, Collins B, Mohammadmirzaei N, Knox D. Fear learning-induced changes in
902 AMPAR and NMDAR expression in the fear circuit. Learn Mem. 2022;29(3):83-92.
903 34. Feyissa AM, Chandran A, Stockmeier CA, Karolewicz B. Reduced levels of NR2A and NR2B subunits
904 of NMDA receptor and PSD-95 in the prefrontal cortex in major depression. Prog Neuropsychopharmacol Biol
905 Psychiatry. 2009;33(1):70-5.
906 35. Yamamoto H, Kamegaya E, Hagino Y, Takamatsu Y, Sawada W, Matsuzawa M, et al. Loss of GluN2D
907 subunit results in social recognition deficit, social stress, 5-HT(2C) receptor dysfunction, and anhedonia in
908 mice. Neuropharmacology. 2017;112(Pt A):188-97.

909 36. Gorard DA, Gomborone JE, Libby GW, Farthing MJ. Intestinal transit in anxiety and depression. Gut.
910 1996;39(4):551-5.
911 37. Li X, Zhou L, Zhang X, Jin Y, Zhao B, Zhang D, et al. Proteins secreted by brain arteriolar smooth
912 muscle cells are instructive for neural development. Mol Brain. 2022;15(1):97.
913 38. Yu XD, Zhu Y, Sun QX, Deng F, Wan J, Zheng D, et al. Distinct serotonergic pathways to the amygdala
914 underlie separate behavioral features of anxiety. Nat Neurosci. 2022;25(12):1651-63.
915 39. Boas DA, Dunn AK. Laser speckle contrast imaging in biomedical optics. J Biomed Opt.
916 2010;15(1):011109.
917 40. Jin Y, Shi P, Wang Y, Li J, Zhang J, Zhao X, et al. Precise control of embolic stroke with magnetized
918 red blood cells in mice. Commun Biol. 2022;5(1):136.
919 41. Liu CY, Chen JB, Liu YY, Zhou XM, Zhang M, Jiang YM, et al. Saikosaponin D exerts antidepressant
920 effect by regulating Homer1-mGluR5 and mTOR signaling in a rat model of chronic unpredictable mild stress.
921 Chin Med. 2022;17(1):60.
922 42. Guo Z, Li S, Wu J, Zhu X, Zhang Y. Maternal Deprivation Increased Vulnerability to Depression in
923 Adult Rats Through DRD2 Promoter Methylation in the Ventral Tegmental Area. Front Psychiatry.
924 2022;13:827667.
925 43. Kim S, Hong KB, Kim S, Suh HJ, Jo K. Creatine and taurine mixtures alleviate depressive-like
926 behaviour in Drosophila melanogaster and mice via regulating Akt and ERK/BDNF pathways. Sci Rep.
927 2020;10(1):11370.
928 44. Lapmanee S, Charoenphandhu J, Teerapornpuntakit J, Krishnamra N, Charoenphandhu N.
929 Agomelatine, venlafaxine, and running exercise effectively prevent anxiety- and depression-like behaviors and
930 memory impairment in restraint stressed rats. PLoS One. 2017;12(11):e0187671.
931 45. Borelli KG, Blanchard DC, Javier LK, Defensor EB, Brandao ML, Blanchard RJ. Neural correlates of
932 scent marking behavior in C57BL/6J mice: detection and recognition of a social stimulus. Neuroscience.
933 2009;162(4):914-23.
934 46. Arakawa H, Arakawa K, Blanchard DC, Blanchard RJ. Scent marking behavior in male C57BL/6J mice:
935 sexual and developmental determination. Behav Brain Res. 2007;182(1):73-9.
936 47. Arakawa H, Arakawa K, Blanchard DC, Blanchard RJ. A new test paradigm for social recognition
937 evidenced by urinary scent marking behavior in C57BL/6J mice. Behav Brain Res. 2008;190(1):97-104.

938 48. McQuaid RJ, Audet MC, Anisman H. Environmental enrichment in male CD-1 mice promotes
939 aggressive behaviors and elevated corticosterone and brain norepinephrine activity in response to a mild
940 stressor. Stress. 2012;15(3):354-60.
941 49. Liu J, Li D, Huang J, Cao J, Cai G, Guo Y, et al. Glutamatergic Neurons in the Amygdala Are Involved
942 in Paclitaxel-Induced Pain and Anxiety. Front Psychiatry. 2022;13:869544.
943 50. Traynelis SF, Wollmuth LP, McBain CJ, Menniti FS, Vance KM, Ogden KK, et al. Glutamate receptor
944 ion channels: structure, regulation, and function. Pharmacol Rev. 2010;62(3):405-96.
945 51. Monyer H, Burnashev N, Laurie DJ, Sakmann B, Seeburg PH. Developmental and regional expression
946 in the rat brain and functional properties of four NMDA receptors. Neuron. 1994;12(3):529-40.
947 52. Laurie DJ, Bartke I, Schoepfer R, Naujoks K, Seeburg PH. Regional, developmental and interspecies
948 expression of the four NMDAR2 subunits, examined using monoclonal antibodies. Brain Res Mol Brain Res.
949 1997;51(1-2):23-32.
950 53. Slattery P, Frolich S, Goren I, Nusing RM. Salt supplementation ameliorates developmental kidney
951 defects in COX-2(-/-) mice. Am J Physiol Renal Physiol. 2017;312(6):F1044-F55.
952 54. Huber G, Ogrodnik M, Wenzel J, Stolting I, Huber L, Will O, et al. Telmisartan prevents high-fat diet-
953 induced neurovascular impairments and reduces anxiety-like behavior. J Cereb Blood Flow Metab.
954 2021;41(9):2356-69.
955 55. Niwa K, Araki E, Morham SG, Ross ME, Iadecola C. Cyclooxygenase-2 contributes to functional
956 hyperemia in whisker-barrel cortex. J Neurosci. 2000;20(2):763-70.
957 56. Yamagata K, Andreasson KI, Kaufmann WE, Barnes CA, Worley PF. Expression of a mitogen-
958 inducible cyclooxygenase in brain neurons: regulation by synaptic activity and glucocorticoids. Neuron.
959 1993;11(2):371-86.
960 57. Breder CD, Dewitt D, Kraig RP. Characterization of inducible cyclooxygenase in rat brain. J Comp
961 Neurol. 1995;355(2):296-315.
962 58. Kaufmann WE, Worley PF, Pegg J, Bremer M, Isakson P. COX-2, a synaptically induced enzyme, is
963 expressed by excitatory neurons at postsynaptic sites in rat cerebral cortex. Proc Natl Acad Sci U S A.
964 1996;93(6):2317-21.
965 59. Lacroix A, Toussay X, Anenberg E, Lecrux C, Ferreiros N, Karagiannis A, et al. COX-2-Derived
966 Prostaglandin E2 Produced by Pyramidal Neurons Contributes to Neurovascular Coupling in the Rodent
967 Cerebral Cortex. J Neurosci. 2015;35(34):11791-810.

968 60. Lecrux C, Toussay X, Kocharyan A, Fernandes P, Neupane S, Levesque M, et al. Pyramidal neurons
969 are "neurogenic hubs" in the neurovascular coupling response to whisker stimulation. J Neurosci.
970 2011;31(27):9836-47.
971 61. Koizumi K, Hattori Y, Ahn SJ, Buendia I, Ciacciarelli A, Uekawa K, et al. Apoepsilon4 disrupts
972 neurovascular regulation and undermines white matter integrity and cognitive function. Nat Commun.
973 2018;9(1):3816.
974 62. Kordowska J, Huang R, Wang CL. Phosphorylation of caldesmon during smooth muscle contraction
975 and cell migration or proliferation. J Biomed Sci. 2006;13(2):159-72.
976 63. Wang CL. Caldesmon and smooth-muscle regulation. Cell Biochem Biophys. 2001;35(3):275-88.
977 64. Hai CM, Gu Z. Caldesmon phosphorylation in actin cytoskeletal remodeling. Eur J Cell Biol. 2006;85(3-
978 4):305-9.
979 65. Wang CL. Caldesmon and the regulation of cytoskeletal functions. Adv Exp Med Biol. 2008;644:250-
980 72.
981 66. Childs TJ, Watson MH, Sanghera JS, Campbell DL, Pelech SL, Mak AS. Phosphorylation of smooth
982 muscle caldesmon by mitogen-activated protein (MAP) kinase and expression of MAP kinase in differentiated
983 smooth muscle cells. J Biol Chem. 1992;267(32):22853-9.
984 67. Foster DB, Shen LH, Kelly J, Thibault P, Van Eyk JE, Mak AS. Phosphorylation of caldesmon by p21-
985 activated kinase. Implications for the Ca(2+) sensitivity of smooth muscle contraction. J Biol Chem.
986 2000;275(3):1959-65.
987 68. Janovick JA, Natarajan K, Longo F, Conn PM. Caldesmon: a bifunctional (calmodulin and actin)
988 binding protein which regulates stimulated gonadotropin release. Endocrinology. 1991;129(1):68-74.
989 69. Yamakita Y, Oosawa F, Yamashiro S, Matsumura F. Caldesmon inhibits Arp2/3-mediated actin
990 nucleation. J Biol Chem. 2003;278(20):17937-44.
991 70. Morita T, Mayanagi T, Yoshio T, Sobue K. Changes in the balance between caldesmon regulated by
992 p21-activated kinases and the Arp2/3 complex govern podosome formation. J Biol Chem. 2007;282(11):8454-
993 63.
994 71. Ho TC, Wu J, Shin DD, Liu TT, Tapert SF, Yang G, et al. Altered cerebral perfusion in executive,
995 affective, and motor networks during adolescent depression. J Am Acad Child Adolesc Psychiatry.
996 2013;52(10):1076-91 e2.
997

998 **Figure legends**

Main Figures

Figure 1. Expression of *Grin2d*/NR2D in cerebral aSMCs. A) Expression of all NMDAR receptors in mRNA level detected by RT-PCR. B) Statistical data of Figure 1A. Each dot indicates an independent experiment, and the data are mean ±s.e.m. C) RNA scope results of *Grin2d* expression in cerebral aSMCs. Red is the signal of aSMCs. Green is the signal of the *Grin2d* probe. Blue is the signal of the nucleus. Histogram of the red, green, and blue fluorescent intensities of the *Grin2d* signal inside the nucleus of smooth muscle cells pointed out by the red arrow. D) WB of NR2D expression in P0 Nestin-cre^{-}:*Grin2d*$^{f/f}$ cerebellum, Adult Nestin-cre^{-}:*Grin2d*$^{f/f}$ cerebellum, and P0 Nestin-cre^{+}:*Grin2d*$^{f/f}$ cerebellum. E) WB of NR2D expression in P10 SMAcre^{ER-}:*Grin2d*$^{f/f}$ cerebellum and P10 SMAcre^{ER+}:*Grin2d*$^{f/f}$ cerebellum. F) RT-PCR of *Grin2d* expression in SMAcre^{ER+}:*Grin2d*$^{+/+}$:Ai47 sorted pial aSMCs and SMAcre^{ER+}:*Grin2d*$^{f/f}$:Ai47 sorted pial aSMCs. G) WB of NR2D expression in SMAcre^{ER+}:*Grin2d*$^{+/+}$:Ai47 sorted pial aSMCs and SMAcre^{ER+}:*Grin2d*$^{f/f}$:Ai47 sorted pial aSMCs. H-K), Statistical data of Figure 1D-G. Each dot indicates an independent experiment, and the data are mean ±s.e.m. L) IF of NR2D expression in MCA of SMAcre^{ER-}:*Grin2d*$^{f/f}$ and SMAcre^{ER+}:*Grin2d*$^{f/f}$ (Top two rows). Red is the signal of smoothelin. Green is the signal of NR2D. Blue is the signal of the nucleus. The bottom row is the IF of NR2D in SMAcre^{ER+}:*Grin2d*$^{+/+}$:Ai47 sorted pial aSMCs and SMAcre^{ER+}:*Grin2d*$^{f/f}$:Ai47 sorted pial aSMCs. Red is the signal of NR2D. White is the signal of smooth muscle cells. M) Statistical data of NR2D expression in MCA of Figure 1L. Each dot indicates a smooth muscle cell. Data are mean ±s.e.m. N) Statistical data of Smoothelin expression in MCA of Figure 1L. Each dot indicates a smooth muscle cell. Data are mean ±s.e.m. O) Statistical data of NR2D expression in cultured aSMCs of Figure 1L. Each dot indicates an independent experiment, and the data are mean ±s.e.m. P) Statistical data of SMA expression in cultured aSMCs through WB. Each dot indicates an independent experiment, and the data are mean ± s.e.m. RFI, Relative Fluorescence Intensity. T-test used for statistical analysis. **** means P<0.0001.

Figure 2. Cerebral blood flow variation of SMAcre^{ER+}/Pdgfrβ^{ER+}:*Grin2d*$^{f/f}$ mice during the whisker stimulation. A) Schematic diagram of experimental timeline and operations. B) Schematic diagram of CBF increases in the ROI before, during, and after the whisker stimulation of SMAcre^{ER-}:*Grin2d*$^{f/f}$ mice and SMAcre^{ER+}:*Grin2d*$^{f/f}$ mice. In the right area, the redder the colour is, the more CBF increases, and the bluer the colour is, the more CBF decreases. C) CBF variation before, during, and after the whisker stimulation. The solid line indicates the mean value, and the dotted line indicates ±s.e.m. D) The mean and maximum value of CBF variation during the plateau period. E) The value “Time to plateau” of mice. F) The value “K-slope” of mice. In Figure 2, Each group contains six mice, except the P60 TMX_ Pdgfrβ^{ER+}:*Grin2d*$^{f/f}$ group contains five mice. Each mouse was

1030 stimulated at least twice. Each dot indicates the mean value obtained from one mouse, and the data are mean
1031 ±s.e.m. T-test used for statistical analysis. **** means P<0.0001.
1032
1033 **Figure 3.** Cerebral blood flow variation of SMAcre^{ER+}:*Grin2d*$^{f/f}$ mice and SMAcre^{ER+}:*Grin1*$^{f/f}$:*Grin2d*$^{f/f}$ mice
1034 during the whisker stimulation. A) Schematic diagram of experimental timeline and operations. B) CBF
1035 variation before, during, and after the whisker stimulation. The solid line indicates the mean value, and the
1036 dotted line indicates ±s.e.m. C) The IF of colocalization of NR2D and NR1 in MCA. Blue is the signal of
1037 smooth muscle cells. Green is the signal of NR2D. Red is the signal of NR1. White is the signal of nucleus. D)
1038 Statistical data of Figure 3C. Each dot indicates an independent experiment. Data are mean ±s.e.m. E) The
1039 mean and maximum value of CBF variation during the plateau period. F) The value "Time to plateau" of mice.
1040 G) The value "K-slope" of mice. In Figure 3, each group contains four mice. Each mouse was stimulated at
1041 least twice. Each dot indicates the mean value obtained from one mouse, and the data are mean ±s.e.m. T-
1042 test used for statistical analysis. **** means P<0.0001.
1043
1044 **Figure 4.** Cerebral blood flow variation of SMAcre^{ER-}:*Grin2d*$^{f/f}$ mice and SMAcre^{ER+}:*Grin2d*$^{f/f}$ mice with COX-2
1045 inhibition and HFD challenge during the whisker stimulation. A) Schematic diagram of experimental timeline
1046 and operations. B) Schematic diagram of the validation of cistern magnum injection. NS-398 mixed with FITC.
1047 The green signal of FITC can be detected in the Virchow-Robin spaces of cerebral blood vessels. C) RT-PCR
1048 of *Ptgs2* expression in adult cortex and sorted SMAcre^{ER+}:Ai47 parenchymal aSMCs. D) IF of COX-2 in
1049 cerebral smooth muscle cells in the cortex of mice. The red signal is smooth muscle cells, green is the signal
1050 of COX-2, and white is the signal of the nucleus. The Arrow shows the signal of COX-2 expressed inside the
1051 signal of smooth muscle cells. E) WB of COX-2 expression validation in the IP products. F) CBF variation
1052 before, during, and after the whisker stimulation. The solid line indicates the mean value, and the dotted line
1053 indicates ± s.e.m. G) Statistical data of Figure 4C. H) The mean and maximum value of CBF variation during
1054 the plateau period. I) The value "Time to plateau" of mice. J) The value "K-slope" of mice. In Figure 4, each
1055 group contains three mice. Each mouse was stimulated at least twice. Each dot indicates an independent
1056 experiment, and the data are mean ±s.e.m. T-test used for statistical analysis. **** means P<0.0001.
1057
1058 **Figure 5.** Downstream signal pathways analysis of NR2D in aSMCs. A) Veen diagram of NR2D-related
1059 proteins obtained from three independent mass spectrum data. B) KEGG pathway analysis of 915 proteins
1060 selected from three independent mass spectrum data. C) WB of NR2D and caldesmon expression validation

1061 in the IP products. D-F) GO analysis of 915 proteins selected from three independent mass spectrum data.
1062 They are GO_BP, GO_CC, and GO_MF, respectively.
1063
1064 **Figure 6.** The open field-like test (OFLT) of SMAcre^{ER-}:*Grin2d*$^{f/f}$ (WT) mice and SMAcre^{ER+}:*Grin2d*$^{f/f}$ (cKO)
1065 mice. A) Schematic diagram of the box used for the OFLT. B) Schematic diagram of the heat map of WT and
1066 cKO mice in the box during 20min. C) Running distance of WT and cKo mice. D) Urine volume of WT and cKo
1067 mice. E) Fecal particles of WT and cKo mice in OFT and OFLT. F) Box area preference of WT and cKo mice.
1068 G) Ratio of time spent in the right and left area of WT and cKO mice. Data presented in log10 format. H) Ratio
1069 of time spent in the right and the rest of area of WT and cKO mice. Data presented in log10 format. T-test used
1070 for statistical analysis. Each dot indicates one mouse, and the data are mean ±s.e.m.
1071
1072 **Figure 7.** CD-1 fear assay of SMAcre^{ER-}:*Grin2d*$^{f/f}$ (WT) mice and SMAcre^{ER+}:*Grin2d*$^{f/f}$ (cKO) mice. A)
1073 Schematic diagram of the cage for CD-1 fear assay. B) The value “Number of active sniffing” of mice. C) The
1074 value “First fight latency” of mice. D) The value “Number of fights” of mice. E) The value “Two mice in tiny
1075 space together” of mice. F) The value “Total fighting duration” of mice. G) The percentage of “Who triggered
1076 the fight” of mice. H) The percentage of “Who flighted after the fight” of mice. I-L) IF of c-Fos expression in the
1077 amygdala, S1BF, pir cortex, and hippocampus of WT and cKO mice. Red, the signal of NeuN. Green, the
1078 signal of c-Fos. M) Statistical data of Figure 7I-L, including the data of controls (Figure S6B-E). Each dot
1079 indicates one mouse, and the data are mean ±s.e.m. T-test used for statistical analysis. **** means P<0.0001.
1080
1081 **Supplementary Figures**
1082 **Figure S1.** RNA scope probe specificity, SMAcreER specificity, and NR2D expression specificity validation.
1083 A) RNA scope of *Grin2d* and *Grin1* in mice cerebellum. Red is the signal of the *Grin1* probe. Green is the
1084 signal of the *Grin2d* probe. Blue is the signal of the nucleus. B) IF of NeuN in the brain slices of SMAcre^{ER+}:Ai14
1085 mice. Red is the signal of the smooth muscle cell. Green is the signal of CD-31. Blue is the signal of NeuN,
1086 and the white signal is for the nucleus. In the statistical data, each dot indicates an ROI of analysis. Three
1087 independent experiments were performed, and the data are mean ±s.e.m. C) IF of NR2D expression in heart,
1088 liver, spleen, lung, kidney, and small intestine of SMAcre^{ER+}:Ai14 mice. Red is the signal of the smooth muscle
1089 cell. Green is the signal of NR2D. Blue is the signal of the nucleus. The first row is zoom-out images of six
1090 organs, the second row is zoom-in images of white circles in the first row, and the third row is histograms of

1091 the red and green fluorescent intensities of the indicated sites in the second row. RFI, Relative Fluorescence
1092 Intensity. T-test used for statistical analysis. **** means P<0.001.
1093
1094 **Figure S2.** Physical parameters of SMAcre^{ER-}:*Grin2d*$^{f/f}$ mice and SMAcre^{ER+}:*Grin2d*$^{f/f}$ mice. A) The absolute
1095 weight change of SMAcre^{ER-}:*Grin2d*$^{f/f}$ mice and SMAcre^{ER+}:*Grin2d*$^{f/f}$ mice. Tamoxifen was administrated at P5.
1096 The solid line indicates the mean value, and the dotted line indicates ±s.e.m. B) The relative weight change
1097 in Figure S2A. The solid line indicates the mean value, and the dotted line indicates ±s.e.m. C) The absolute
1098 weight change of SMAcre^{ER-}:*Grin2d*$^{f/f}$ mice and SMAcre^{ER+}:*Grin2d*$^{f/f}$ mice. Tamoxifen was administrated at P60.
1099 The solid line indicates the mean value, and the dotted line indicates ±s.e.m. D) The relative weight change
1100 in Figure S2C. The solid line indicates the mean value, and the dotted line indicates ±s.e.m. E) The blood
1101 pressure of mice. F) The body weight of SMAcre^{ER-}:*Grin2d*$^{f/f}$ mice and SMAcre^{ER+}:*Grin2d*$^{f/f}$ mice before the
1102 whisker stimulation at P65. G) High-fat food consumption of SMAcre^{ER-}:*Grin2d*$^{f/f}$ mice and SMAcre^{ER+}:*Grin2d*$^{f/f}$
1103 mice. H) Fat/lean/total water of SMAcre^{ER-}:*Grin2d*$^{f/f}$ mice and SMAcre^{ER+}:*Grin2d*$^{f/f}$ mice under HFD challenge.
1104 Each dot indicates one mouse, and the data are mean ±s.e.m. T-test used for statistical analysis. * means
1105 P=0.01-0.05, and ** means P<0.01. **** means P<0.0001.
1106
1107 **Figure S3.** Cerebral blood flow variation of SMAcre^{ER-}:*Grin2d*$^{f/f}$ mice in the whisker stimulation before and after
1108 long-term stimulation. A) CBF variation before, during, and after the whisker stimulation. The solid line indicates
1109 the mean value, and the dotted line indicates ±s.e.m. B) The mean and maximum value of CBF variation
1110 during the plateau period. C) The value “Time to plateau” of mice. D) The value “K-slope” of mice. In figure S3,
1111 four SMAcre^{ER-}:*Grin2d*$^{f/f}$ mice were used in the experiment. T-test used for statistical analysis. Each dot
1112 indicates the mean value obtained from one mouse, and the data are mean ±s.e.m.
1113
1114 **Figure S4.** Cerebral blood flow variation of SMAcre^{ER-}:*Grin2d*$^{f/f}$ mice in the whisker stimulation before and after
1115 Tamoxifen administration. A) CBF variation before, during, and after the whisker stimulation. The solid line
1116 indicates the mean value, and the dotted line indicates ±s.e.m. B) The mean and maximum value of CBF
1117 variation during the plateau period. C) The value “Time to plateau” of mice. D) The value “K-slope” of mice. In
1118 figure S4, five SMAcre^{ER-}:*Grin2d*$^{f/f}$ mice were used in the experiment. T-test used for statistical analysis. Each
1119 dot indicates the mean value obtained from one mouse, and the data are mean ±s.e.m.
1120

1121 **Figure S5.** The open field test (OFT) of SMAcre^{ER-}:*Grin2d*$^{f/f}$ (WT) mice and SMAcre^{ER+}:*Grin2d*$^{f/f}$ (cKO) mice.
1122 A) Schematic diagram of the box used for the Open Field Test. B) Time of WT and cKO mice spent in the
1123 central area of the box. C) Time of WT and cKO mice spent in the non-central area of the box. D) Running
1124 distance of WT and cKO mice spent in the center of the box. E) Rate of fecal production for WT and cKO mice.
1125 F) Rate of urine production for WT and cKO mice. G) Fecal latency for WT and cKO mice. T-test used for
1126 statistical analysis. Each dot indicates one mouse, and the data are mean ±s.e.m.
1127
1128 **Figure S6.** Blood vessel distribution in the amygdala and negative control of CD-1 fear assay. A) The blood
1129 vessel distribution in the amygdala. Red is the signal of mural cells. Green is the signal of NeuN. Blue is the
1130 signal of nucleus. B-E) The negative control IF staining of CD-1 fear assay. They are amygdala, pir cortex,
1131 S1BF, and hippocampus.
1132
1133 **Figure S7.** Elevated plus maze (EPM) test of SMAcre^{ER-}:*Grin2d*$^{f/f}$ (WT) mice and SMAcre^{ER+}:*Grin2d*$^{f/f}$ (cKO)
1134 mice. A) Schematic diagram and representative diagram of WT and cKO mice in EPM, B) Running distance
1135 of WT and cKO mice spent in the EPM. C) Time percentage of WT and cKO mice spent in the central area of
1136 the EPM. D) Time percentage of WT and cKO mice spent in close arms of the EPM E) Time percentage of
1137 WT and cKO mice spent in open arms of the EPM. F) Ratio of time spent in open and closed arms of WT and
1138 cKO mice. Data presented as - log10 format. G) Ratio of time spent in the central and non-central area of WT
1139 and cKO mice. Data presented in - log10 format. T-test used for statistical analysis. Each dot indicates one
1140 mouse, and the data are mean ±s.e.m.
1141

1142 # Tables

1143 **Table 1. List of Mice Genetics**

Common name	Strain name	Resource
Nestin-cre	B6.Cg-Tg(Nes-cre)1Kln/J	Yanmei Tao, Hangzhou Normal University/ Southeast University
Grin2d	B6/JGpt-Grin2d^{em1Cflox}/Gpt	GemPharmatech
SMAcre^{ER}	Tg(Acta2-cre/ERT2)12Pcn	Bo Zhou, ShanghaiInstitutes for Biological Sciences, Chinese Academy of Sciences
Ai47	Gt(ROSA)26Sor$^{tm47(CAG-EGFP*)Hze}$	Zilong Qiu, Chinese Academy of Sciences Center for Excellence in Brain Science and Intelligence Technology, Chinese Academy of Sciences.
PdgfrβCre^{ER}	Tg(Pdgfrb-cre/ERT2)6096Rha	Xiang Yu, Peking University
Grin1	*Grin1*^{tm2Stl}	Yangang Sun, Chinese Academy of Sciences Center for Excellence in Brain Science and Intelligence Technology, Chinese Academy of Sciences
Ai14	B6.Cg-Gt(ROSA)26Sor$^{tm14(CAG-tdTomato)Hze}$/J	Woo-Ping Ge, Chinese Institute of Brain Research (CIBR)

1144

1145 **Table 2. List of Primer Pairs (Some primers referred to the published PrimerBank database)**

Name		Sequence
Grin1	F	AAGAACCTGCAGCAGTACCA
	R	GCAGCAGGACTCATCAGTGT
Grin2a	F	TCAGGGACTTTGGAAAACGCT
	R	AAGTCATGCAGGGTTGGTTG
Grin2b	F	ACTAACTATCAATGAAGAACGGT
	R	CCAGACCCCAGAGTAACCA
Grin2c	F	TGTGGGCCTTCTTCGCTGTCATCT
	R	TGCCATTAGGTACCGTGCCAAAAC
Grin2d	F	TGGAGGAGTACGACTGGACAT
	R	CGCACTGACACTACGGAGC
Grin3a	F	CTGCACACCAGTCAGAGGTT
	R	TTCGTTGGTTGTCGTGACTC
Grin3b	F	TGGGGGTCTACCACTTGTCA
	R	TGGATCTTCTGGCTCGTGTG
Ptgs2	F	TTCAACACACTCTATCACTGGC
	R	AGAAGCGTTTGCGGTACTCAT
18s	F	CGGACACGGACAGGATTGACA
	R	CCAGACAAATCGCTCCACCAACTA

1146

1147 **Table 3. List of Antibodies**

Name	Host	Cat#	Dilution	Company
Anti-NMDAR2D Antibody	Mouse	MAB5578	1:400 (IF) 1:2,500 (WB) 1:1,000 (IP)	Merck
Anti-Smoothelin antibody	Rabbit	ab219652	1:400 (IF)	abcam
α-Smooth Muscle Actin (ACTA2) Rabbit mAb	Rabbit	A17910	1:2,500 (WB)	ABclonal
Anti-NeuN purified Antibody	Guinea Pig	ABN90P	1:800 (IF)	Merck
Anti-NMDAR1 Antibody, clone 54.1	Mouse	MAB363	1:400 (IF)	Merck
COX2/PTGS2 Rabbit pAb	Rabbit	A1253	1:400 (IF)	ABclonal
c-Fos antibody	Rabbit	226 003	1:1,000 (IF)	SYSY
Recombinant Alexa Fluor® 488 Anti-Caldesmon/CDM antibody	Rabbit	ab208116	1:400 (IF) 1:2,500 (WB)	abcam
Mice IgG	Mouse	A7028	1:1,000 (IP)	Beyotime
Goat anti-Mouse IgG (H+L) Cross-Adsorbed Secondary Antibody, Alexa Fluor™ 488	Goat	A-11001	1:1,000 (IF)	Invitrogen
Goat anti-Rabbit IgG (H+L) Cross-Adsorbed Secondary Antibody, Alexa Fluor™ 546	Goat	A-11010	1:1,000 (IF)	Invitrogen
Goat anti-Rabbit IgG (H+L) Highly Cross-Adsorbed Secondary Antibody, Alexa Fluor™ 488	Goat	A-11034	1:1,000 (IF)	Invitrogen
Donkey anti-Goat IgG (H+L) Cross-Adsorbed Secondary Antibody, Alexa Fluor™ 647	Donkey	A-21447	1:1,000 (IF)	Invitrogen
Goat Anti-Guinea pig IgG H&L (Alexa Fluor® 488)	Goat	ab150185	1:1,000 (IF)	abcam
Goat Anti-Guinea pig IgG H&L (Alexa Fluor® 555)	Goat	ab150186	1:1,000 (IF)	abcam
Goat Anti-Guinea pig IgG H&L (Alexa Fluor® 647)	Goat	Ab150187	1:1000 (IF)	abcam
β-Tubulin Mouse mAb	Mouse	AC021	1:5,000 (WB)	ABclonal
Goat Anti-Mouse IgG, HRP Conjugated	Goat	CW0102	1:10,000 (WB)	CWBIO
Goat Anti-Rabbit IgG, HRP Conjugated	Goat	CW0103	1:10,000 (WB)	CWBIO
Goat Anti-Mouse IgG (H+L)	Goat	AS071	1:500 (IF)	ABclonal
DDDDK-Tag Rabbit mAb	Rabbit	AE063	1:5000 (WB)	ABclonal
BD Pharmingen™ Purified Rat Anti-Mouse CD31	Rat	557355	1:400 (IF)	BD
Alexa Fluor® 488 AffiniPure Donkey Anti-Rat IgG (H+L)	Donkeny	712-545-453	1:500 (IF)	Jackson ImmunoResearch

Data availability

All codes involved in this study are available at https://github.com/JialabEleven/Neurovascular_coupling with citation. Another data is available from authors upon reasonable request.

Author contributions

Jie-Min Jia conceived the project, designed the experiments, and supervised this study. Jiayu Ruan did all main experiments, obtained all main original data, and wrote the manuscript. Yiyi Zhang wrote main MATLAB code. Dongdong Zhang provided primer pairs of *Grin1* and provided critical suggestions. Huiqi Xie participated in blood pressure measurement, long-term whisker stimulation, and provided suggestion for manuscript writing. Xinghua Quan participated in all behavioral tests and IF staining of blood vessel distribution in the Amygdala. Wentao Wang participated in the writing of MATLAB code. Xu Hu provided primer pairs of *Grin2a*, *Grin2b*, *Grin2c*, *Grin3a*, *Grin3b*, and *18s*. Yanmei Tao provided Nestin-cre mice. Bingrui Zhao participated in genotyping of all mice and cell sorting. Danping Lu participated in brain slice acquisition.

Figure 1

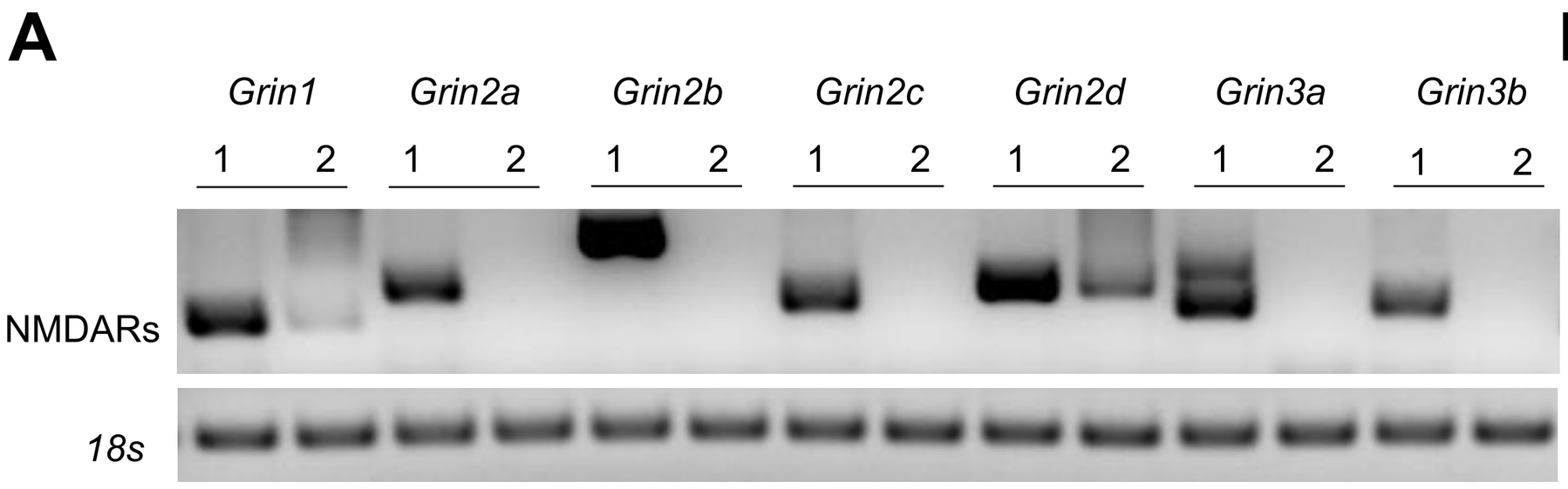

1: P0 cerebellum
2: SMAcre^{ER+}:Ai47 sorted parenchymal aSMCs

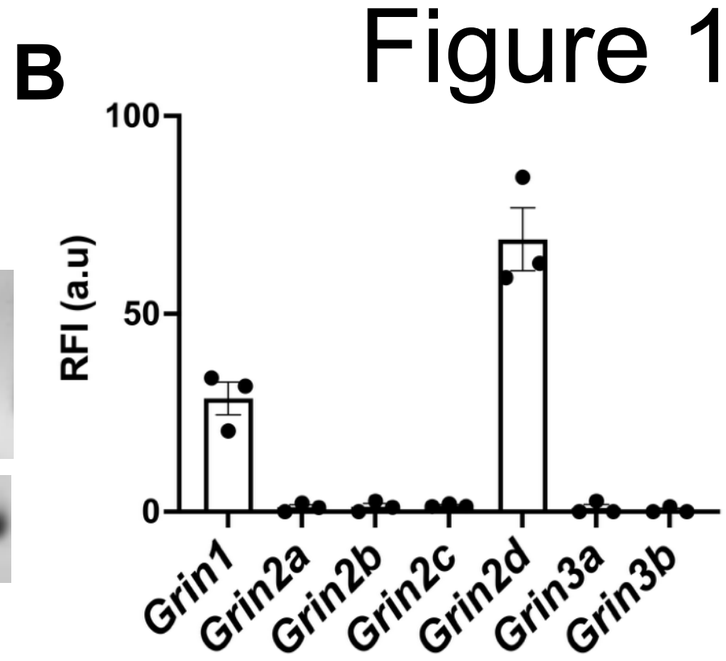

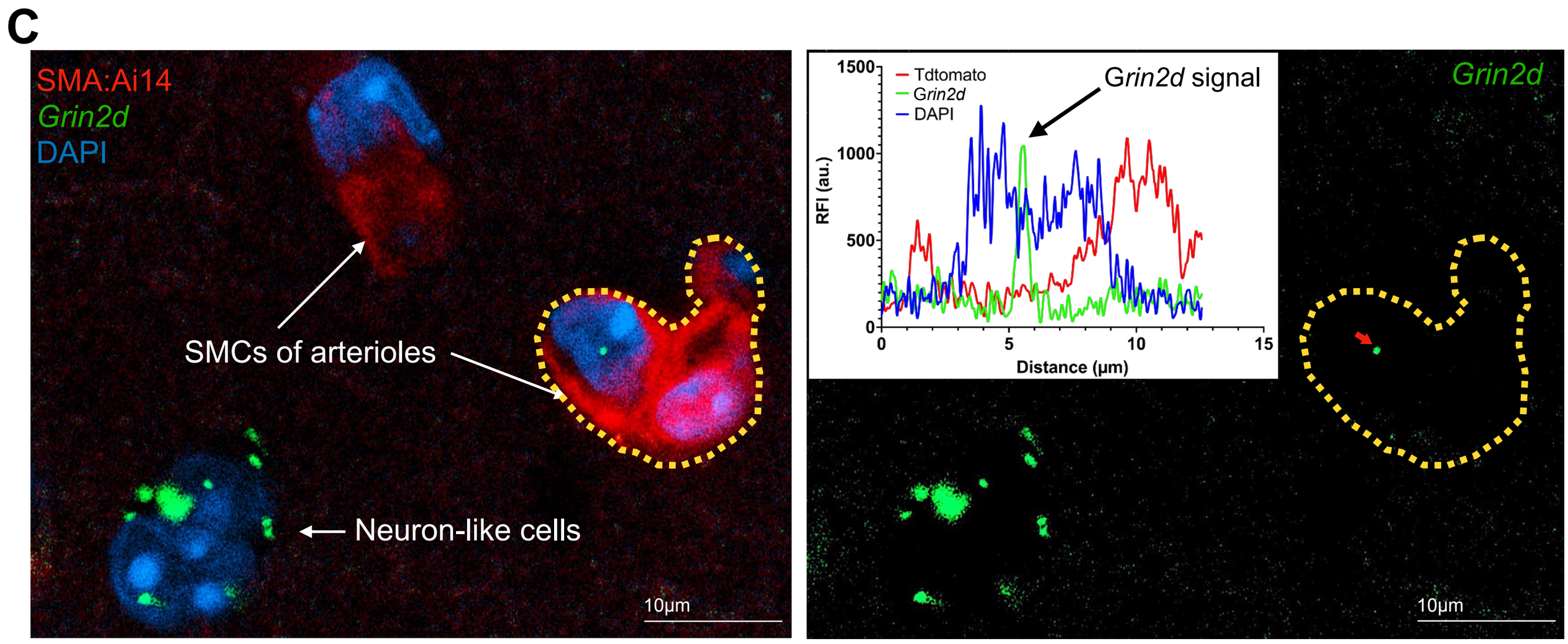

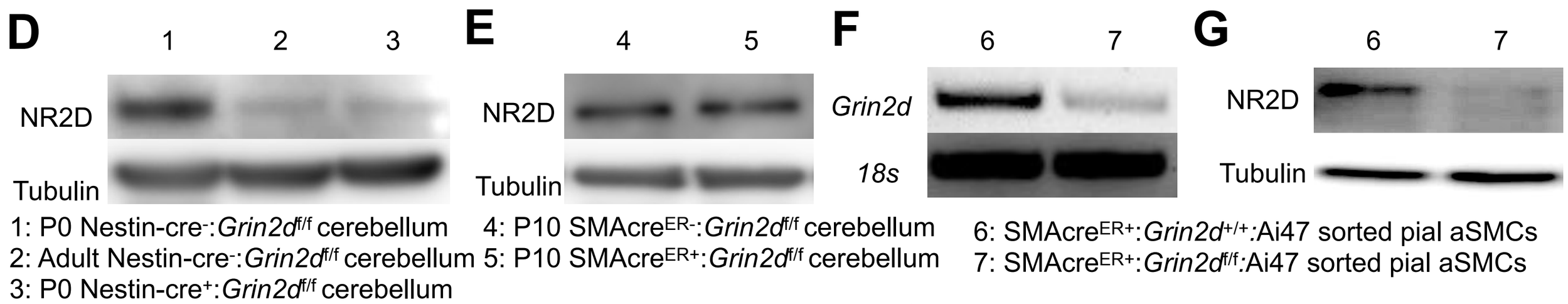

1: P0 Nestin-cre^{-}:*Grin2d*$^{f/f}$ cerebellum
2: Adult Nestin-cre^{-}:*Grin2d*$^{f/f}$ cerebellum
3: P0 Nestin-cre^{+}:*Grin2d*$^{f/f}$ cerebellum
4: P10 SMAcre^{ER-}:*Grin2d*$^{f/f}$ cerebellum
5: P10 SMAcre^{ER+}:*Grin2d*$^{f/f}$ cerebellum
6: SMAcre^{ER+}:*Grin2d*$^{+/+}$:Ai47 sorted pial aSMCs
7: SMAcre^{ER+}:*Grin2d*$^{f/f}$:Ai47 sorted pial aSMCs

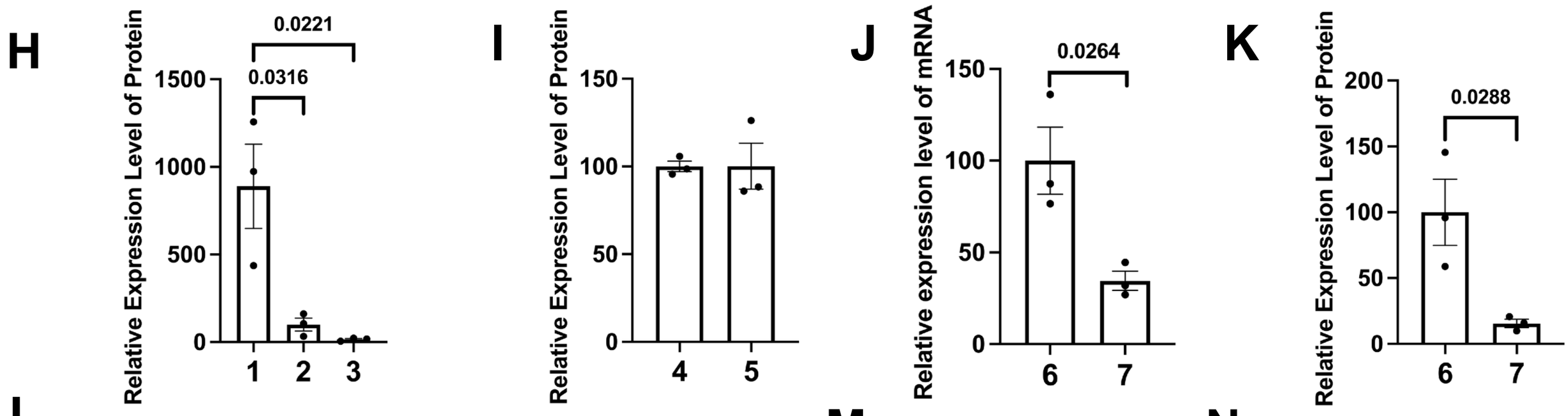

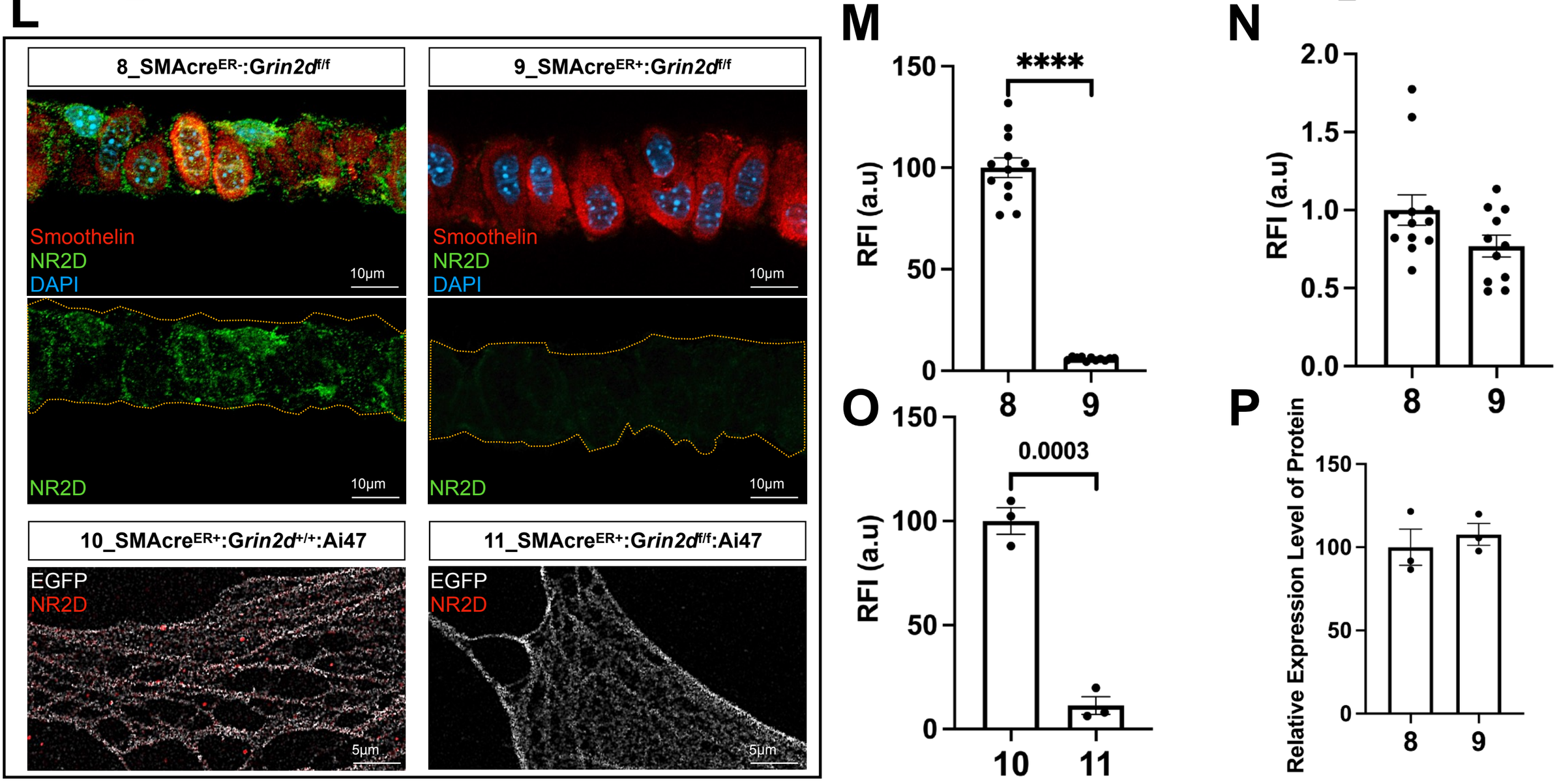

Figure 2

A

TMX administration
(P5 to P8)
(P5_cKO group & littermate control)

Whisker trimming, scalp open
(P63)

Whisker stimulation 4Hz, 1min
(P65)

TMX administration
(P60 to P63)
(P60_cKO group & littermate control)

Rest
(P64)

B

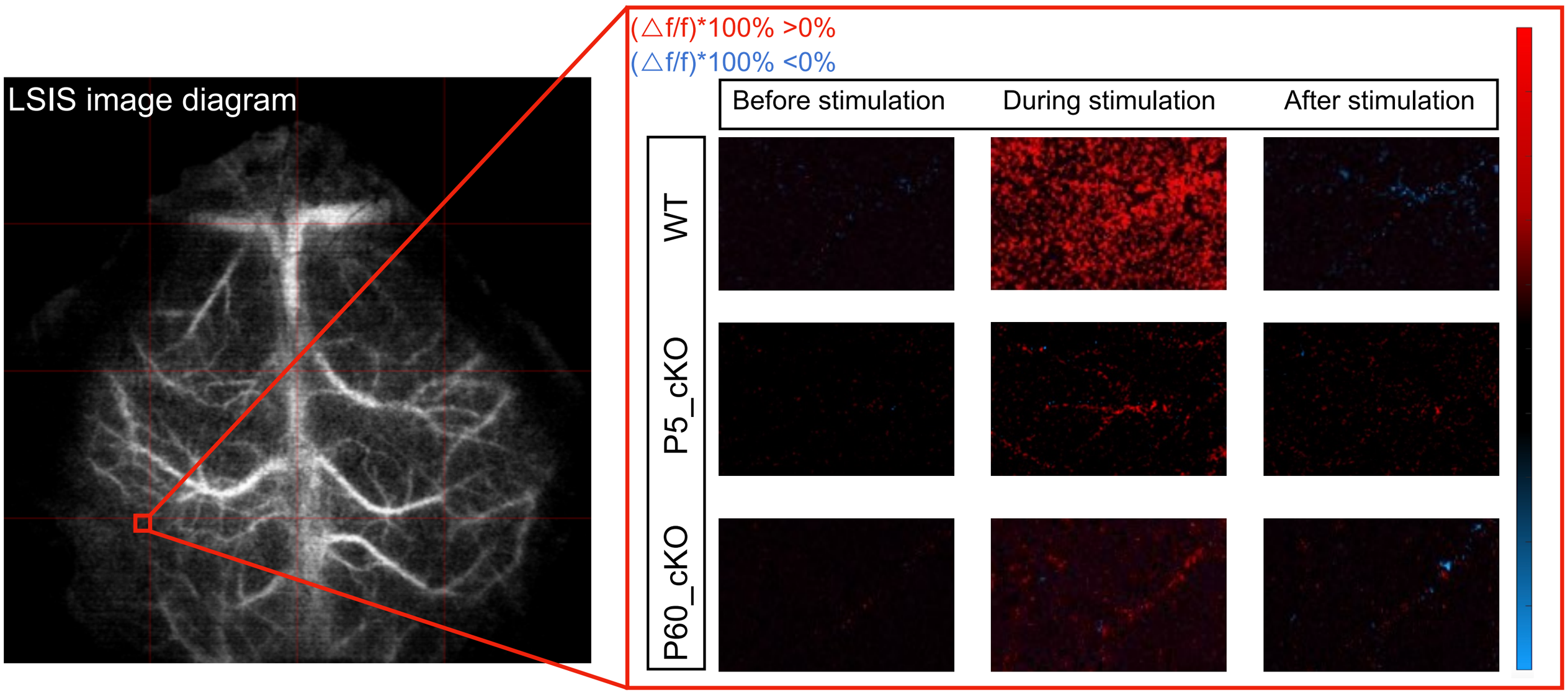

C

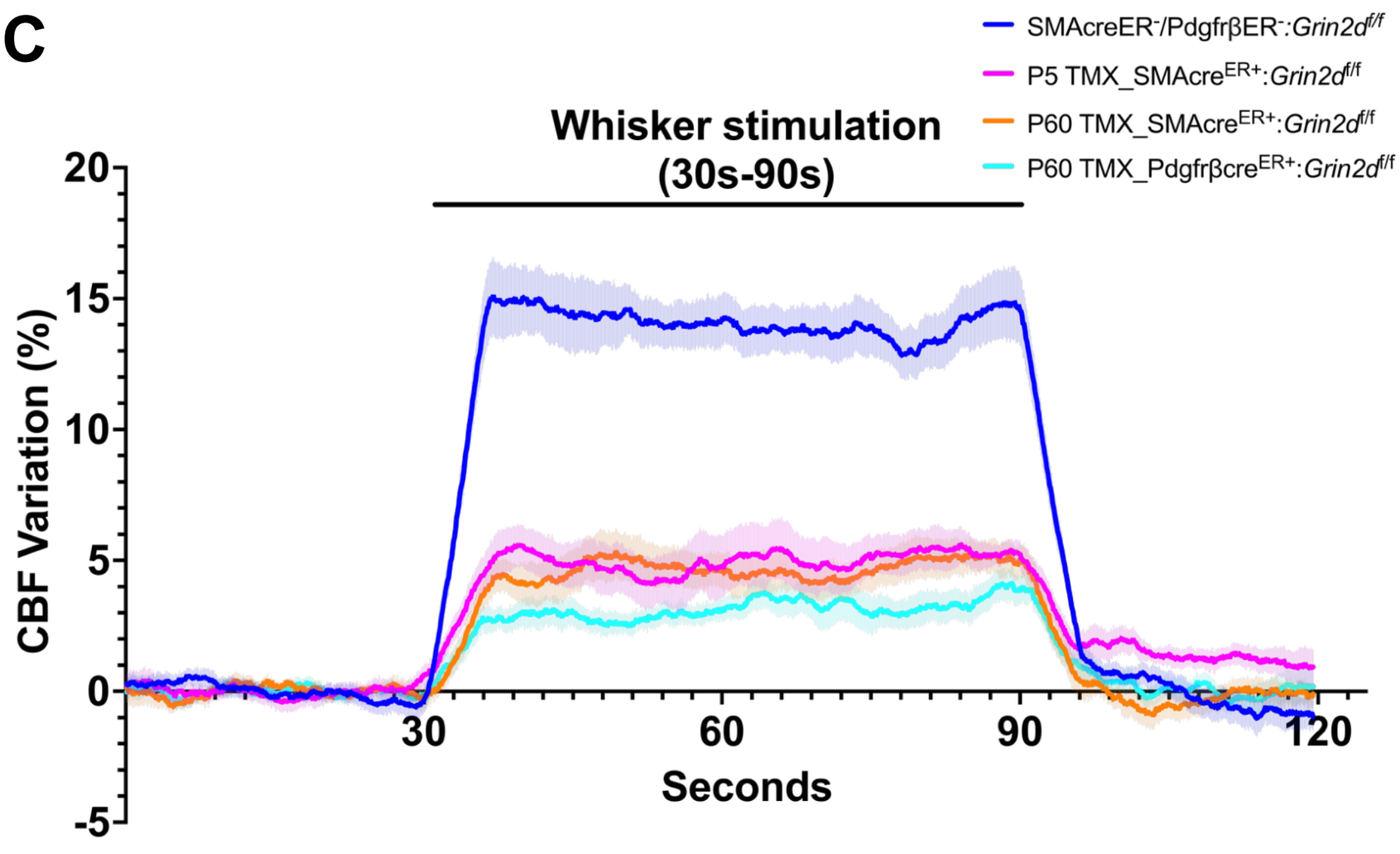

E

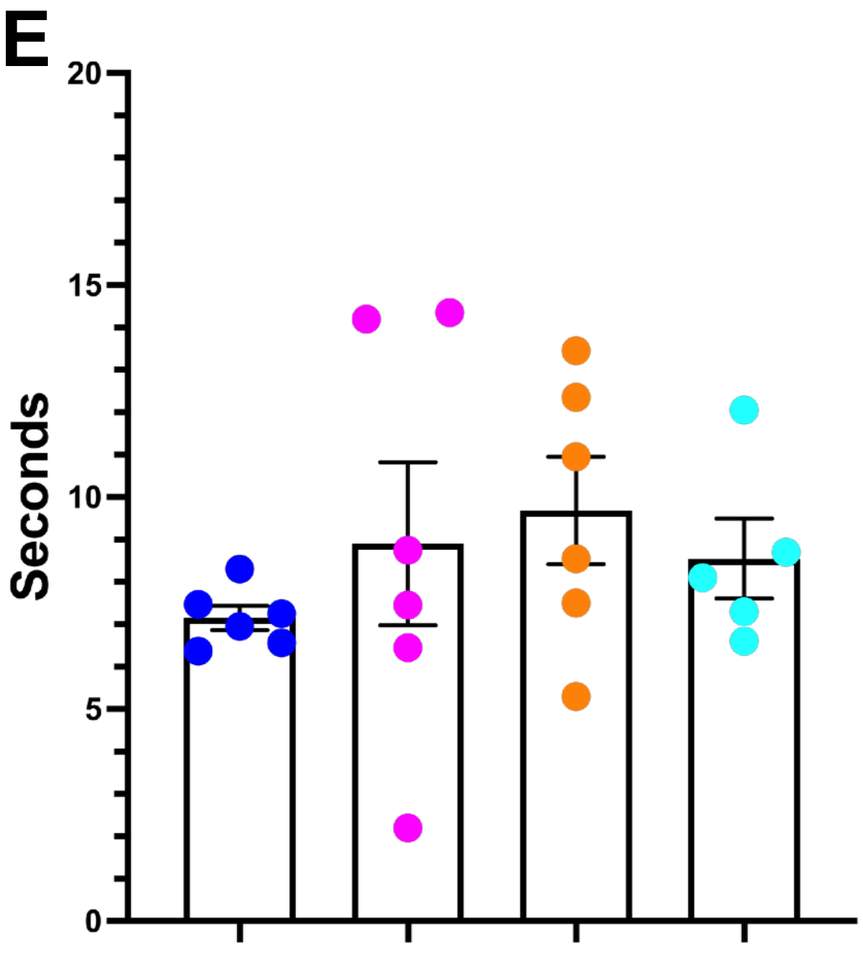

D

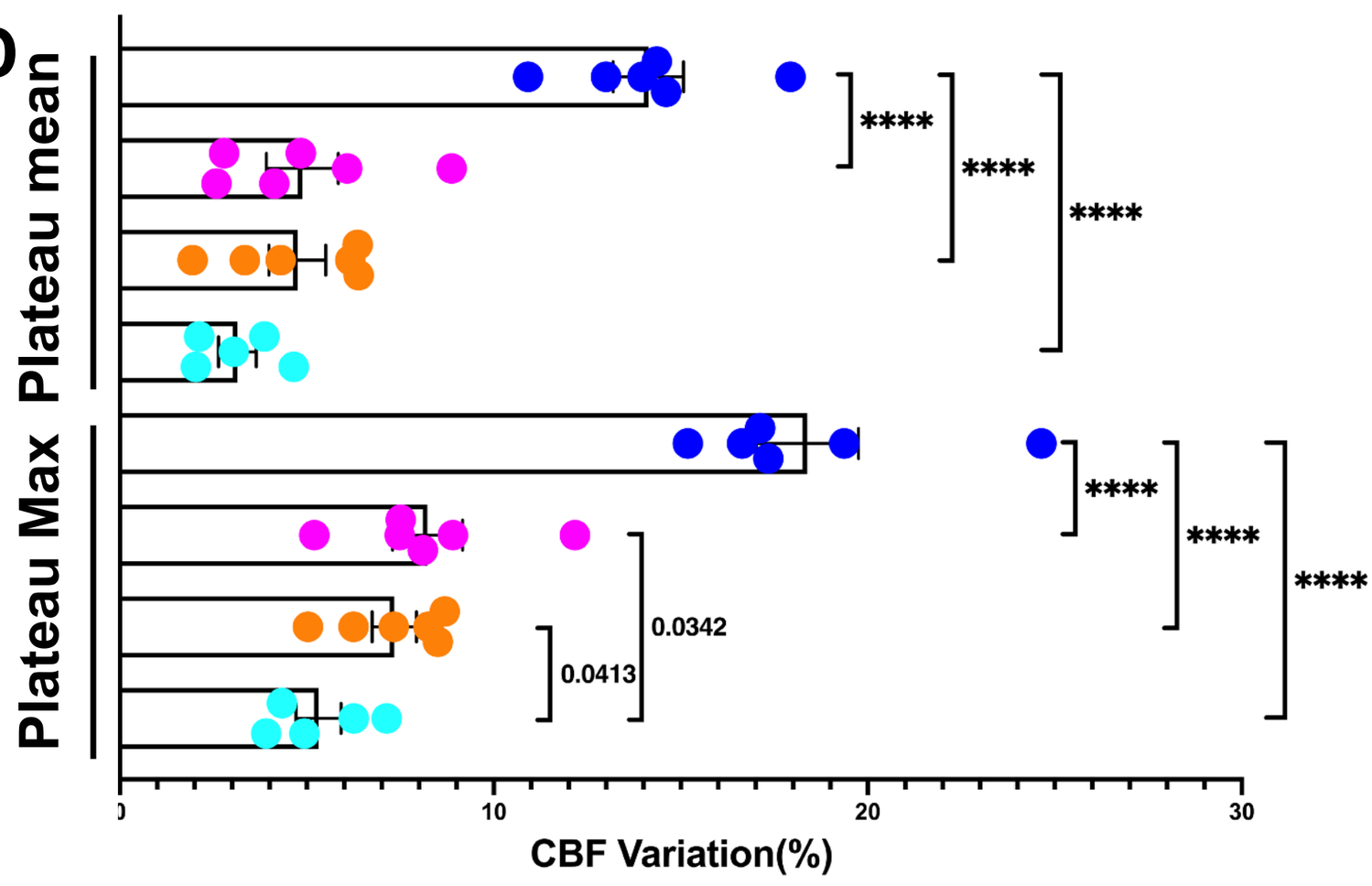

F

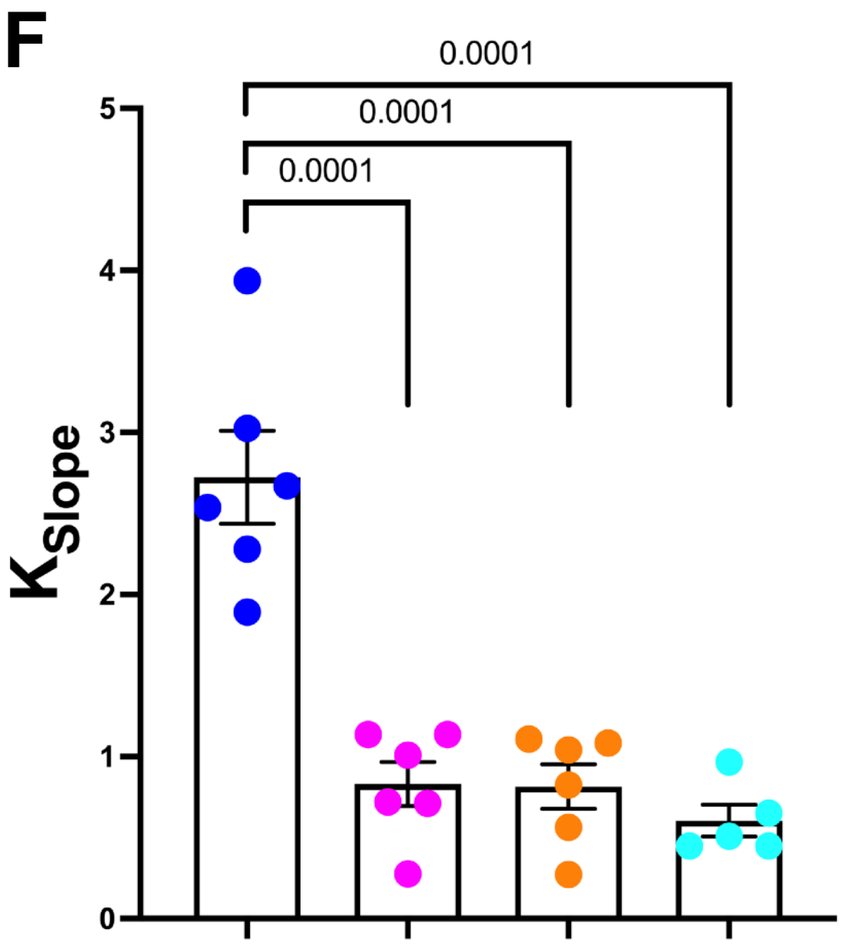

Figure 3

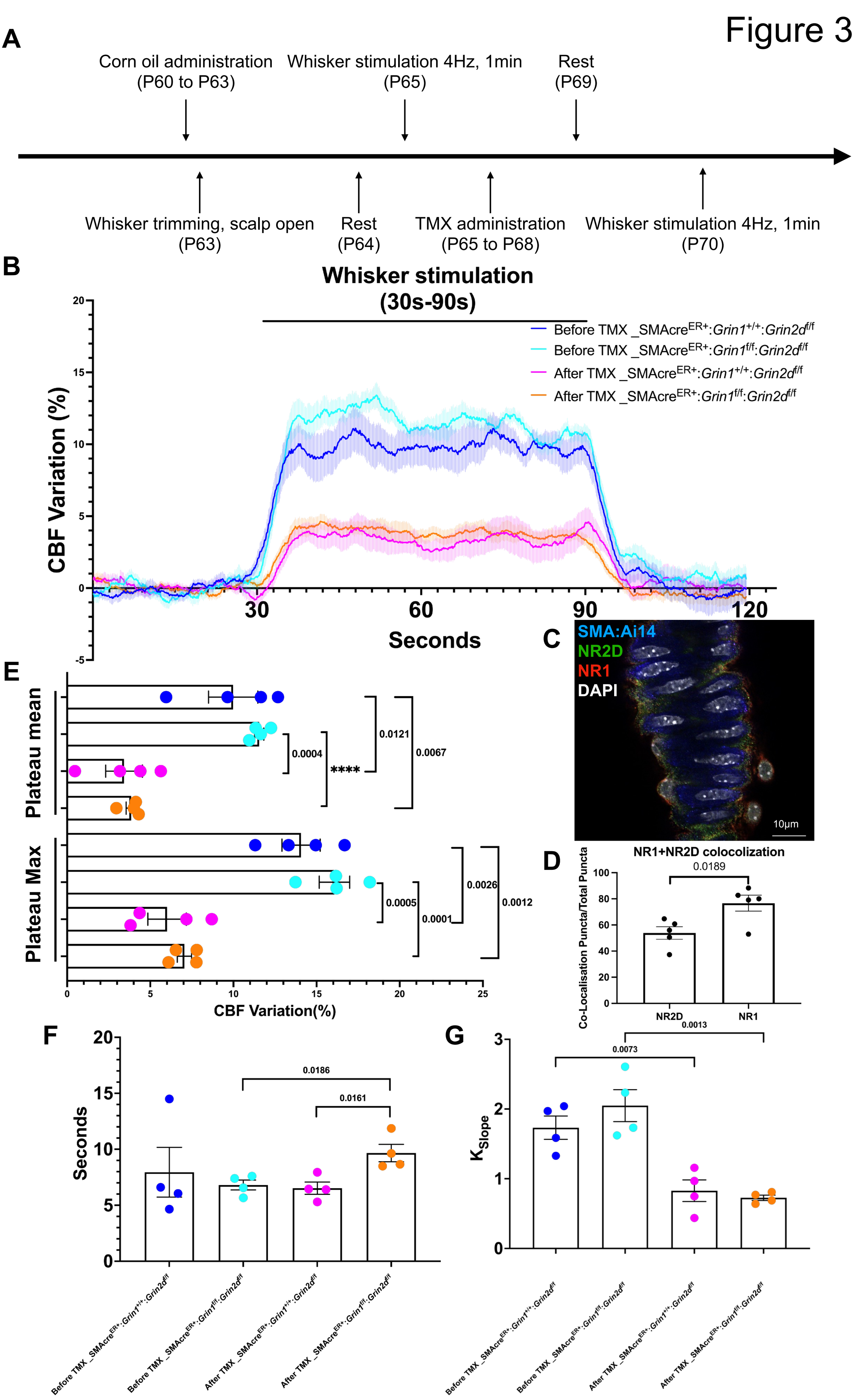
A
Corn oil administration (P60 to P63)
Whisker stimulation 4Hz, 1min (P65)
Rest (P69)
Whisker trimming, scalp open (P63)
Rest (P64)
TMX administration (P65 to P68)
Whisker stimulation 4Hz, 1min (P70)
B
Whisker stimulation (30s-90s)
CBF Variation (%)
Seconds
Before TMX _SMAcre^{ER+}:Grin1$^{+/+}$:Grin2d$^{f/f}$
Before TMX _SMAcre^{ER+}:Grin1$^{f/f}$:Grin2d$^{f/f}$
After TMX _SMAcre^{ER+}:Grin1$^{+/+}$:Grin2d$^{f/f}$
After TMX _SMAcre^{ER+}:Grin1$^{f/f}$:Grin2d$^{f/f}$
C
SMA:Ai14
NR2D
NR1
DAPI
10µm
D
NR1+NR2D colocolization
Co-Localisation Puncta/Total Puncta
0.0189
NR2D
NR1
E
Plateau mean
Plateau Max
CBF Variation(%)
0.0121
0.0067
0.0004
****
0.0026
0.0012
0.0005
0.0001
F
Seconds
0.0186
0.0161
G
K_{Slope}
0.0073
0.0013

Figure 4

A

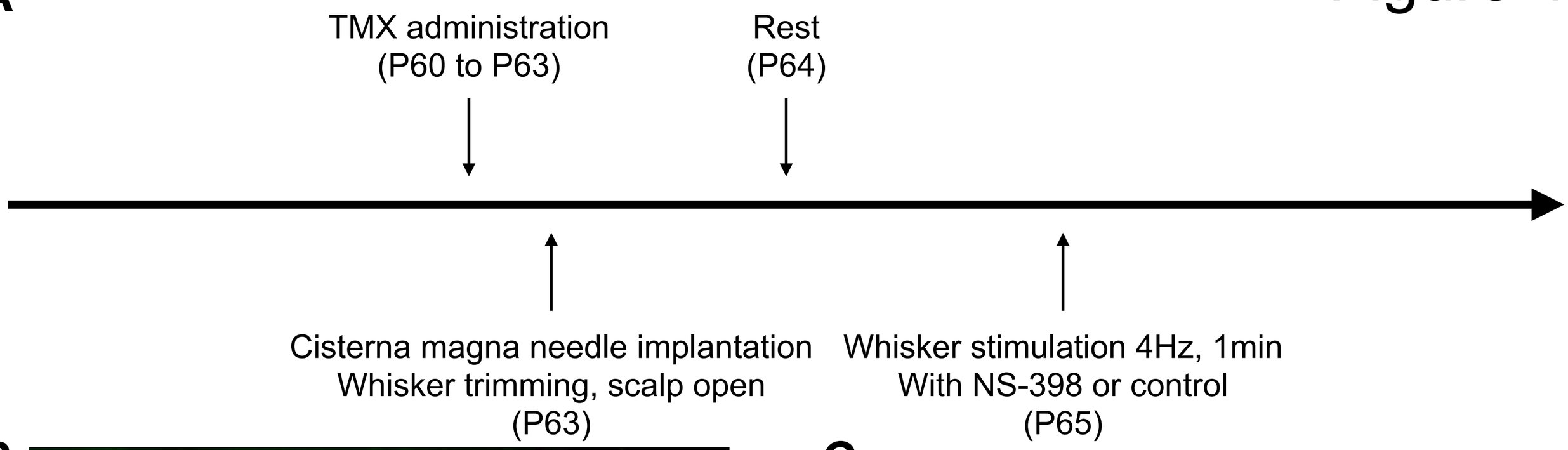

B

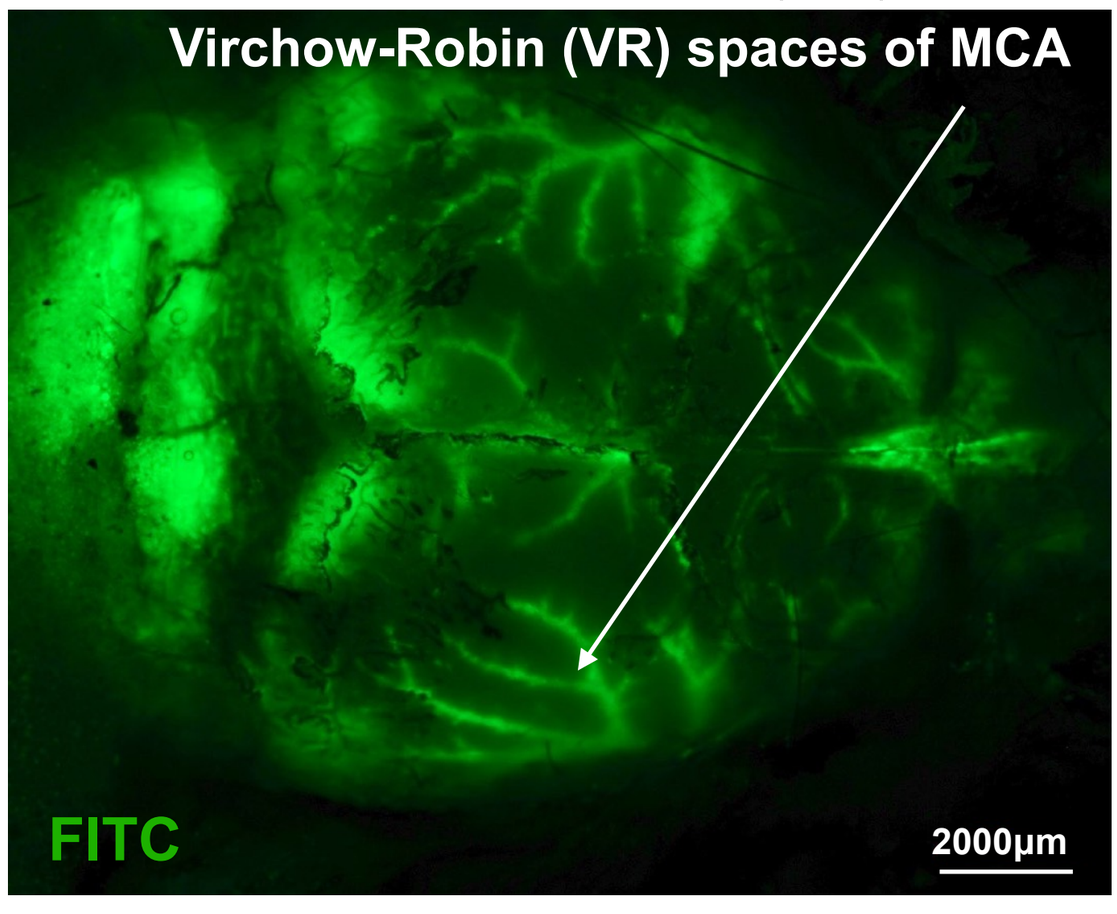

C

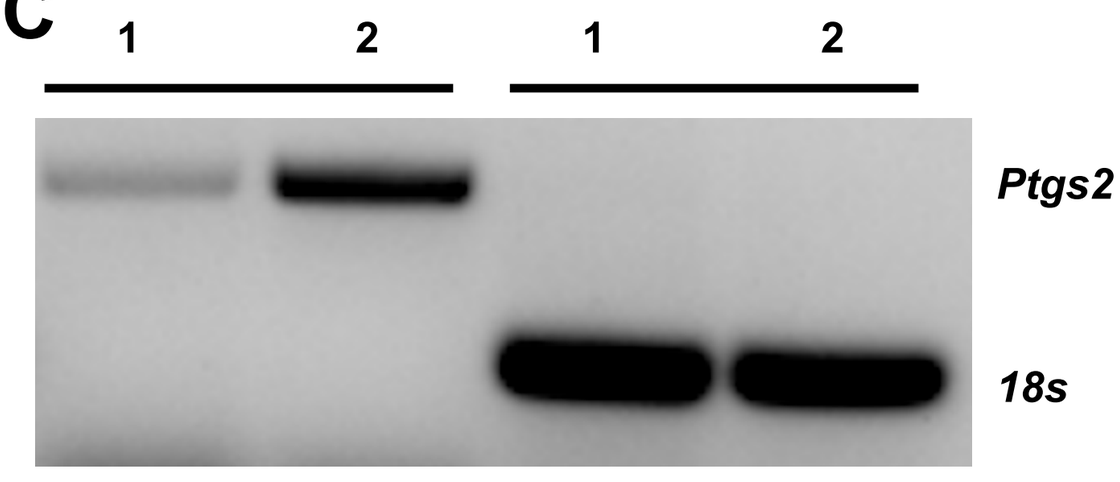

1: Adult cortex lysis
2: sorted SMAcre^{ER+}:Ai47 parenchymal aSMCs

D

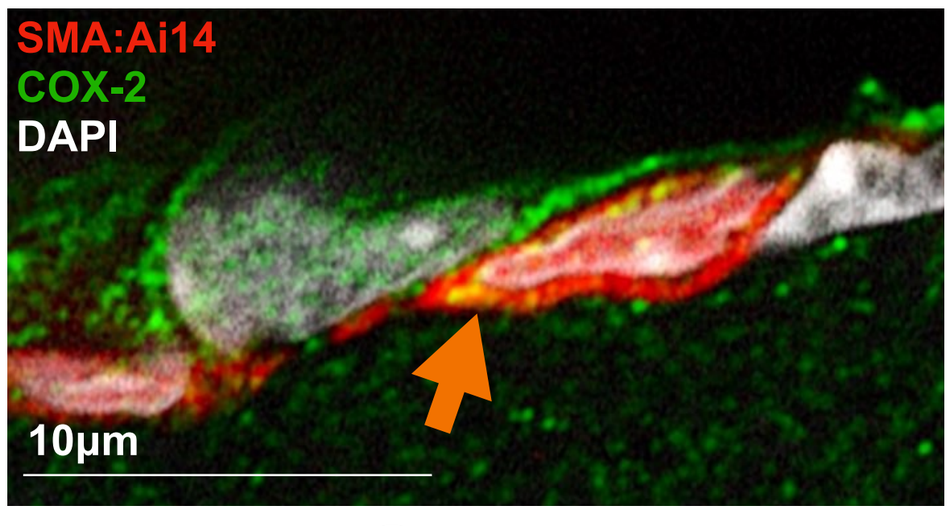

E

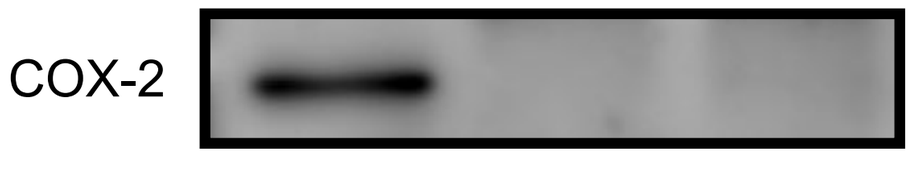

F

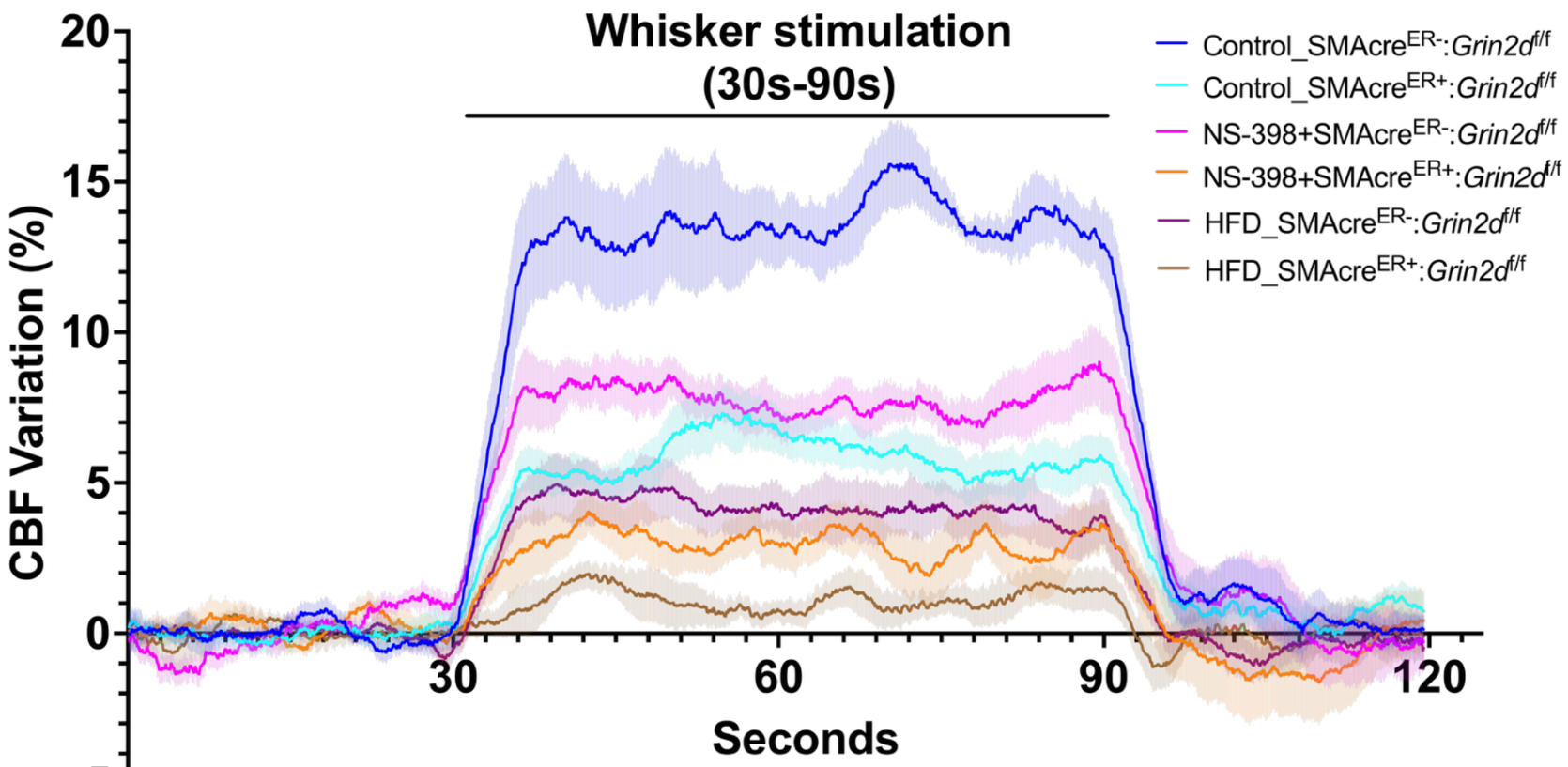

G

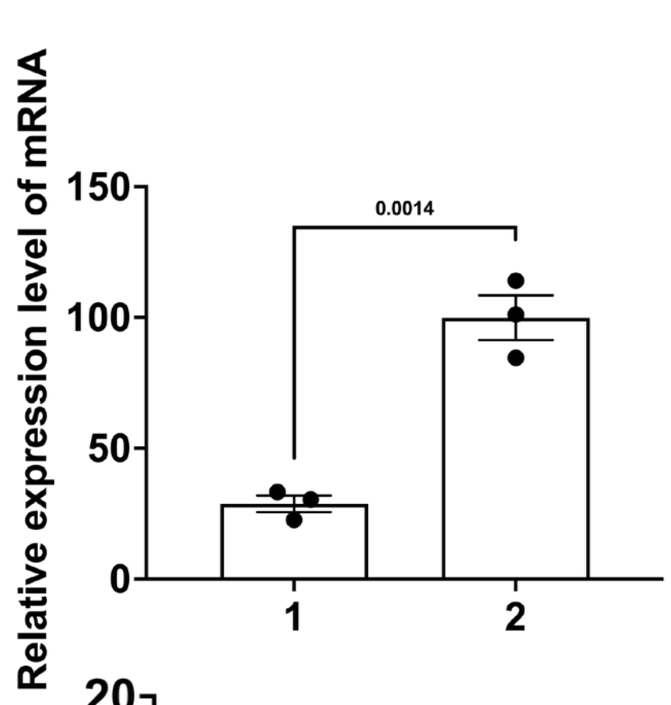

H

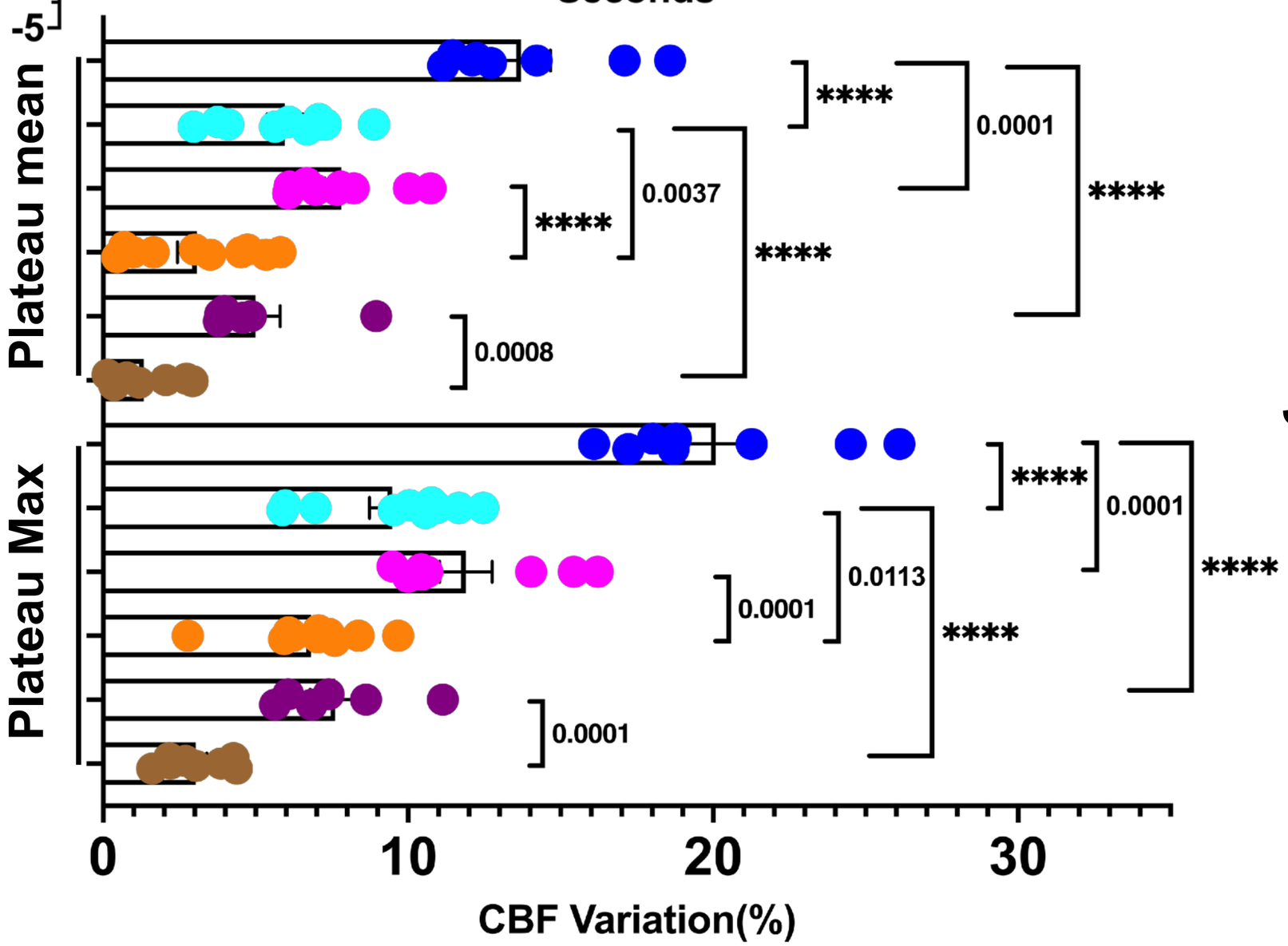

I

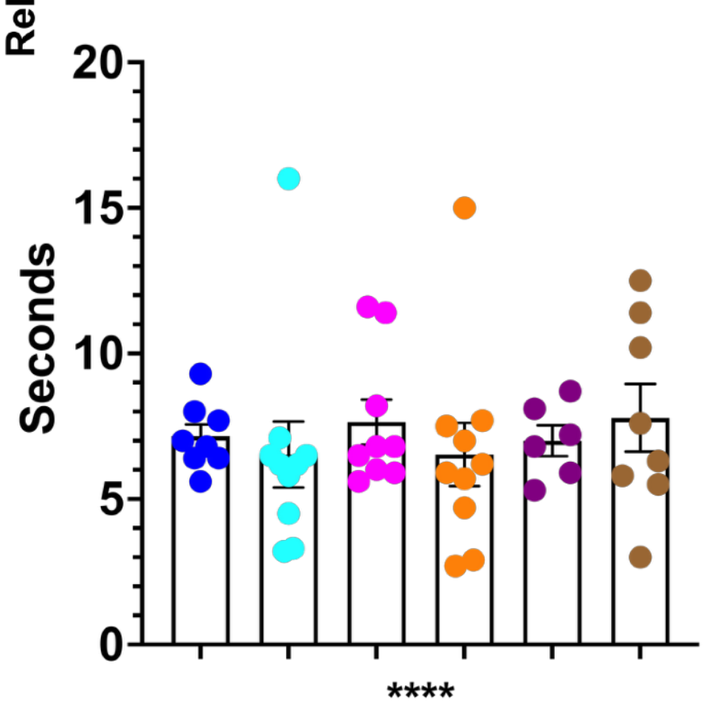

J

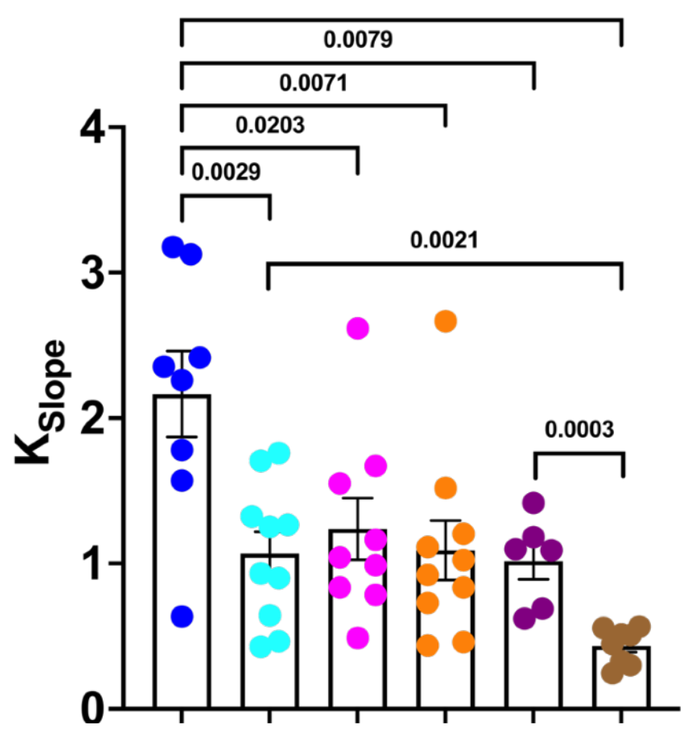

Figure 5

A

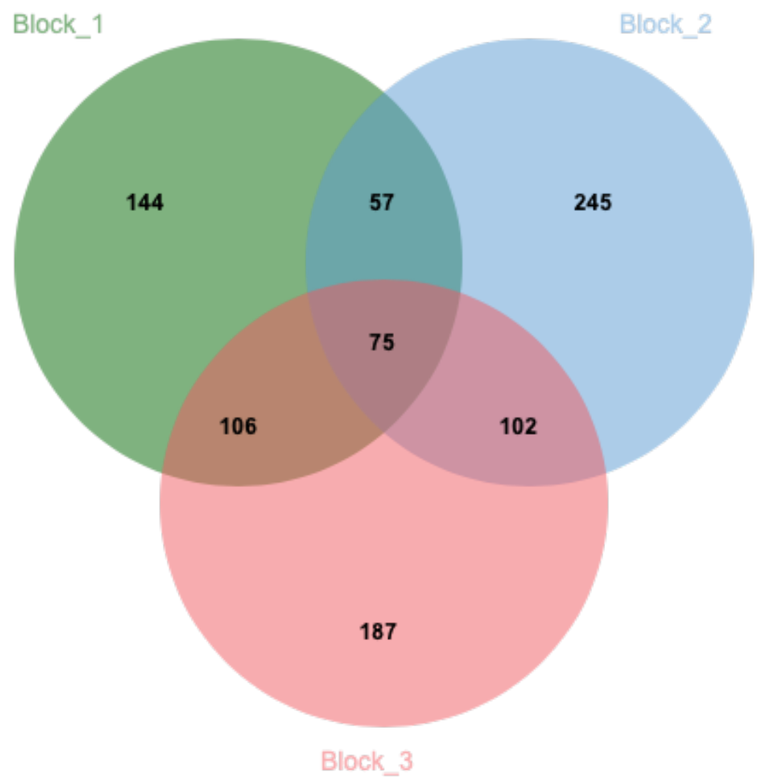

B

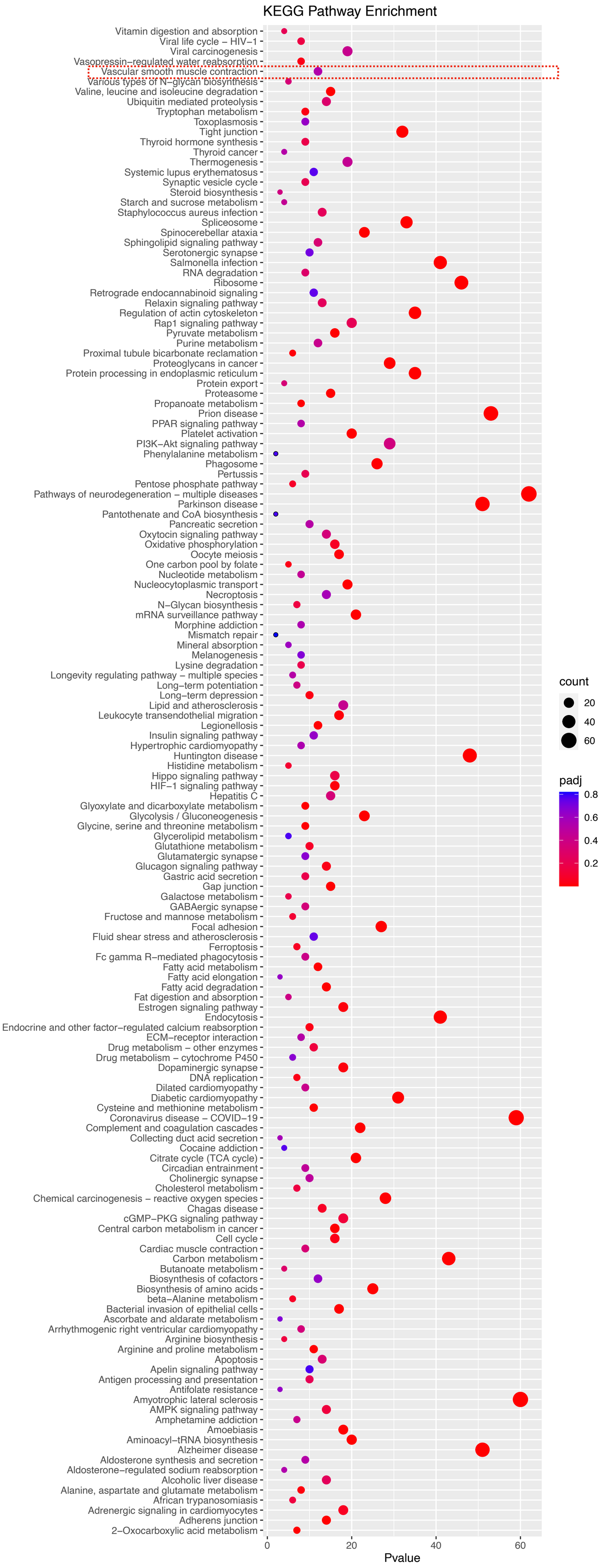

C

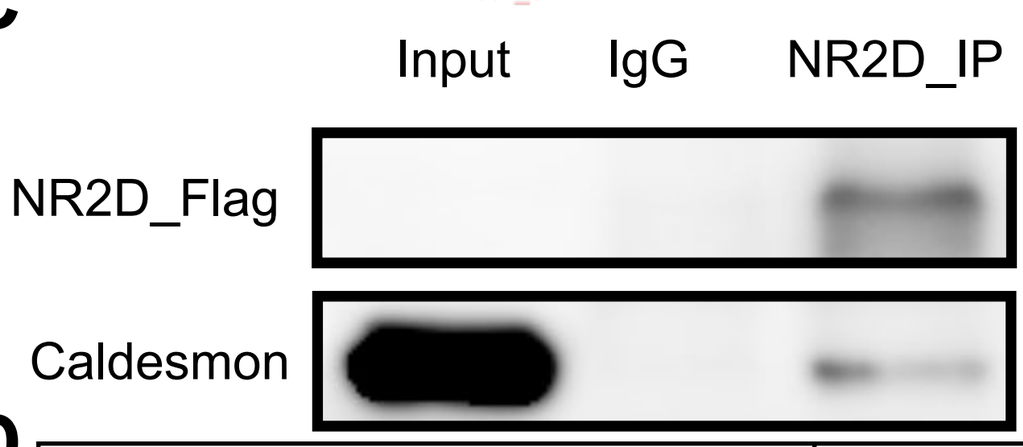

D

Go-BP	No. of proteins
Translation	86
Protein Transport	69
mRNA Processing	63
RNA Splicing	52
Intracellular Protein Transport	45
Cytoplasmic Translation	44
Negative Regulation Of Apoptotic Process	44
Lipid Metabolic Process	44
Cell Cycle	42
Protein Stabilization	38
Immune System Process	36
Positive Regulation Of Gene Expression	34
Vesicle-Mediated Transport	33
Response To Drug	33
mRNA Splicing, Via Spliceosome	32
Cell Division	32
Protein Folding	29
Regulation Of Translation	29
Endocytosis	27
Actin Cytoskeleton Organization	26

E

Go-CC	No. of proteins
Cytoplasm	536
Cytosol	403
Nucleus	380
Nucleoplasm	233
Mitochondrion	182
Macromolecular Complex	122
Endoplasmic Reticulum	121
Cytoskeleton	119
Myelin Sheath	96
Synapse	96
Intracellular Membrane-Bounded Organelle	88
Perinuclear Region Of Cytoplasm	86
Nucleolus	76
Cell Projection	76
Golgi Apparatus	72
Ribonucleoprotein Complex	70
Neuronal Cell Body	67
Cytoplasmic Vesicle	60
Cell Junction	58
Cell Surface	55

F

Go-MF	No. of proteins
Protein Binding	430
Nucleotide Binding	202
Identical Protein Binding	183
RNA Binding	176
ATP Binding	153
Hydrolase Activity	114
Nucleic Acid Binding	96
Macromolecular Complex Binding	81
mRNA Binding	64
Protein Domain Specific Binding	64
GTP Binding	63
Actin Binding	62
Protein Homodimerization Activity	60
Oxidoreductase Activity	59
Enzyme Binding	57
Protein Kinase Binding	55
GTPase Activity	52
ATPase Activity	51
Catalytic Activity	47
Structural Constituent Of Ribosome	46

Figure 6

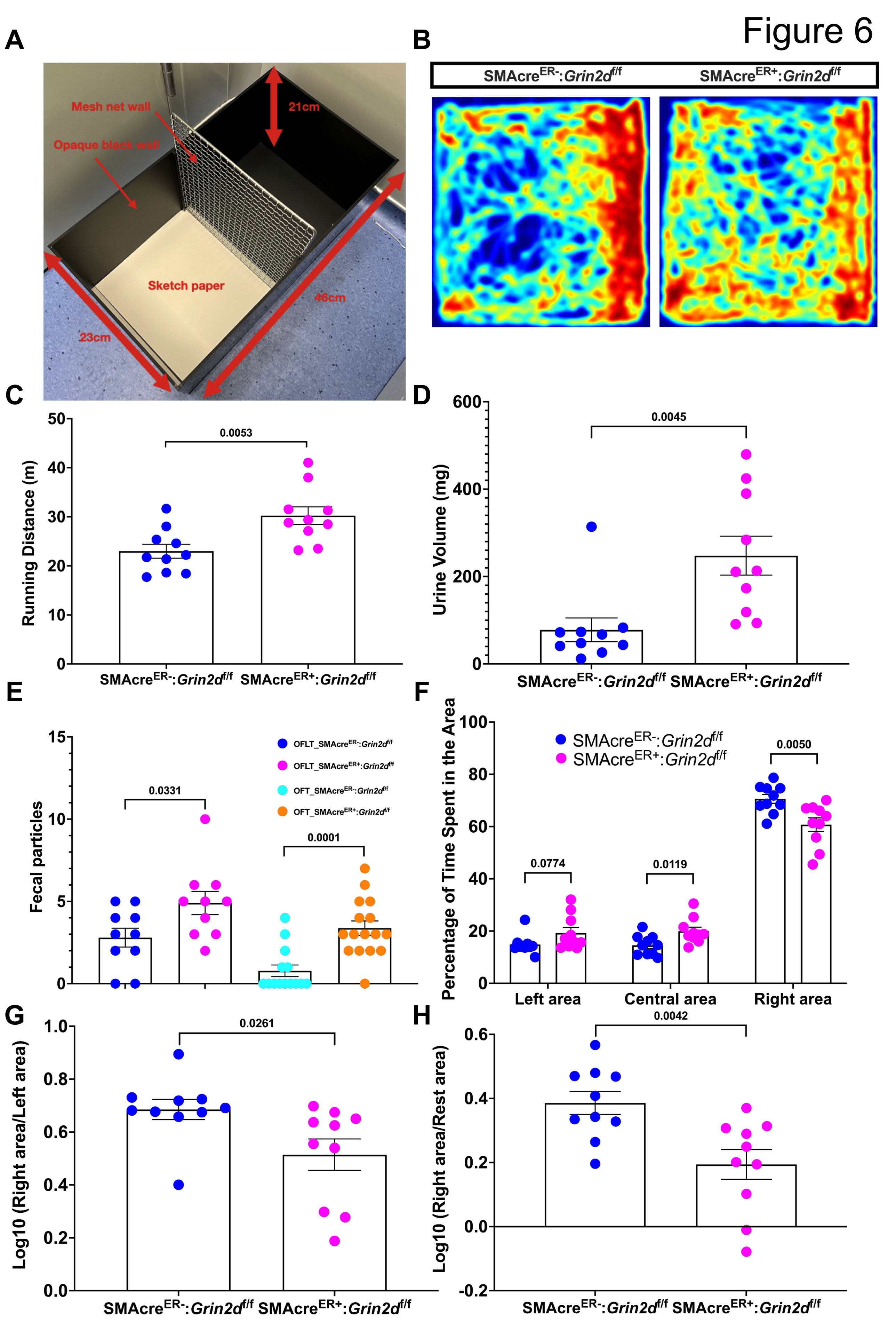
A
Mesh net wall
Opaque black wall
21cm
Sketch paper
46cm
23cm
B
SMAcre^{ER-}:*Grin2d*$^{f/f}$
SMAcre^{ER+}:*Grin2d*$^{f/f}$
C
Running Distance (m)
0.0053
SMAcre^{ER-}:*Grin2d*$^{f/f}$
SMAcre^{ER+}:*Grin2d*$^{f/f}$
D
Urine Volume (mg)
0.0045
SMAcre^{ER-}:*Grin2d*$^{f/f}$
SMAcre^{ER+}:*Grin2d*$^{f/f}$
E
Fecal particles
OFLT_SMAcre^{ER-}:*Grin2d*$^{f/f}$
OFLT_SMAcre^{ER+}:*Grin2d*$^{f/f}$
OFT_SMAcre^{ER-}:*Grin2d*$^{f/f}$
OFT_SMAcre^{ER+}:*Grin2d*$^{f/f}$
0.0331
0.0001
F
Percentage of Time Spent in the Area
SMAcre^{ER-}:*Grin2d*$^{f/f}$
SMAcre^{ER+}:*Grin2d*$^{f/f}$
0.0774
0.0119
0.0050
Left area
Central area
Right area
G
Log10 (Right area/Left area)
0.0261
SMAcre^{ER-}:*Grin2d*$^{f/f}$
SMAcre^{ER+}:*Grin2d*$^{f/f}$
H
Log10 (Right area/Rest area)
0.0042
SMAcre^{ER-}:*Grin2d*$^{f/f}$
SMAcre^{ER+}:*Grin2d*$^{f/f}$

Figure 7

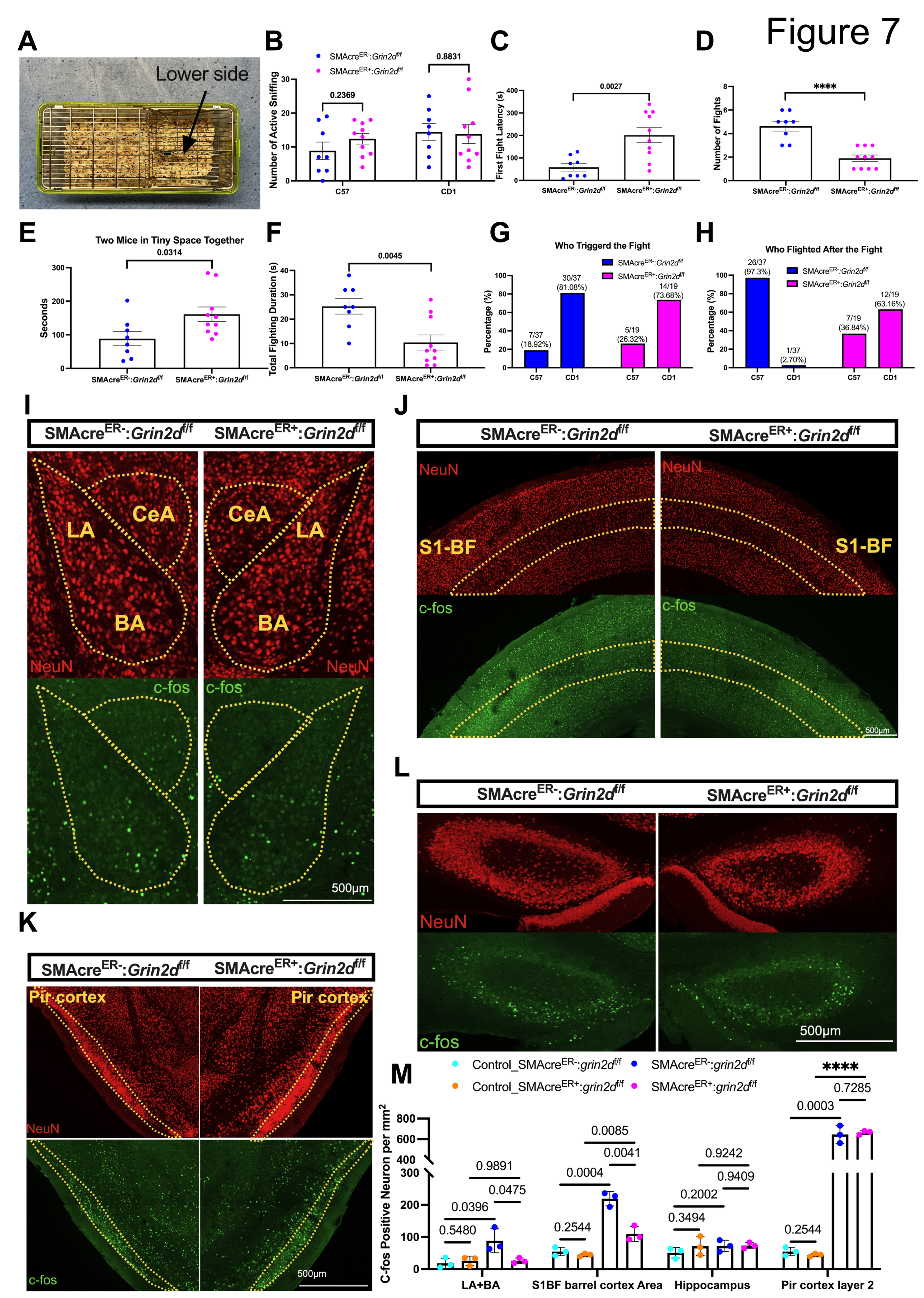
A
Lower side
B
SMAcre^{ER-}:Grin2d$^{f/f}$
SMAcre^{ER+}:Grin2d$^{f/f}$
Number of Active Sniffing
0.2369
0.8831
C57
CD1
C
First Fight Latency (s)
0.0027
D
Number of Fights
****
E
Two Mice in Tiny Space Together
Seconds
0.0314
F
Total Fighting Duration (s)
0.0045
G
Who Triggerd the Fight
Percentage (%)
7/37 (18.92%)
30/37 (81.08%)
5/19 (26.32%)
14/19 (73.68%)
H
Who Flighted After the Fight
26/37 (97.3%)
1/37 (2.70%)
7/19 (36.84%)
12/19 (63.16%)
I
LA
CeA
BA
NeuN
c-fos
500μm
J
S1-BF
500μm
K
Pir cortex
L
M
Control_SMAcre^{ER-}:grin2d$^{f/f}$
SMAcre^{ER-}:grin2d$^{f/f}$
Control_SMAcre^{ER+}:grin2d$^{f/f}$
SMAcre^{ER+}:grin2d$^{f/f}$
C-fos Positive Neuron per mm^2
LA+BA
S1BF barrel cortex Area
Hippocampus
Pir cortex layer 2

Figure S1

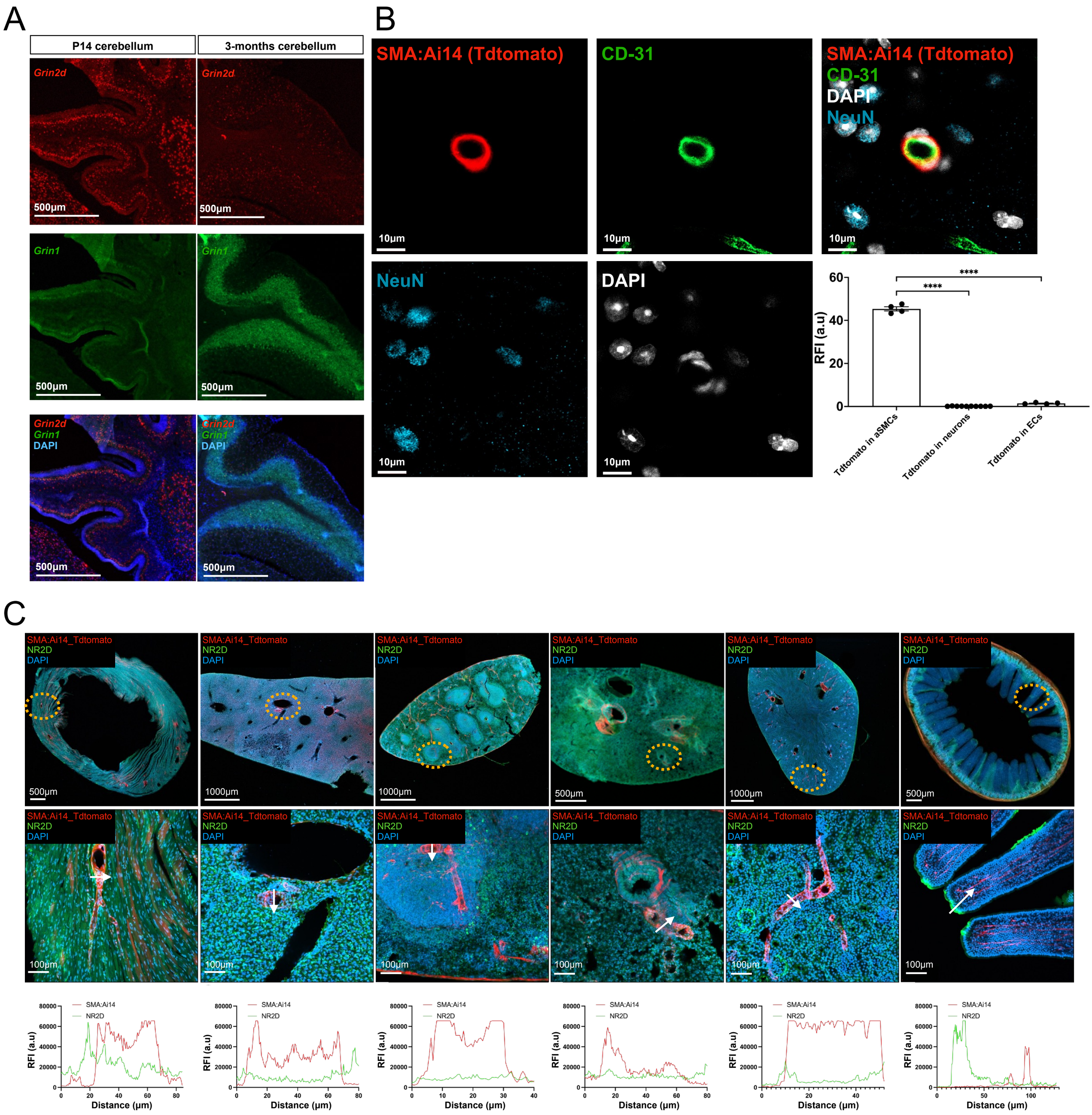
A
P14 cerebellum
3-months cerebellum
Grin2d
Grin1
DAPI
500µm
B
SMA:Ai14 (Tdtomato)
CD-31
NeuN
DAPI
10µm
RFI (a.u)
Tdtomato in aSMCs
Tdtomato in neurons
Tdtomato in ECs
****
C
SMA:Ai14_Tdtomato
NR2D
DAPI
500µm
1000µm
100µm
SMA:Ai14
Distance (µm)

Figure S2

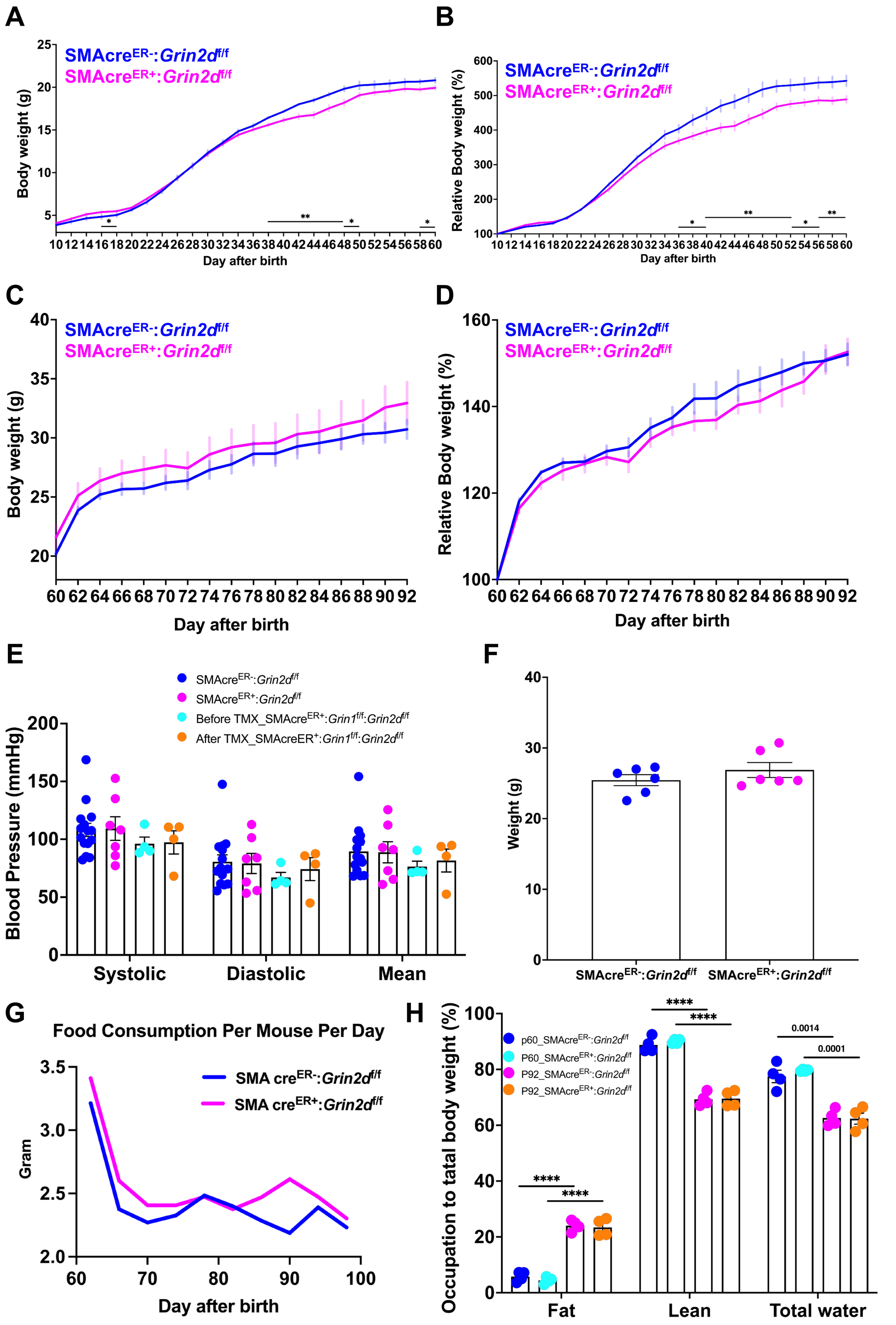
A
SMAcreER-:Grin2df/f
SMAcreER+:Grin2df/f
Body weight (g)
Day after birth
B
Relative Body weight (%)
Day after birth
C
Body weight (g)
Day after birth
D
Relative Body weight (%)
Day after birth
E
SMAcreER-:Grin2df/f
SMAcreER+:Grin2df/f
Before TMX_SMAcreER+:Grin1f/f:Grin2df/f
After TMX_SMAcreER+:Grin1f/f:Grin2df/f
Blood Pressure (mmHg)
Systolic
Diastolic
Mean
F
Weight (g)
SMAcreER-:Grin2df/f
SMAcreER+:Grin2df/f
G
Food Consumption Per Mouse Per Day
SMA creER-:Grin2df/f
SMA creER+:Grin2df/f
Gram
Day after birth
H
p60_SMAcreER-:Grin2df/f
P60_SMAcreER+:Grin2df/f
P92_SMAcreER-:Grin2df/f
P92_SMAcreER+:Grin2df/f
Occupation to tatal body weight (%)
Fat
Lean
Total water
0.0014
0.0001

Figure S3

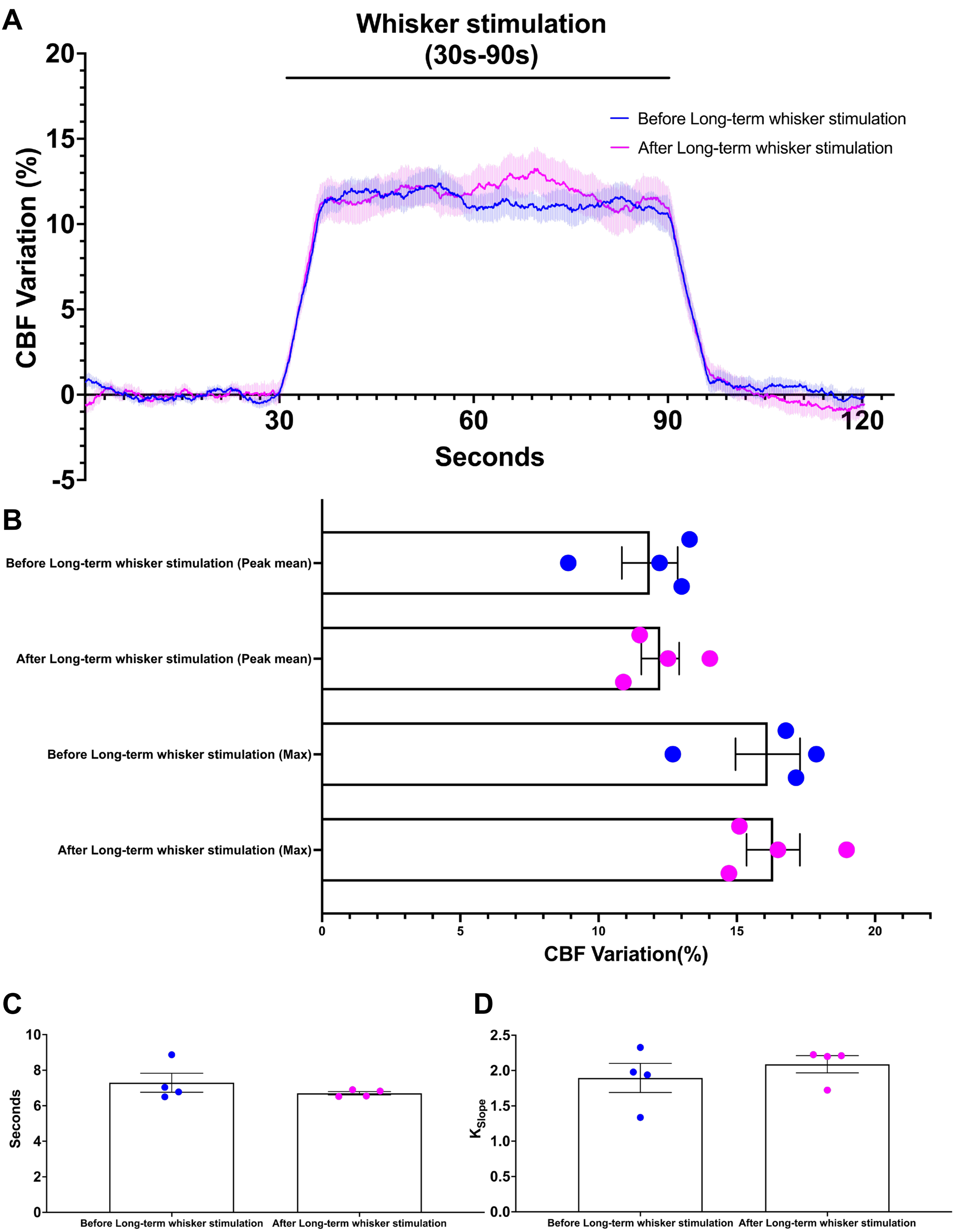
A
Whisker stimulation
(30s-90s)
Before Long-term whisker stimulation
After Long-term whisker stimulation
CBF Variation (%)
Seconds
B
Before Long-term whisker stimulation (Peak mean)
After Long-term whisker stimulation (Peak mean)
Before Long-term whisker stimulation (Max)
After Long-term whisker stimulation (Max)
CBF Variation(%)
C
Seconds
Before Long-term whisker stimulation
After Long-term whisker stimulation
D
K Slope
Before Long-term whisker stimulation
After Long-term whisker stimulation

Figure S4

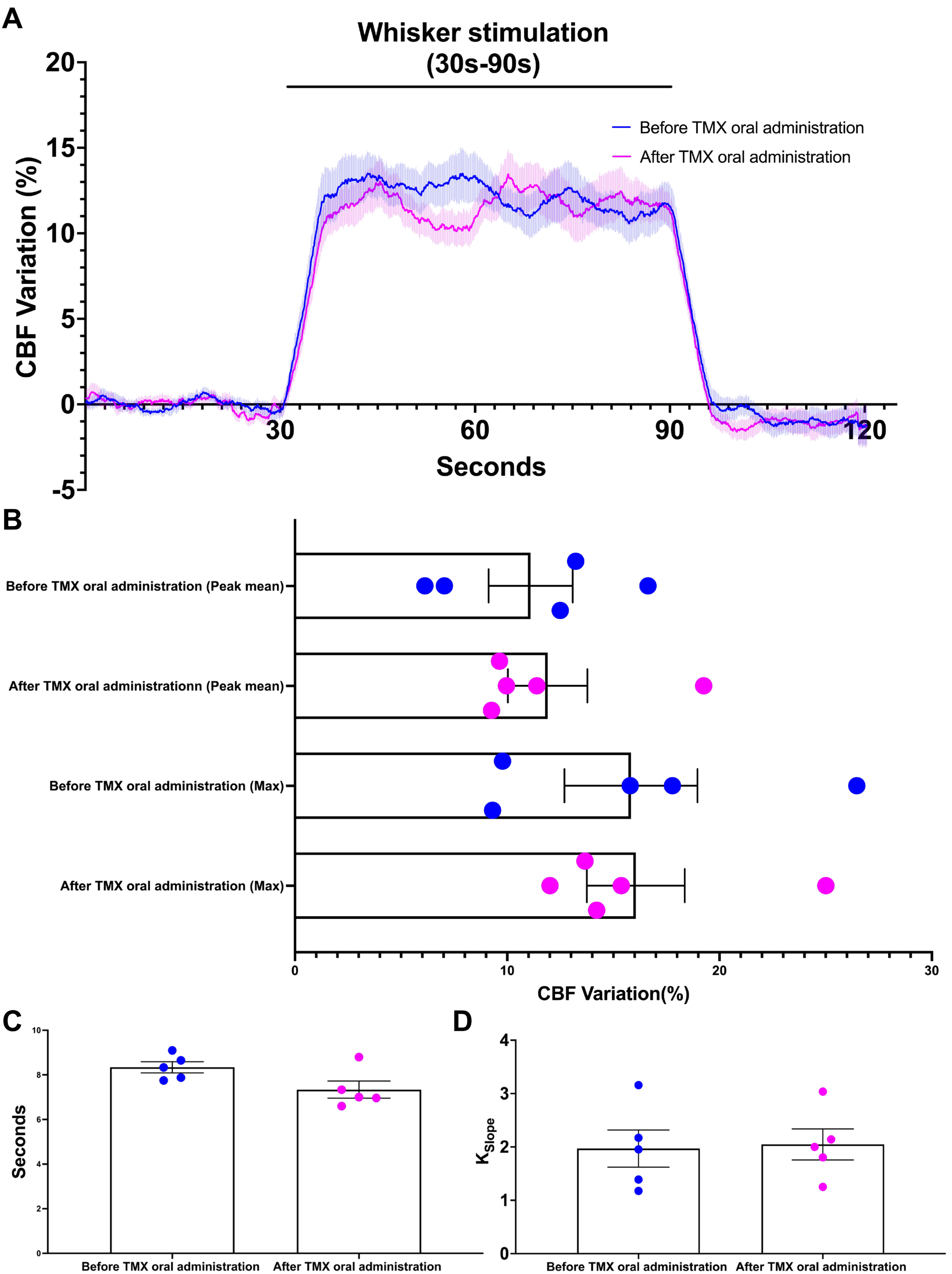
A
Whisker stimulation
(30s-90s)
Before TMX oral administration
After TMX oral administration
CBF Variation (%)
20
15
10
5
0
-5
30
60
90
120
Seconds
B
Before TMX oral administration (Peak mean)
After TMX oral administrationn (Peak mean)
Before TMX oral administration (Max)
After TMX oral administration (Max)
0
10
20
30
CBF Variation(%)
C
Seconds
10
8
6
4
2
0
Before TMX oral administration
After TMX oral administration
D
K_{Slope}
4
3
2
1
0
Before TMX oral administration
After TMX oral administration

Figure S5

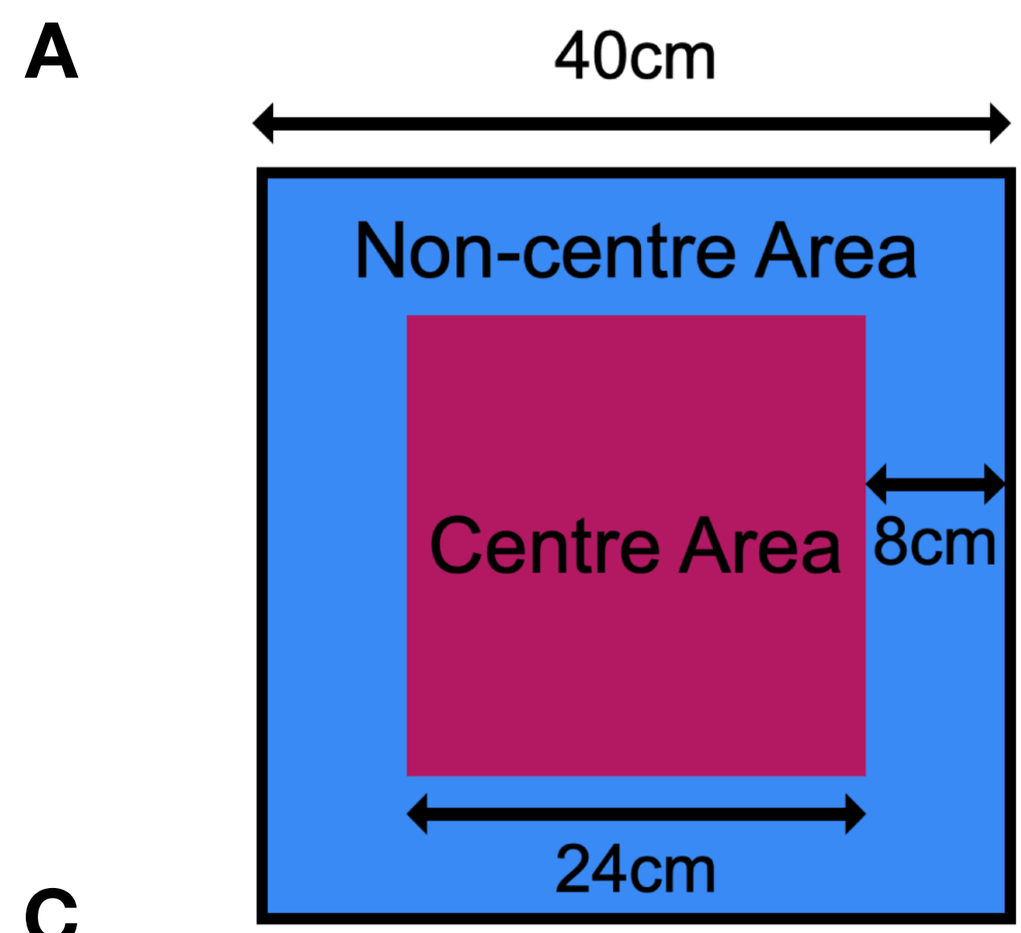
A
40cm
Non-centre Area
Centre Area
8cm
24cm

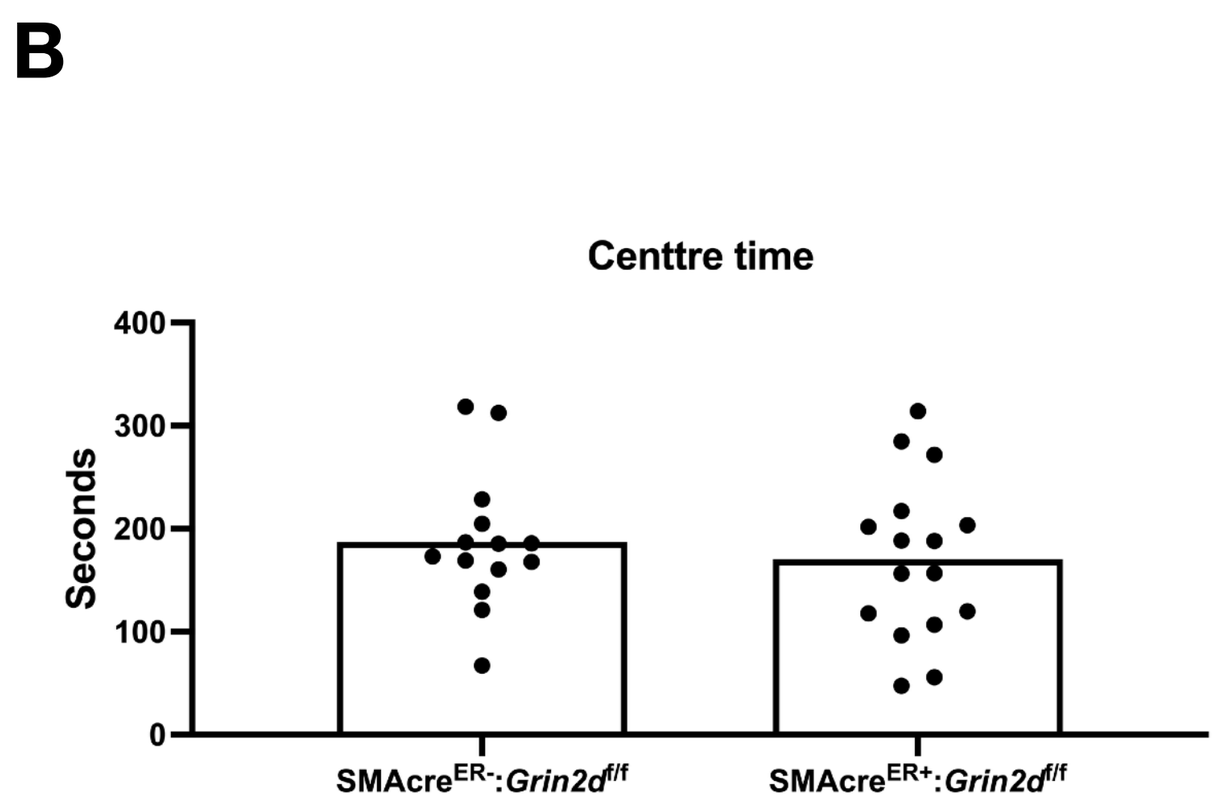
B
Centtre time
Seconds
400
300
200
100
0
SMAcre^{ER-}:*Grin2d*$^{f/f}$
SMAcre^{ER+}:*Grin2d*$^{f/f}$

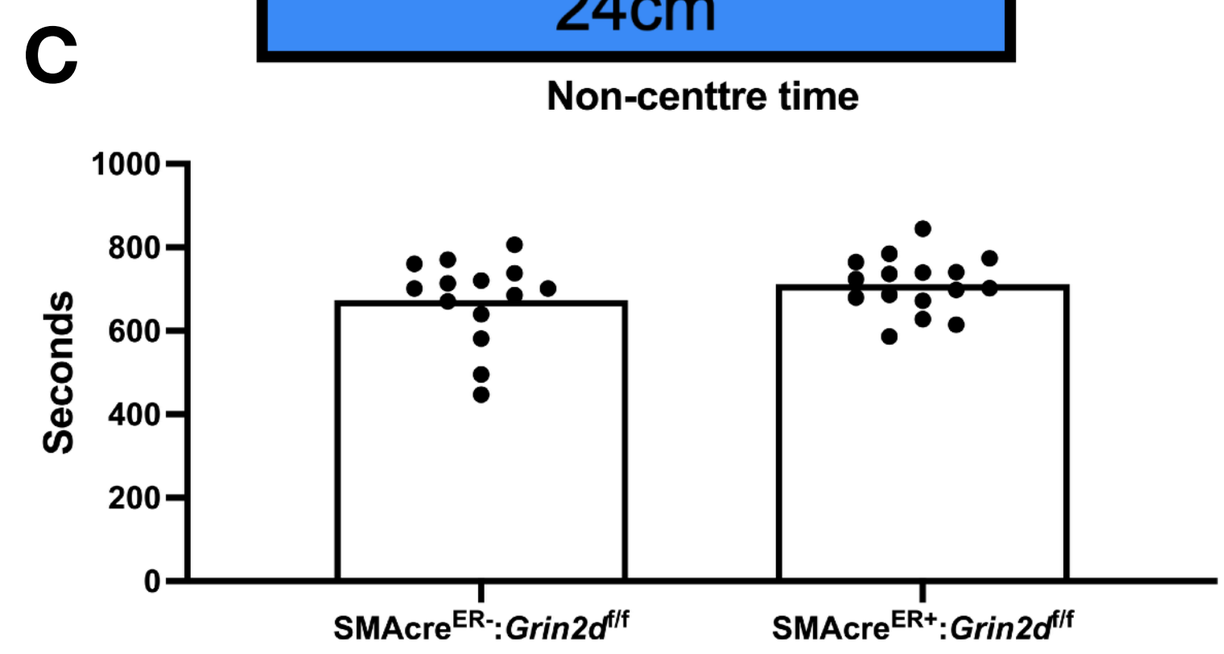
C
Non-centtre time
Seconds
1000
800
600
400
200
0
SMAcre^{ER-}:*Grin2d*$^{f/f}$
SMAcre^{ER+}:*Grin2d*$^{f/f}$

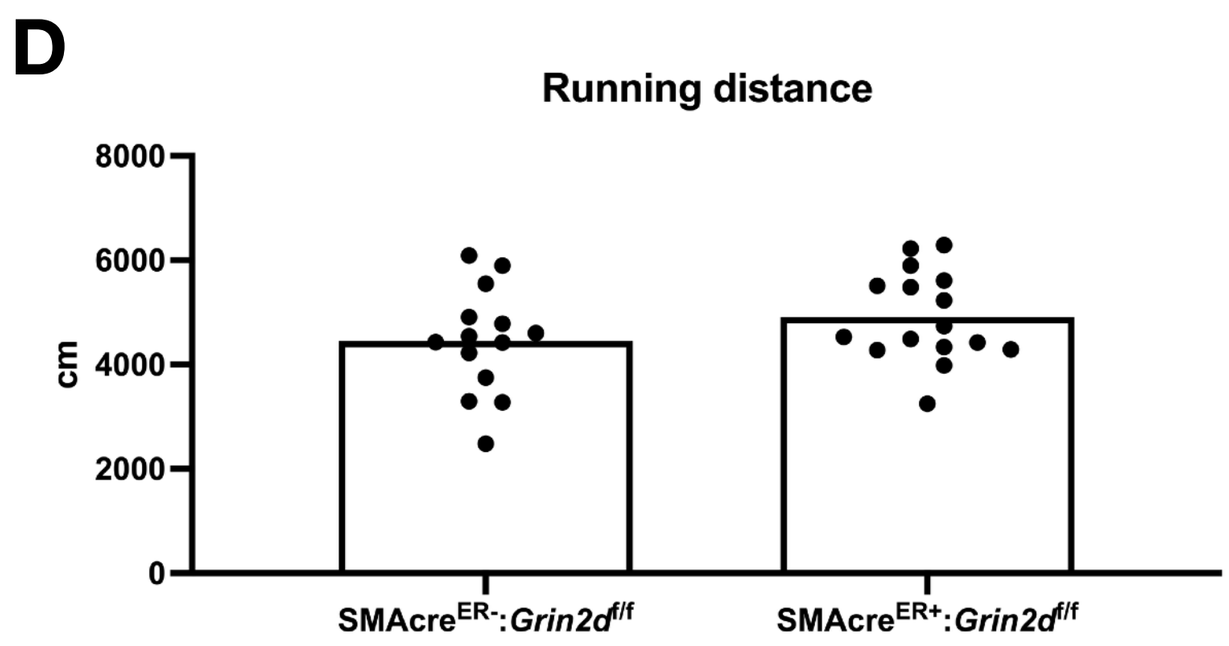
D
Running distance
cm
8000
6000
4000
2000
0
SMAcre^{ER-}:*Grin2d*$^{f/f}$
SMAcre^{ER+}:*Grin2d*$^{f/f}$

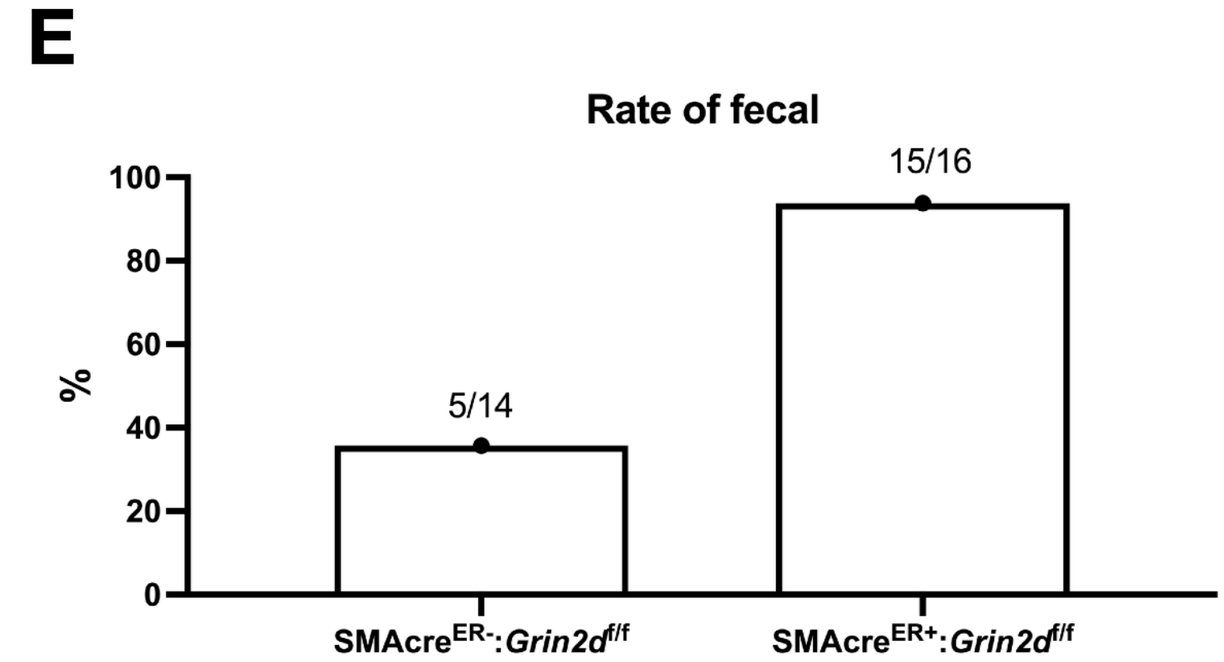
E
Rate of fecal
%
100
80
60
40
20
0
5/14
15/16
SMAcre^{ER-}:*Grin2d*$^{f/f}$
SMAcre^{ER+}:*Grin2d*$^{f/f}$

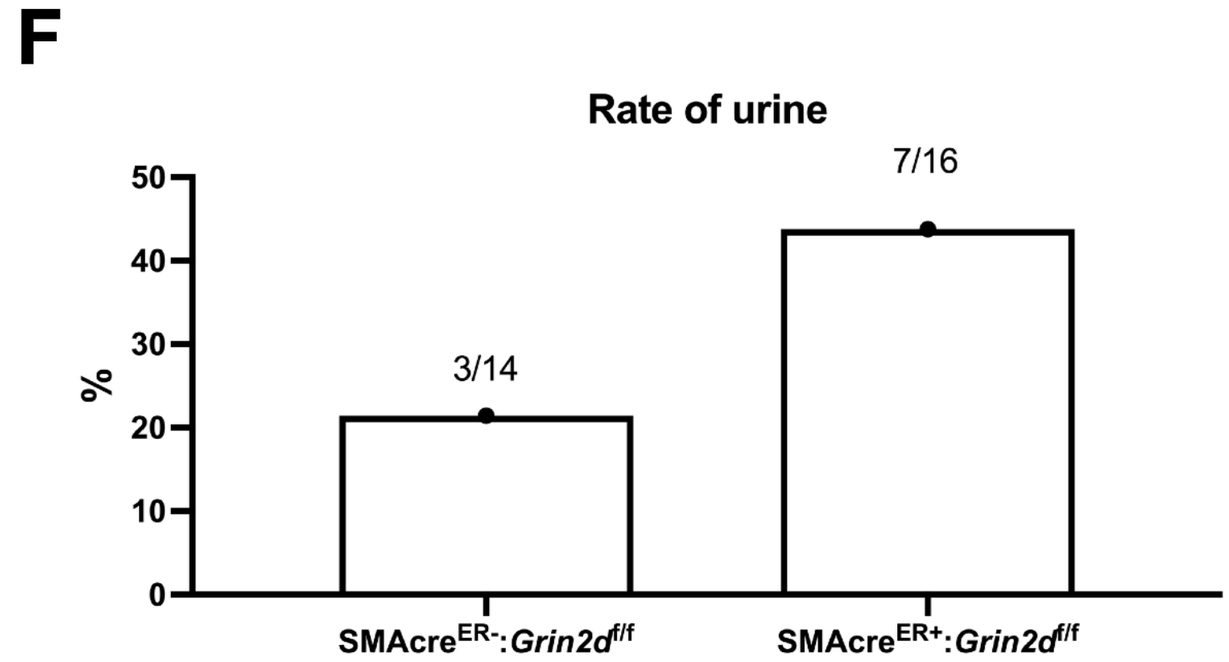
F
Rate of urine
%
50
40
30
20
10
0
3/14
7/16
SMAcre^{ER-}:*Grin2d*$^{f/f}$
SMAcre^{ER+}:*Grin2d*$^{f/f}$

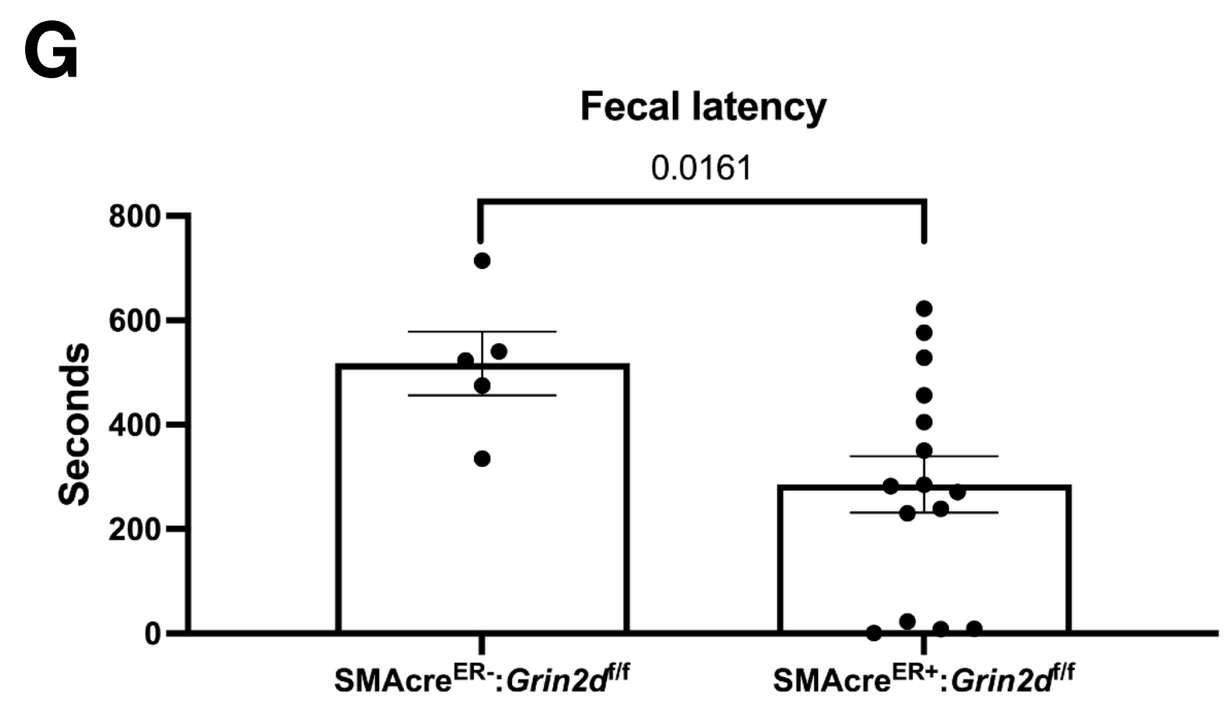
G
Fecal latency
0.0161
Seconds
800
600
400
200
0
SMAcre^{ER-}:*Grin2d*$^{f/f}$
SMAcre^{ER+}:*Grin2d*$^{f/f}$

Figure S6

A

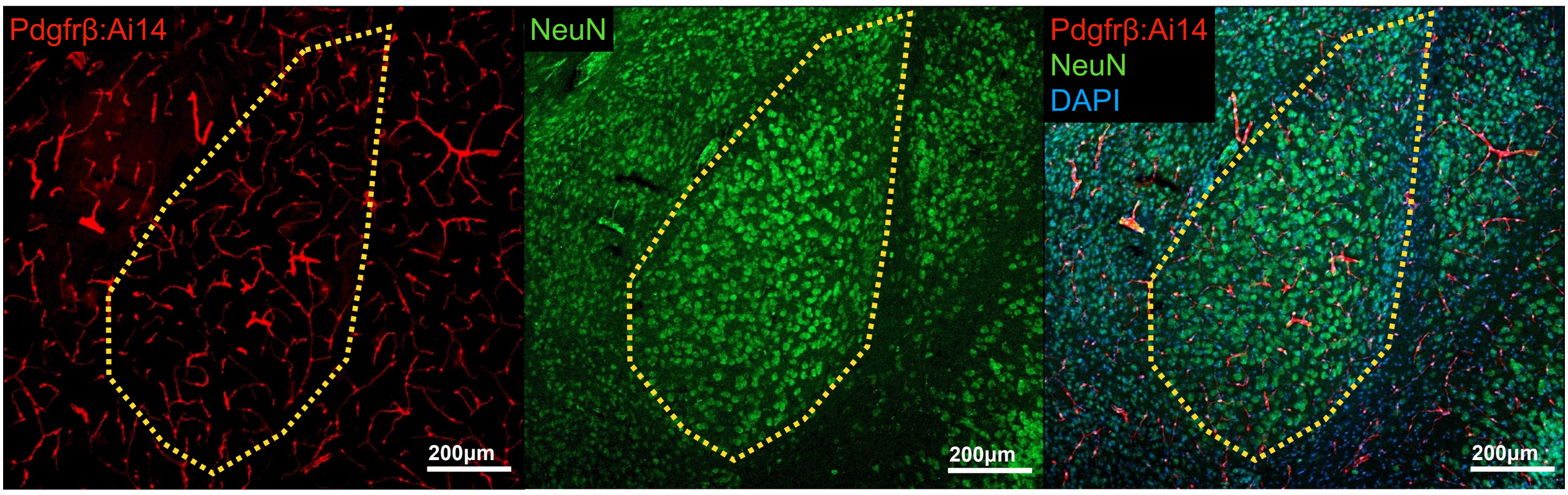

B SMAcre^{ER-}:*Grin2d*$^{f/f}$ SMAcre^{ER+}:*Grin2d*$^{f/f}$

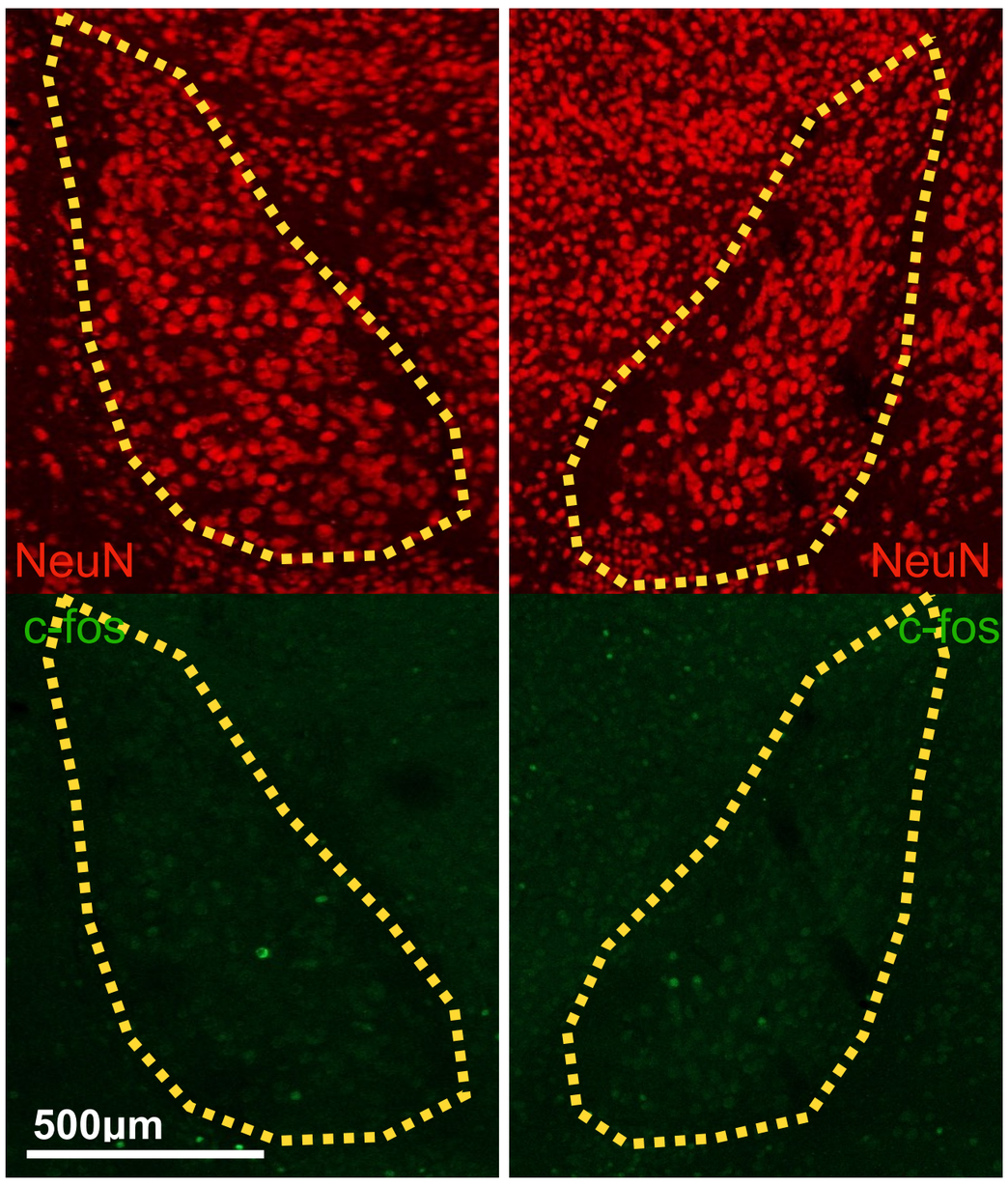

C SMAcre^{ER-}:*Grin2d*$^{f/f}$ SMAcre^{ER+}:*Grin2d*$^{f/f}$

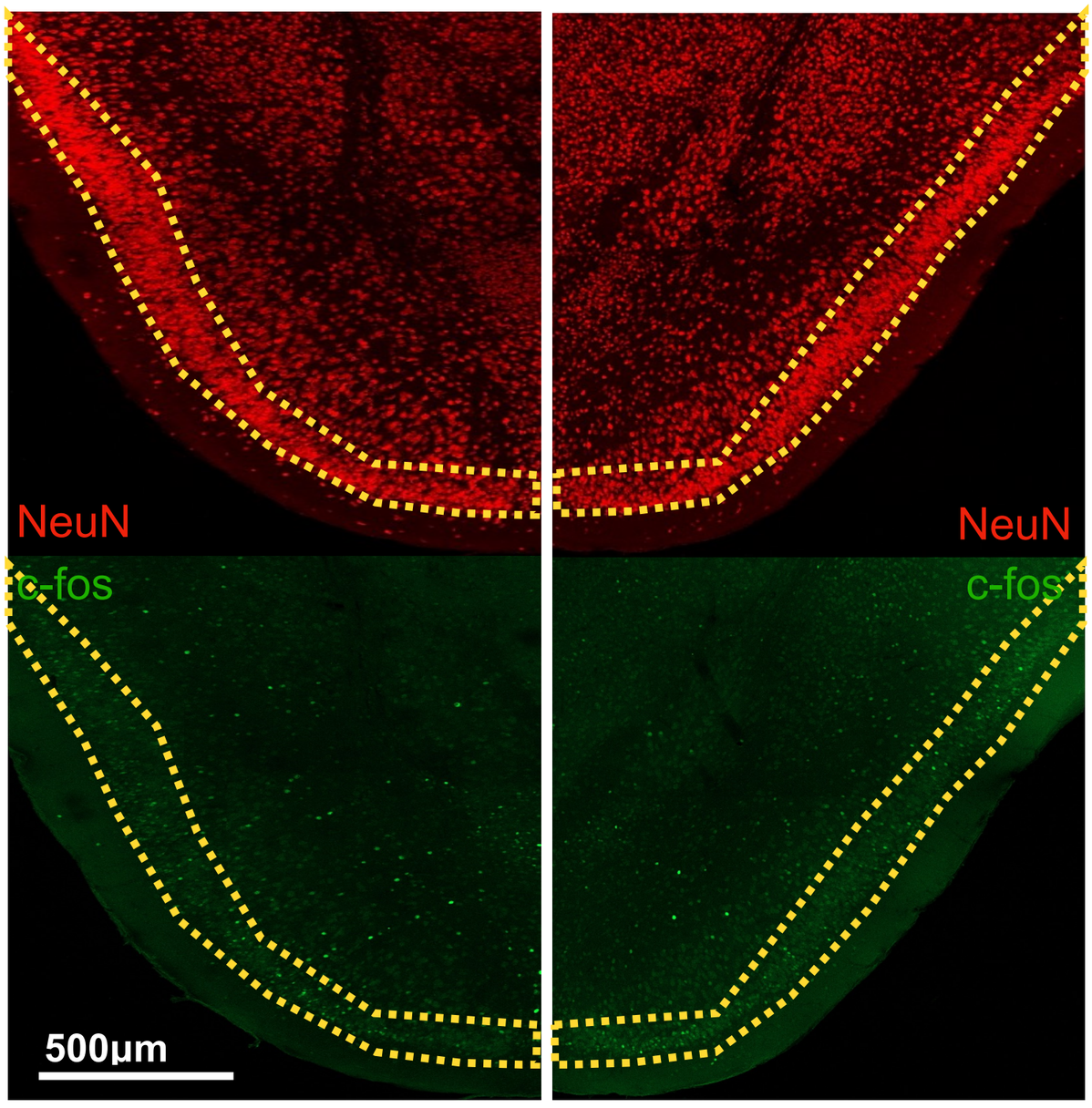

D SMAcre^{ER-}:*Grin2d*$^{f/f}$ SMAcre^{ER+}:*Grin2d*$^{f/f}$

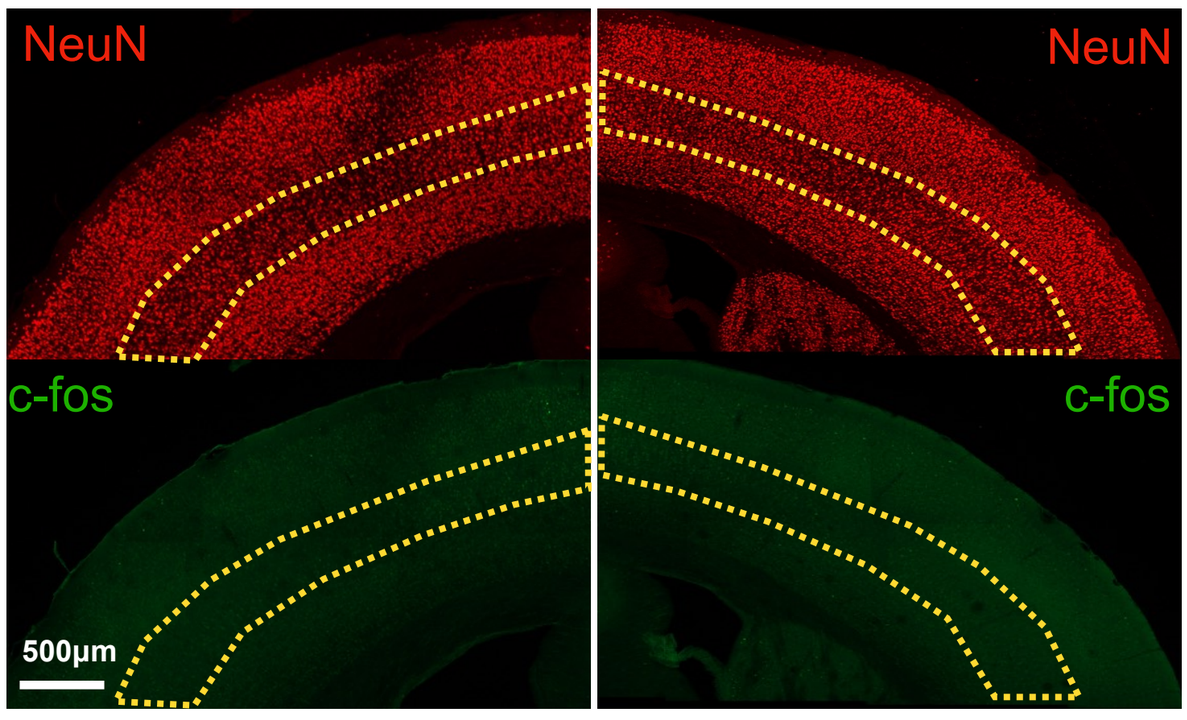

E SMAcre^{ER-}:*Grin2d*$^{f/f}$ SMAcre^{ER+}:*Grin2d*$^{f/f}$

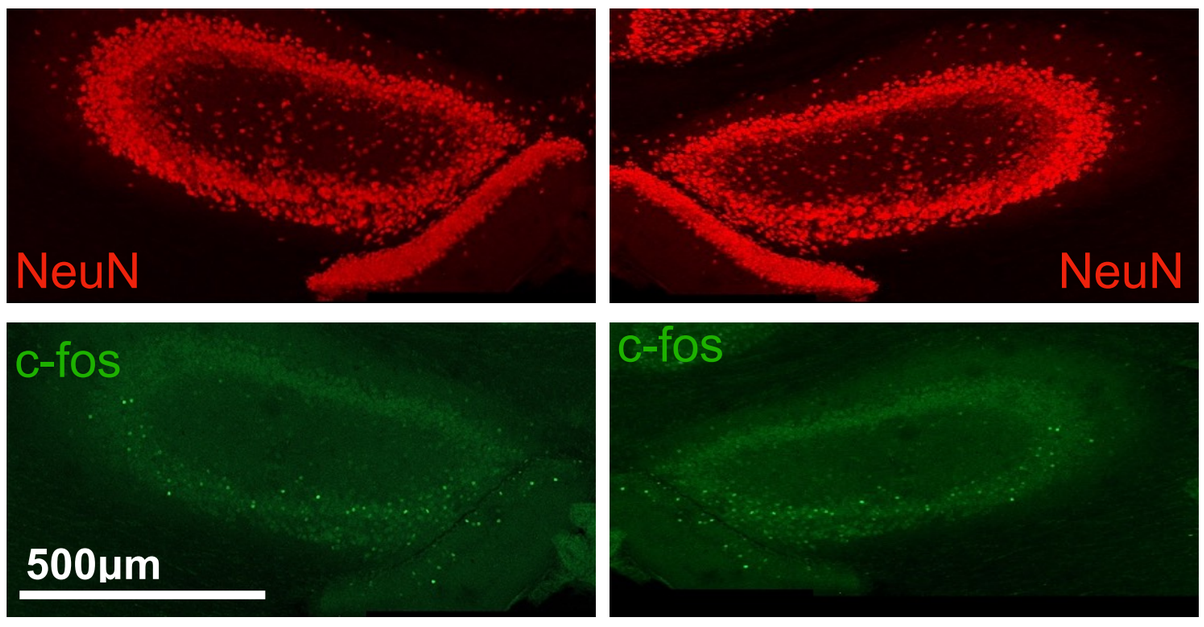

Figure S7

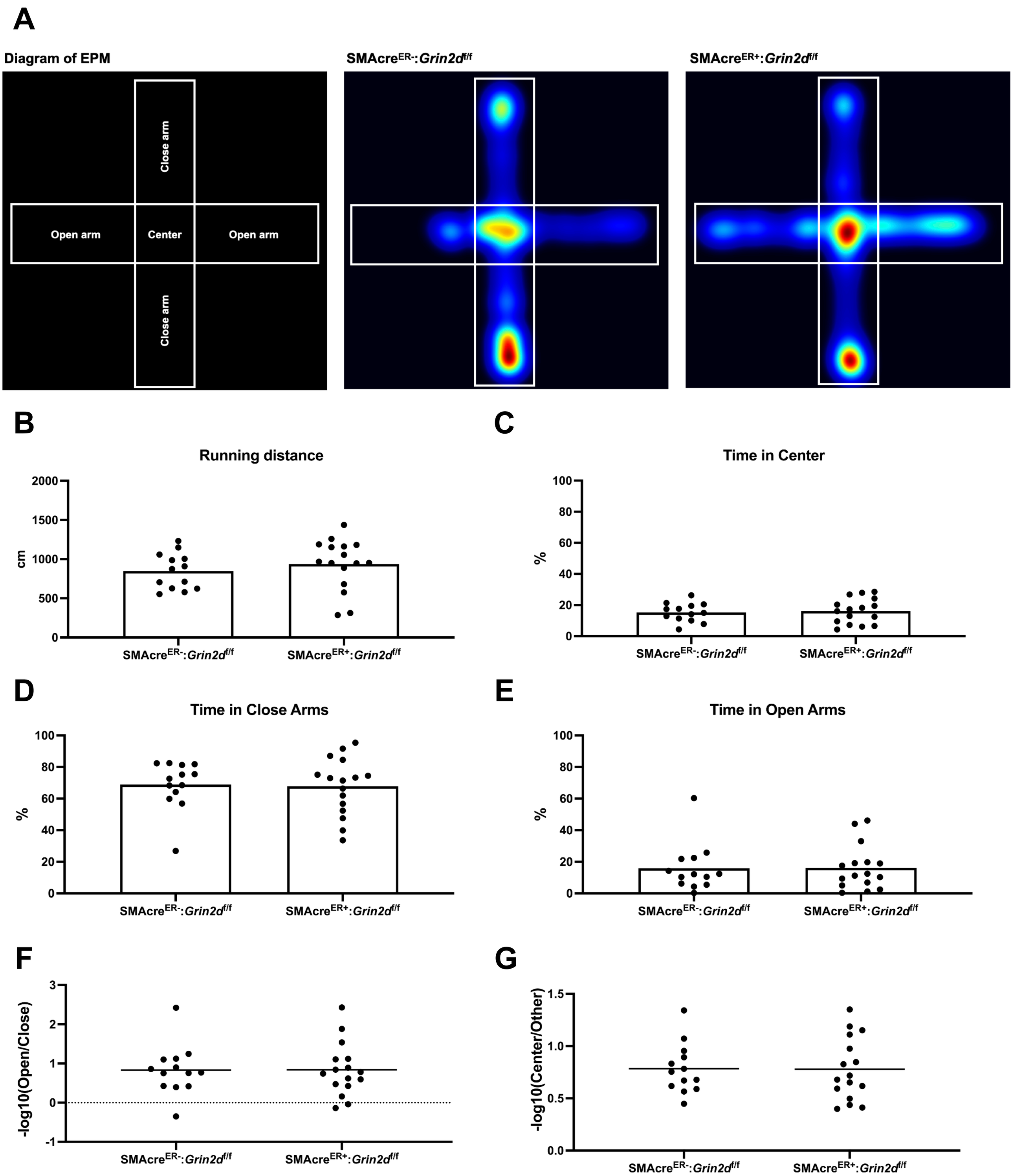
A
Diagram of EPM
Close arm
Open arm
Center
Open arm
Close arm
SMAcreER-:Grin2df/f
SMAcreER+:Grin2df/f
B
Running distance
cm
2000
1500
1000
500
0
SMAcreER-:Grin2df/f
SMAcreER+:Grin2df/f
C
Time in Center
%
100
80
60
40
20
0
SMAcreER-:Grin2df/f
SMAcreER+:Grin2df/f
D
Time in Close Arms
%
100
80
60
40
20
0
SMAcreER-:Grin2df/f
SMAcreER+:Grin2df/f
E
Time in Open Arms
%
100
80
60
40
20
0
SMAcreER-:Grin2df/f
SMAcreER+:Grin2df/f
F
-log10(Open/Close)
3
2
1
0
-1
SMAcreER-:Grin2df/f
SMAcreER+:Grin2df/f
G
-log10(Center/Other)
1.5
1.0
0.5
0.0
SMAcreER-:Grin2df/f
SMAcreER+:Grin2df/f